A response-rescaling property revealed by single-cell analysis of cAMP signaling response in the social amoeba *Dictyostelium discoideum*

(社会性アメーバ *Dictyostelium discoideum* が示す cAMP 応答のリスケーリング特性の一細胞解析)

神野　圭太

Contents

Chapter 1

Introduction

1.1 Intercellular communication in the development of the social amoeba *Dictyostelium discoideum*

The social amoeba *Dictyostelium discoideum* (figure 1.1) is one of the most studied organisms both in cell biology and developmental biology [65]. The main reason why the amoeba have attracted researchers to date is that the cells transition from a unicellular stage into a multicellular stage during their life cycle. The life cycle of each amoeba begins with the germination of a spore. The cell germinated from the spore continues to grow and divide as long as it finds bacteria on which it can feed. Upon starvation, however, the cells start to communicate with each other by means of a chemical mechanism. The intercellular signaling results in a macroscopic spatio-temporal pattern of a signaling molecule. At a certain point, the cells start to aggregate to a center of the pattern following a chemical gradient of the signaling molecule. The resultant collection of the cells makes a mound-like aggregate containing about 10^5 cells. The aggregate then takes the form of a slug that can migrate a long distance and finally culminates in a multicellular structure called fruiting body.

In this study, we try to gain insights into the relation between collective behaviors of cells and properties of constituent cells through the analysis of cAMP signaling in the early stage of *Dictyostelium* development. The collective behavior observed at the early stage of the development is periodic synthesis and secretion of cAMP called cAMP oscillation. Two to three hours after a layer of starved *Dictyostelium* cells are placed on an agar substrate, a macroscopic pattern consisting of dark and light bands of a few millimeters wavelength appears on the agar surface (figure 1.2). The pattern propagates unidirectionally as waves and forms a spiral pattern in a self-organized manner until the cells start to aggregate to the center of the spiral pattern [34, 35]. It has been revealed that the pattern results from shape changes of the cells [2], which alter the intensity of scattered light, caused by the stimulation of waves of cAMP [66, 13, 93, 109]. Because the periodic nature of cAMP can be observed even in a continuously stirred cell suspensions (i.e., in a spatially-uniform conditions)(Gerisch 1974), we call the phenomenon cAMP oscillation instead of cAMP wave. The several dynamic properties of cAMP oscillation is the key in successfully carrying out their development. The temporally periodic stimulation of cAMP cause the cells to express

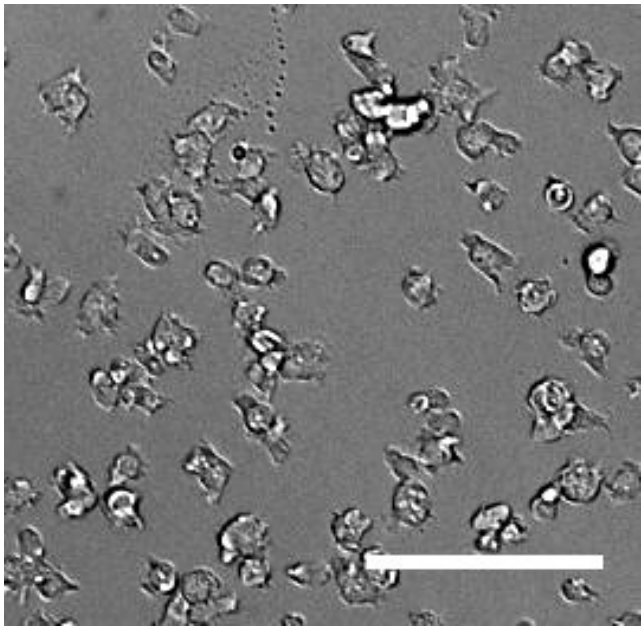

Fig. 1.1 Microscopic image of free-living *Dictyostelium* cells in a unicellular stage. Scale bar: 100 μm.

several genes required at later stages of the development [82]. In addition to that, the spatial pattern of the cAMP wave determines the point to which the cells migrate.

It is interesting to note that the dynamics of extracellular cAMP that stimulates the cells are created by their own. Therefore a natural question here is that what kind of rules governing each cell make it possible for a genetically identical cell population to self-organize such spatio-temporal patterning. To understand the origin of the collective behavior, cellular level properties of the signaling system has been intensely investigated. One fundamental process underlying the oscillation is cAMP signaling response in which binding of extracellular cAMP to receptors on the membrane cause the cells to synthesize cAMP intracellularly and to secrete it to extracellular space [25]. As will be described later in this chapter, we try to characterizes the response in a quantitative way and then relate it to the population-level behavior.

How can it contribute to understand biological phenomena in general to solve the problem specific to *Dictyostelium*? Because of the singularity of their life cycle and resultant tractability in doing experiment, *Dictyostelium* cells offer substantial advantage over other model organisms in addressing several fundamental questions concerning multicellularity. In the following sections, we introduce a few ubiquitous phenomena in biology: cellular information processing, cell-cell signaling and pattern formation in development. In each section, we discuss basic idea in the field and how it is related to *Dictyostelium* development.

1.2 Cellular information processing

The survival of cells depends on appropriate response to diverse external cues and stimuli and therefore cells must have developed mechanisms for responding to changes

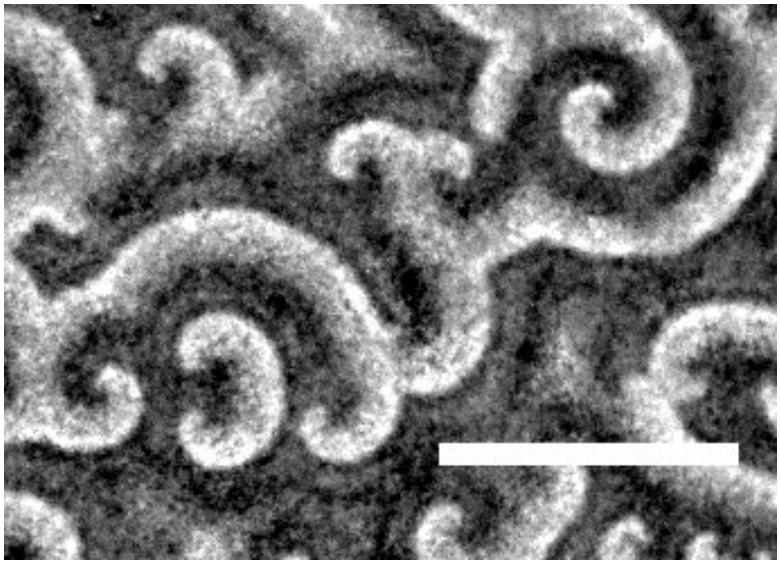

Fig. 1.2 Optical-density waves observed by a dark-field microscopy in the course of *Dictyostelium* development on an agar substrate. The contrast of the image was enhanced by frame subtraction. Scale bar: 5 mm.

in their environment during the course of evolution. One of the typical information that cells utilize is the amount of molecules existing in extracellular space. External molecule is usually detected by cells by receptor proteins at the cell surface (figure 1.3). The binding of the molecules to receptors activates the receptor, which in turn activates one or more intracellular signaling pathways (or signal transduction systems) composed mainly of cascades and networks of intracellular signaling proteins. The activation of the pathways results in the alteration in the states of effector proteins, which finally determine or shape cellular response. In general, the effector proteins and resultant cellular response depend on the identity of the stimulus and the state of the receiving cell. Examples of cellular responses evoked by chemical stimuli are gene regulation, opening and closing of ion channels, modification of components of metabolic pathway, or shaping of the cytoskeleton and so on.

A challenging problem in this field is to understand the molecular mechanism by which information embedded in extracellular space is read out and transformed into a cellular behavior. Such attempts can be difficult because of the 'complexity' of the network structures of signal transduction system. The network is often characterized by redundancy and cross-talk among pathways and full of feedback and feedforward loops in it. To elucidate the mechanism, it is essential to characterize temporal behavior of a system responding to a stimulus. The characterization of temporal behavior, however, is often difficult because the cellular information processing is intrinsically dynamic [91]: even if the same cells (in the same state) are stimulated by the same species of molecule, the cellular response often depends on one or more properties of the stimuli, such as amplitude, rate of increase, duration, or rate of decrease.

Because of these properties, it is often required to measure the cellular behavior in a quantitative way. Moreover, to obtain reliable data, the measurement of cellular

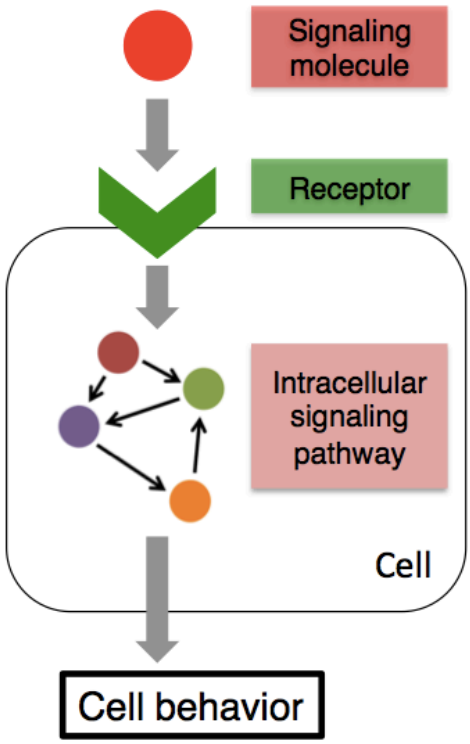

Fig. 1.3 A conceptual diagram of cellular information processing by a intracellular signaling pathway. Extracellular signaling molecule are detected by receptor proteins at the cell surface. The event activates one or more signaling pathways, which causes the activation of effector molecules and resultant cellular behavior.

dynamics should be at the single-cell level [98, 81]. Experiments that average over cell populations can mask events that occur only in a subset of cells, all-or-none effects and cell-cell variability. Furthermore, a cell must be placed in a well-controlled environment because a quantitative difference between two input signals can cause qualitatively different responses. Therefore, as will be explained in chapter 2, we used an experimental system where we can observe how the cells synthesize intracellular cAMP or another signaling molecule at the single-cell level in a well-controlled environment.

In the following subsection, we will introduce two common cellular dynamics in biology: adaptation and directional sensing. Both cellular responses are quite important for cells to behave appropriately in an ever-changing environment. *Dictyostelium* cells show both types of responses and their molecular mechanisms are under intense investigation.

1.2.1 Adaptation

Adaptation refers to a system's ability to respond to a change in input stimulus then return to its prestimulated output level, even when the change in input persists (figure 1.4). Especially when the output level reset exactly to the prestimulus value, the

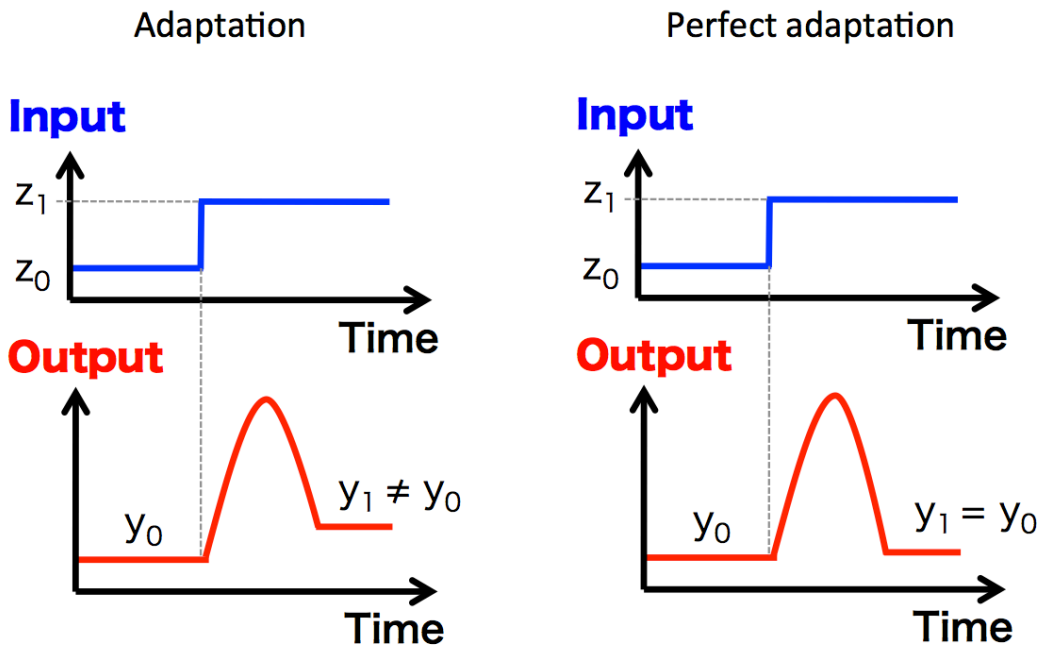

Fig. 1.4 Input-output relations in adaptive responses.

response is called perfect adaptation. Adaptation is widely used in sensory systems, such as vision and hearing, and other signaling systems ranging from the chemotaxis of bacteria [11, 99, 100, 102, 10] to the osmo-response in yeast [76]. Adaptation enables cells to more accurately detect changes in the input stimulus by resetting the sensitivity in accordance with the background stimulus and to maintain homeostasis in the presence of perturbations [72].

Adaptation in cAMP signaling response and its history

cAMP signaling response has been shown to be an adaptive response. Upon binding of extracellular cAMP to the G-protein coupled receptor cAR1, intracellular cAMP is synthesized by adenylyl cyclase ACA, which is activated by PI3 kinase- and PKB-dependent pathways in a transient manner [94, 20, 15, 17]. Before these knowledge of molecular details became available, Steck, Devreotes and his co-workers revealed various dynamic aspects of cAMP signaling response [26, 25, 27, 28, 29, 108]. The key experimental setup in their experiment was a combination of a perfusion system that delivers cAMP stimuli of well-defined magnitude and duration and biochemical assays for cAMP. By using these techniques, they were able to measure intracellular and secreted cAMP under defined concentrations of extracellular cAMP and made quantitative analyses under various conditions to reveal the dynamic property of cAMP signaling response. As shown in figure 1.5, they revealed that the synthesis of cAMP and its secretion peaks at about 2 minutes after application of extracellular cAMP and attenuates within 3-10 minutes. The transient nature, or adaptation, of the response is clearly not due to decrease in extracellular cAMP level by degradation because perfusion was used to "clamp" the level of extracellular cAMP.

In spite of these earlier efforts, a lot remains to be determined regarding the dy-

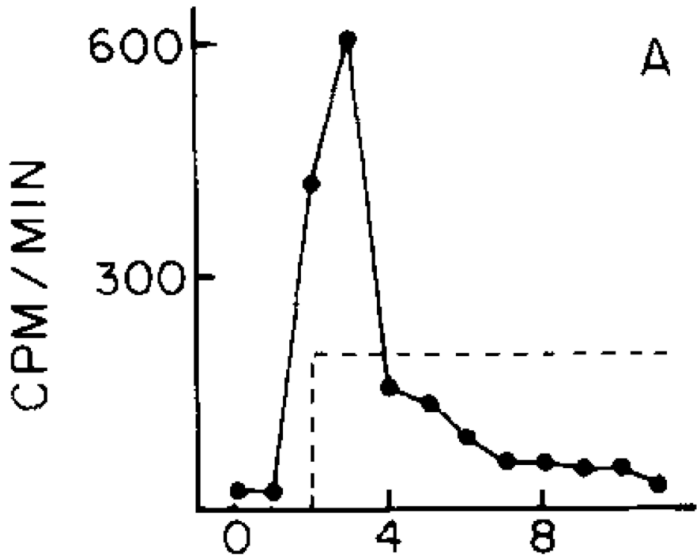

Fig. 1.5 Representative time courses of cAMP signaling response taken from Ref. [108]. The unit of x-axis is minutes. Application of cAMP stimuli is denoted by the dashed rectangle. Rates of radioactively-labeled cAMP secretion were measured by using a population of cells.

namics in cAMP signaling response. One of the main reasons for this is that the measurements were made at the population level in the preceding study. As stated above, such measurements can miss individuality of the cells and more subtle feature by averaging over the population. To circumvent these problems one would ideally like to measure cAMP signaling response of single living cells in isolation. Recently, such experiments have become possible by the development in FRET (förster resonance energy transfer)-based cAMP sensor. By using one of the FRET-based cAMP sensor epac1-camps [84], Gregor et al. have succeeded in observing the dynamics of cAMP signaling response at the single-cell level [47]. When the cells are exposed to a nanomolar level of extracellular cAMP by perfusion, cytosolic cAMP level rises transiently within a few minutes after addition of cAMP. This response attenuates during the next ∼15 minutes showing a trend like a damped oscillation with a periodicity of 3-4 minutes (left panel in figure 1.6). At higher extracellular cAMP level, the damping rate of the oscillation slows down so that the response persists as long as extracellular cAMP is kept elevated. These single-cell analyses have clearly demonstrated the oscillatory property of the response although it has been overlooked in the previous measurements. Importantly the results place strong constraints on potential mechanisms of cAMP signaling response; for a system to be able to show oscillation, it has to contain a negative feedback loop in it [85]. Thus, the result would help us search for the molecular mechanisms for the response.

Response-rescaling properties in cell signaling systems

Recent studies of the input-output relations of cellular signaling systems suggest that a special type of adaptation called fold-change detection (FCD) may be ubiquitous

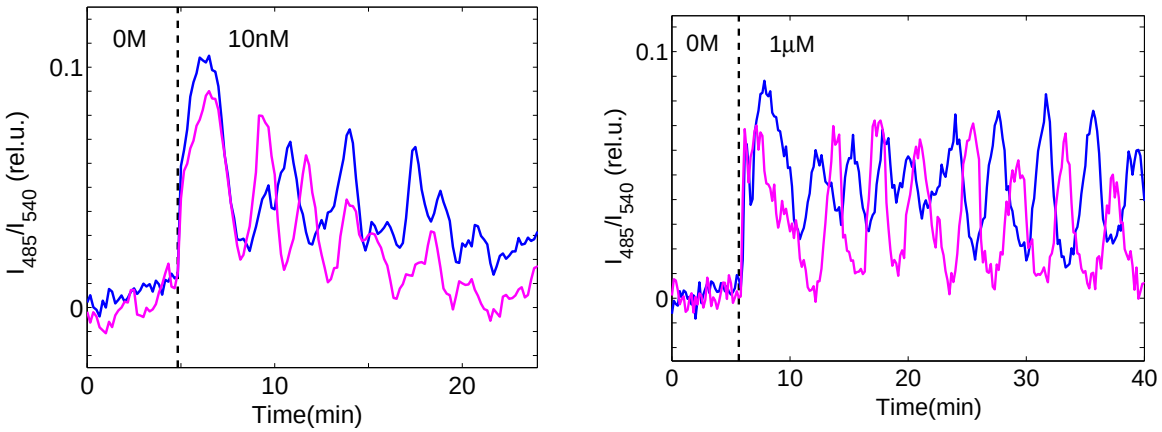

Fig. 1.6 Representative time courses of cAMP signaling response measured at the single-cell level by using FRET-based cAMP sensor. Two cells are represented by different colors. (Left) When perfused with a nanomolar level of extracellular cAMP, the response is gradually damped and adapt to the stimulus. (Right) When perfused with a micromolar level of extracellular cAMP, the response persists.

in biology [19, 42, 97, 68]. FCD refers to a response whose entire shape, including its amplitude and duration, depends only on fold changes in input and not on absolute levels. The feature of FCD is related to Weber's law, an empirical rule originally found in the measurement on psychophysical threshold sensitivity [75, 43, 97]. The law states that the maximal response to a change in signal is inversely proportional to the background signal: $\Delta y = k\Delta z/z_0$, where k is a constant, Δy is the change in the output and Δz is the signal change over the background z_0. FCD is more general than weber's law or perfect adaptation (figure 1.7): Weber's law concerns only the maximal initial response and exact adaptation concerns only the steady state of the response, whereas FCD concerns the entire shape of the response.

The first and only demonstration of FCD was provided in the bacterial chemotactic response of *Escherichia coli* by in vivo FRET measurements on immobilized cell population [68]. In the study, the dynamics of the activity of a kinase, CheA, was analyzed in time-varying stimulus of an attractant α-methylaspartate with various background stimulus level. As a result, it was shown that the response is dictated not by the absolute differences from the background but rather the fold change over the background (figure 1.8). From a theoretical point of view, Shoval and co-workers showed that the FCD property is necessary and sufficient for an organism to be able to move through a spatial sensory field in a way that is independent of multiplications by scalars of the input field [97] For example, bacteria perform a spatial walk through a chemo-attractant field, where the cells climb up the gradient of the field by computing the rate of random direction changes based on the local concentrations of chemo-attractant [10]. Here let us write the spatial position of a bacteria as $\mathbf{R}(t)$. In the chemo-attractant field $u(\mathbf{r}, t)$, the cell senses a series of time changes in input signal as $u(\mathbf{R}(t), t)$. The spatial distribution of chemoattractant $u(\mathbf{r}, t)$ is often governed by

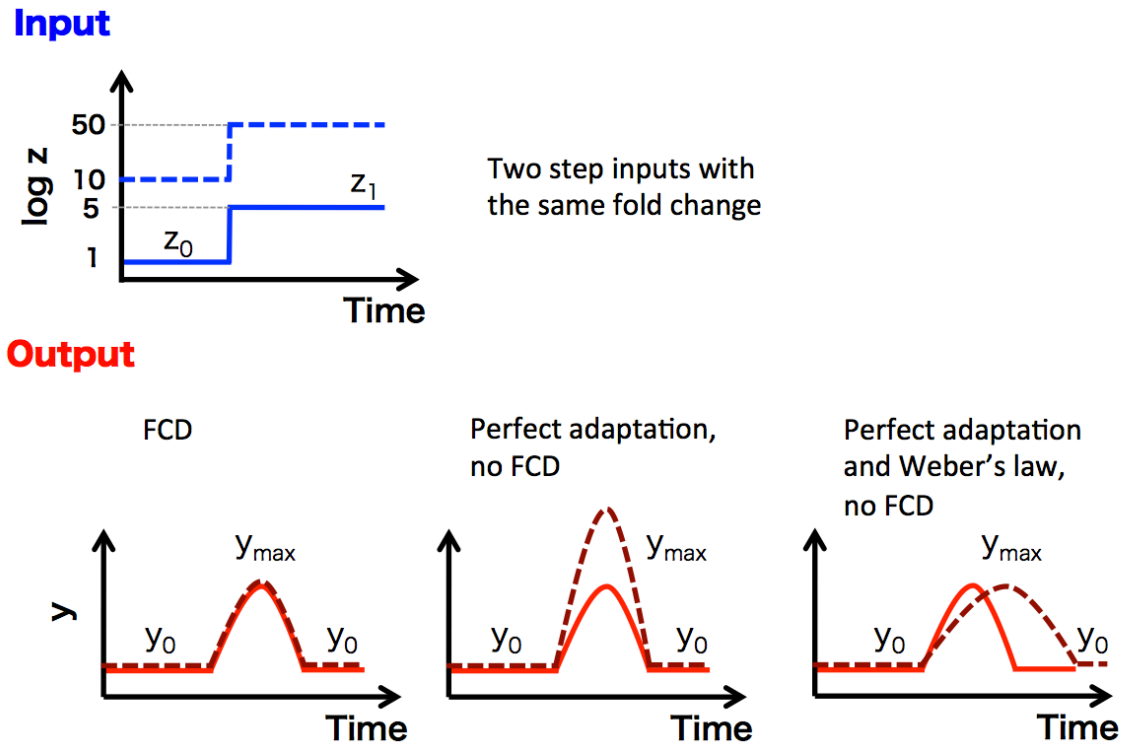

Fig. 1.7 Definitions of fold-change detection, Weber's law and perfect adaptation (modified from [97]). Responses to two step changes with identical fold change and different absolute change are shown. Outputs of the system capable of FCD are identical for the two inputs whereas outputs of the system with exact adaptation, Weber's law and no FCD are not except their amplitudes.

the equations for diffusion or passive scalar convection. Because of the linearity of the equations in terms of the source strength, the sensory field has a scalar symmetry, i.e., the field have the same pattern up to a multiplicative constant (a.k.a. amplitude symmetry) irrespective of the source strength. Therefore a cell capable of fold-change detection of the signal $u(\mathbf{R}(t), t)$ would be dictated not by the absolute level of the signal, which is dependent on the source strength, but by the relative change of the signal. Thus the spatial distribution of the cells would be independent of the source strength [75]. In fact, Lazova and co-workers have demonstrated that the spatial distribution of an ensemble of free-swimming *E.coli* cells changes identically in different absolute levels of an attractant [68].

On the other hand, FCD has been described on the basis of indirect evidence in eukaryotic cell sensory systems. For example in the case of the dynamic response of ERK2, a well-characterized MAPK signaling protein, it was demonstrated that the peak level of the protein concentration is proportional to basal level of it in each cell [19] (figure 1.9). That is, fold change in the activity of the signaling molecule is almost constant even though its absolute level is highly variable between cells. The result strongly suggests that downstream system responds to fold change of the concentration of ERK2 instead of absolute levels. However it remains to be seen whether there really exists such mechanism in the signaling system.

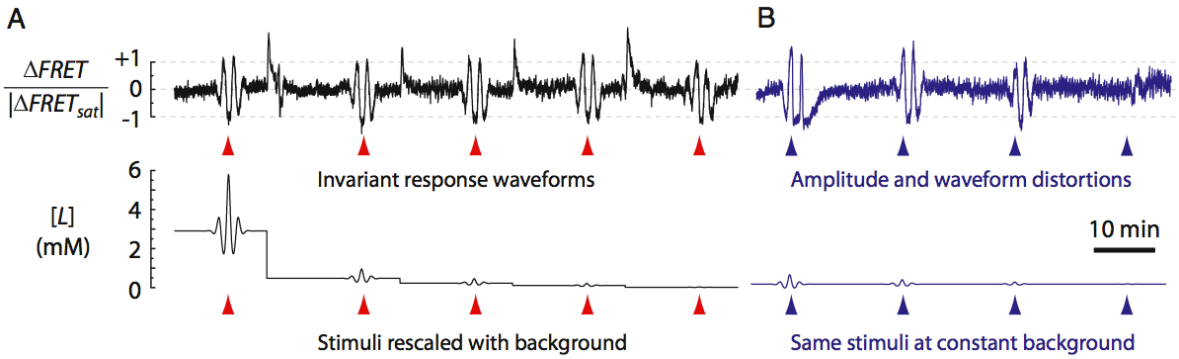

Fig. 1.8 Representative time courses demonstrating that *E.coli* chemotaxis displays FCD taken from Ref. [68]. The cellular response ($\Delta FRET/|\Delta FRET_{sat}|$) remain essentially invariant to identical waveforms and amplitude of input signals ([L]) scaled by the same factor as the background concentration of chemoattractant.

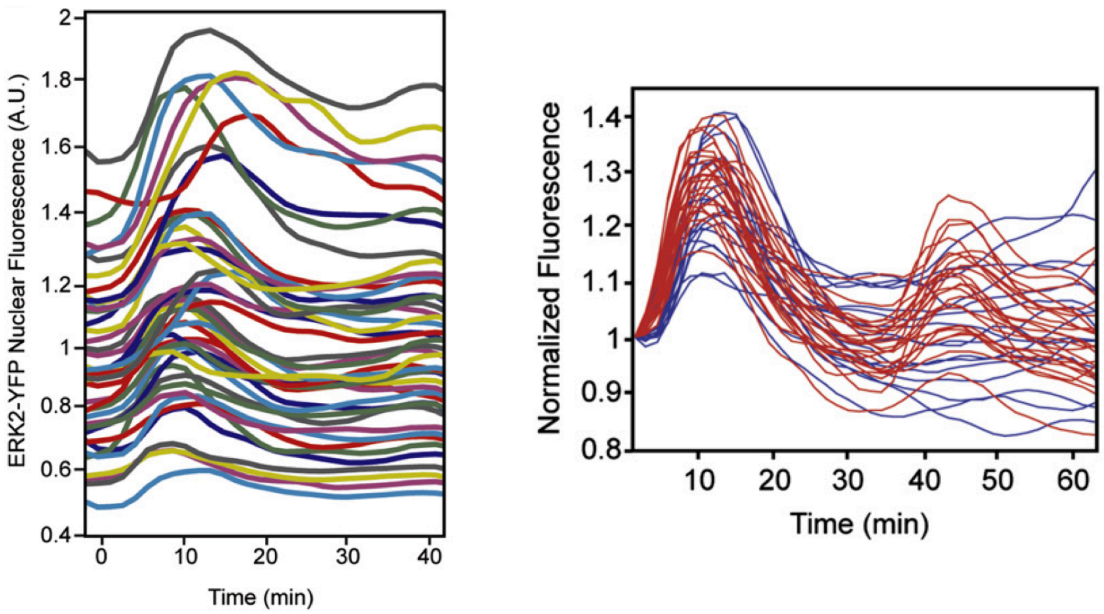

Fig. 1.9 (Left) Representative time courses of ERK2 response taken from Ref. [19]. Different cells are represented by different colors. (Right) ERK2 responses normalized to the initial time point.

A response-rescaling property in cAMP signaling response

Although several features of cAMP signaling response have been clarified by a single-cell analysis using FRET-based cAMP sensor [47], such a response-rescaling property in *Dicyostelium* cell is not yet determined. Investigating the property by using *Dicyostelium* cells can be highly advantageous as it is now possible to observe the

response at the single-cell level[*1]. Moreover, characterizing the property would also be important to understanding cAMP oscillation because the cells experience time-varying input stimuli with nonzero background level during the oscillation [40, 109]. In this study, we conduct single-cell analysis of response-rescaling property in cAMP signaling response by using the cAMP sensor as described in chapter 3.

1.2.2 Directional sensing

Another example of well-characterized cellular dynamics is directional sensing. Directional sensing is one of the key process in chemotaxis by which cells sense and respond to chemoattractant gradients. Interestingly, the process of directional sensing is known to be separable from other processes required for chemotaxis (i.e., polarity and motility) in the signal transduction system [104]; even in a immobilized cell with no polarity, signaling molecules accumulate at the leading edge (the high side of the gradient) of the cell and the location of the leading edge dynamically tracks changes in gradient direction. Because chemotaxis underlies a wide range of biological phenomena such as embryogenesis, the molecular mechanism of directional sensing has been a central theme in cell biology.

Behaviors of the directional sensing module in *Dictyostelium*

In the case of *Dictyostelium* cells, a gradient stimulus of cAMP elicits an accumulation of signaling molecule at the front of the cell [89, 104, 1] (figure 1.10). The initial event of the process is to detect cAMP molecule by a subset of $\sim 80,000$ cAMP receptors cAR1 at the cell surface [112]. The difference in the receptor occupancy by cAMP molecules between the front and the back of the cell leads to a greatly amplified response. That is, the distribution of a signaling molecule, phosphatidylinositol 3,4,5-trisphosphate (PIP_3), on the membrane are sharply localized to the leading edge even when the gradient of the chemoattractant concentration across the cell is very shallow. As shown in figure 1.10, gradient sensing and its resultant localization of the signaling molecule persists as long as the gradient is maintained. Curiously the accumulation of the same signaling molecule appears only transiently when the stimulus is presented in a spatially-uniform manner.

A local-excitation and global-inhibition scheme

Phenomenological models to explain these behaviors of the directional sensing module has been proposed based on a local-excitation, global-inhibition (LEGI) scheme [88, 69] (figure 1.11). In this scheme, the activation of receptors by a external stimulus triggers counteracting processes: a fast excitation of the output signal (PIP_3) and a slow inhibition of the signal. By these processes, a spatially uniform stimulus elicit transient response because of the difference in the time scales of the two processes (figure 1.11 A). The model also explains the spatial distribution of the signaling molecule upon a gradient stimulus by assuming excitation occurs locally near the membrane

[*1] Although there are many biological systems that exhibit adaptation, single-cell analysis of adaptation is often challenging. For example, even in the case of bacterial chemotaxis, a well-characterized adaptive system, the response is often observed at the population level [101, 68].

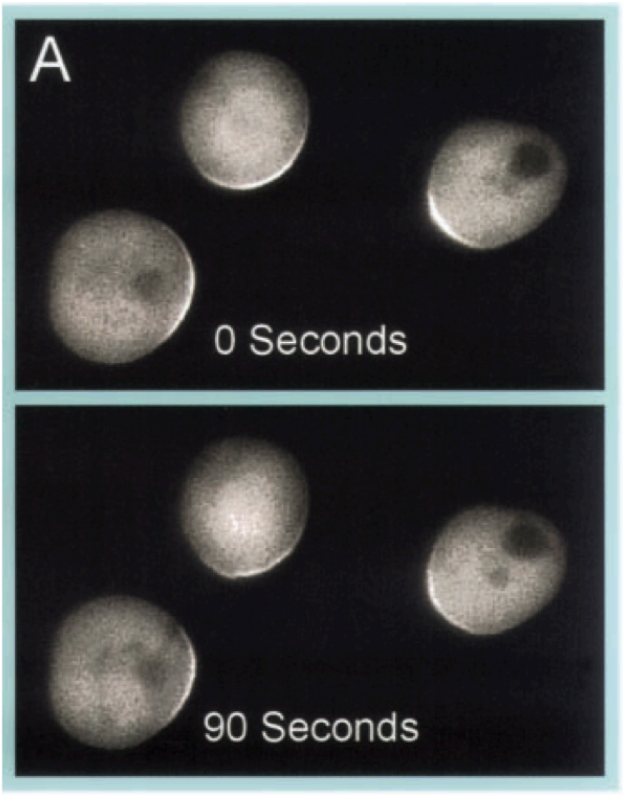

Fig. 1.10 Immobilized *Dictyostelium* cells that shows directional sensing taken from Ref. [88]. The location of the signaling molecule PIP_3 is visualized by CRAC-GRP. The tip of a cAMP filled micropipette is placed in the vicinity of the cells. The response of gradient sensing persists as long as the gradient is maintained.

(local excitation) while inhibition occurs throughout the cells (global inhibition) (figure 1.11 B). At the front of the cell, excitation exceeds inhibition as the excitation continues to reflect the local input level. On the other hand, at the rear of the cell, inhibition exceeds excitation at steady state because of the global effect of inhibition.

A response-rescaling property in PIP_3 response

As mentioned above, PIP_3 is synthesized at the membrane as an output signal in the gradient sensing module. As well as sensing cAMP gradient, the synthesis of PIP_3 regulates a number of critical cellular processes such as cAMP signaling response [74]. Therefore characterizing the dynamics of PIP_3 response would help us understand the molecular mechanism of cAMP signaling response. However, as was the case for cAMP signaling response, a response-rescaling property of the response has not been investigated. In chapter 6, we characterize the property at the PIP_3 level and show how it efficiently constrains possible mechanisms of the directional sensing module.

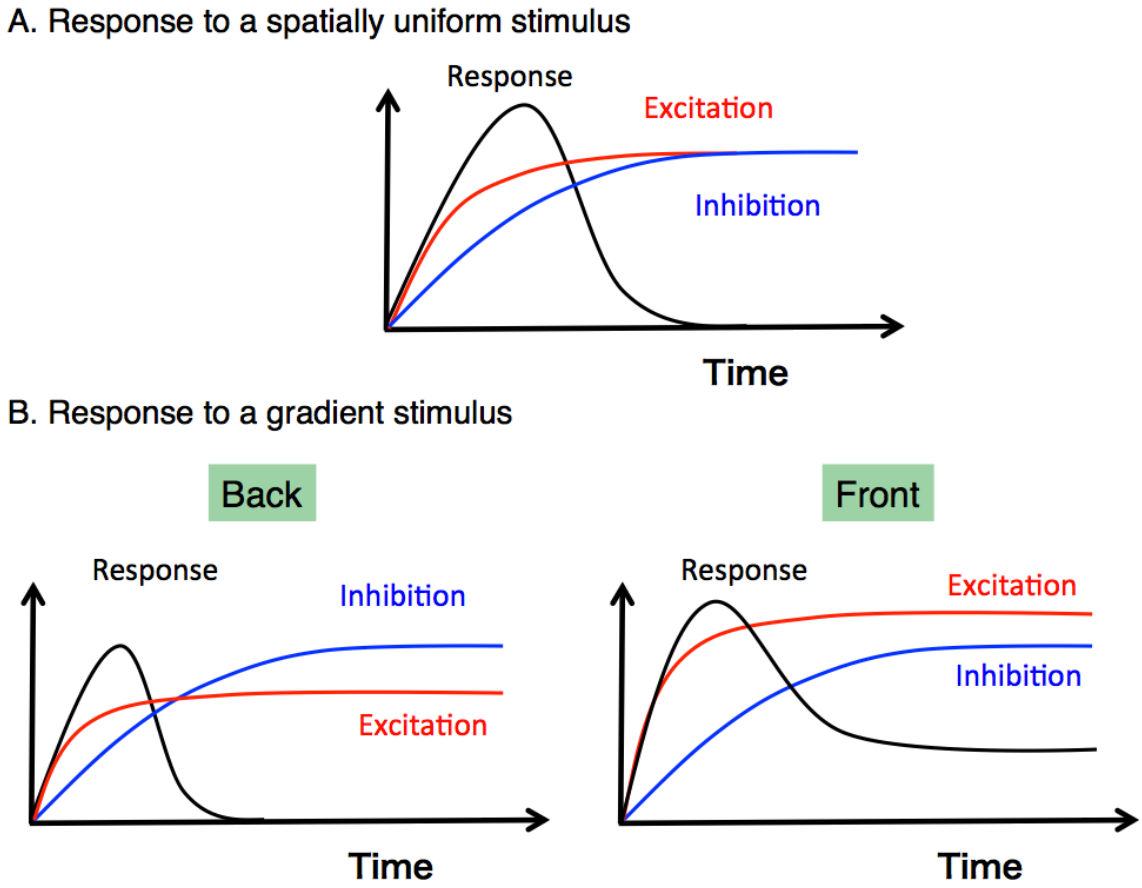

Fig. 1.11 A conceptual diagram of local-excitation, global inhibition model modified from Ref. [88]. (A) The transient response observed in cells when stimulated uniformly is the combined effect of first the fast excitation followed by its quenching by the slower inhibition. Because the stimulus is spatially uniform, the distinction between local and global disappears. (B) In a gradient of receptor occupancy, the excitatory signal at the front is stronger than that of the back. The inhibitory signal equilibrates in space at steady state because of diffusion.

1.3 Cell-cell signaling

Understanding collective behavior of cells in multicellular system is one of the most challenging problem in biology. Multicellularity requires the constituent cells to communicate with each other. The communication is often mediated by transmissions of extracellular signaling molecules across the space between one cell and another. Of course, cell-cell communication include information processing by cells: detection of the signaling molecules secreted by other cells and transformation of the signal into an appropriately response. Therefore, it would be important to investigate the molecular mechanism responsible for the process of information.

However, to understand collective behaviors of cells, just describing single-cell level

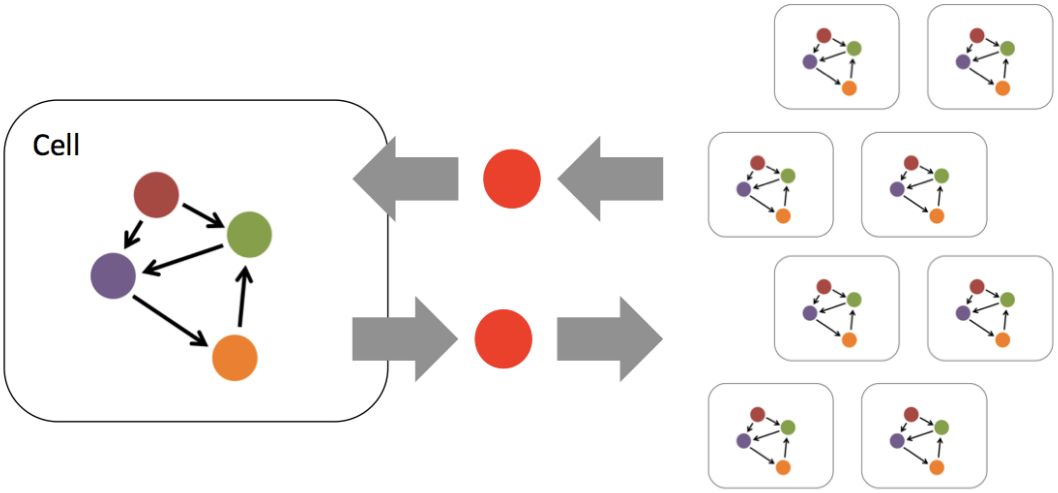

Fig. 1.12 Intercellular signaling includes interaction between two different hierarchical level. That is, a behavior or response of a cell are fed back through strong interactions between cells.

property and its molecular mechanism would not be sufficient. One of the essential features in multicellular system is that each constituent cell is exposed to feedbacks from a higher level of the system [64] (figure 1.12). In other words, the cells not just respond to their environment, which consists of extracellular medium plus all other interacting cells, but also the response does change the environment. To understand such system in a proper way, it is also essential to elucidate the rule describing how the cells interact with each other. In that sense *Dictyostelium* is an ideal model system for the study of cell-cell signaling.

Advantages in making use of *Dictyostelium* cells as a model system for cell-cell signaling

Dictyostelium cells spend as single-celled organism when they grow and divide in a nutrient-rich condition while they can switch to multicellular phase upon starvation. Thanks to this property, the cells can be separated from other cells in a non-invasive manner, which would be difficult in other multicellular system in general. Moreover, the mode of cell-cell signaling in *Dictyostelium* cells are quite simple. The main signaling molecule utilized by the cells is cAMP at least in the early stage of the development although cells in other multicellular system would exchange many species of molecules. Thus, in *Dictyostelium*, it is relatively easy to discriminate single-cell level property from population-level property and to describe how the cells are interacting with each other in comparison to other systems.

Simplification of the mode of cell-cell signaling by a perfusion system

Even though the mode of cell-cell signaling during *Dictyostelium* development is relatively simple, it remains a challenge to accurately describe the way the cells interact with each other. The reason for the difficulty is two-fold: first, concentrations of signaling molecules and the resultant cellular state are spatially heterogenous in the

development, and second, extracellular cAMP is degraded by an enzyme phosphodiesterase (PDE)[*2].

To circumvent the difficulty, Gregor and co-workers have investigated cell-cell signaling of *Dictyostelium* cells by using a perfusion chamber [47]. The system greatly simplifies the kinetics of extracellular cAMP as this:

$$\frac{d[cAMP]_{ext}(t)}{dt} = \rho k_t [cAMP]_{int}(t) - \gamma [cAMP]_{ext}(t), \tag{1.1}$$

where $[cAMP]_{ext}(t)$ and $[cAMP]_{int}(t)$ represent the concentration of extracellular cAMP and intracellular cAMP at time t respectively. The effect of rapid mixture of extracellular buffer by perfusion enables a mean-field approximation and therefore to omit space dimension in the formulation. In addition to that, because the constant flow by perfusion rapidly washes out both extracellular PDE and cAMP, we don't have to consider an enzymatic reaction between the two. Instead, extracellular cAMP in the perfusion chamber is constantly diluted by a factor of γ, which is determined by the flow rate of perfusion. The secretion of cAMP by the cells are supposed to be proportionate to intracellular cAMP [27] and to cell density ρ. Importantly, the system has enabled to control the parameters ρ and γ independently of each other by changing cell density in the chamber and the flow rate of perfusion. We will describe the experimental results obtained by using the perfusion system in the next section. To conclude, although interactions between cells are highly complicated in multicellular organisms in general, cell-cell signaling in *Dictyostelium* cells can now be described in a extremely simple way by using the perfusion chamber.

1.4 Pattern formation in development and its robustness

Spatiotemporal patterning in multicellular development shows high stability to environmental, genetic, or stochastic fluctuations [7, 9]. The stability, or robustness, of the pattern formation of signaling molecules is a prerequisite for the success of multicellular development as such molecules often direct cellular movement and/or state during the course of the development [37]. Here, we describe an example of such robust patterning in multicellular development. Then we show that similar property can also be found in *Dictyostelium* development.

[*2] When the cells are placed on a substrate, the general equation for the kinetics of extracellular cAMP can be written as

$$\begin{aligned}\frac{\partial [cAMP]_{ext}(\mathbf{r},t)}{\partial t} =& \rho(\mathbf{r},t) k_t [cAMP]_{int}(\mathbf{r},t) \\ & - f_\rho([cAMP]_{ext}(\mathbf{r},t), [PDE]_{ext}(\mathbf{r},t)) \\ & + D\nabla^2 [cAMP]_{ext}(\mathbf{r},t).\end{aligned}$$

Here, $[cAMP]_{ext}(\mathbf{r},t)$ and $[cAMP]_{int}(\mathbf{r},t)$ represent the local concentration of extracellular cAMP and intracellular cAMP at time t respectively. The second term f_ρ represents the degradation of extracellular cAMP by extracellular PDE secreted by the cells, which may also be dependent on cell density ρ. The third term represents diffusion of extracellular cAMP.

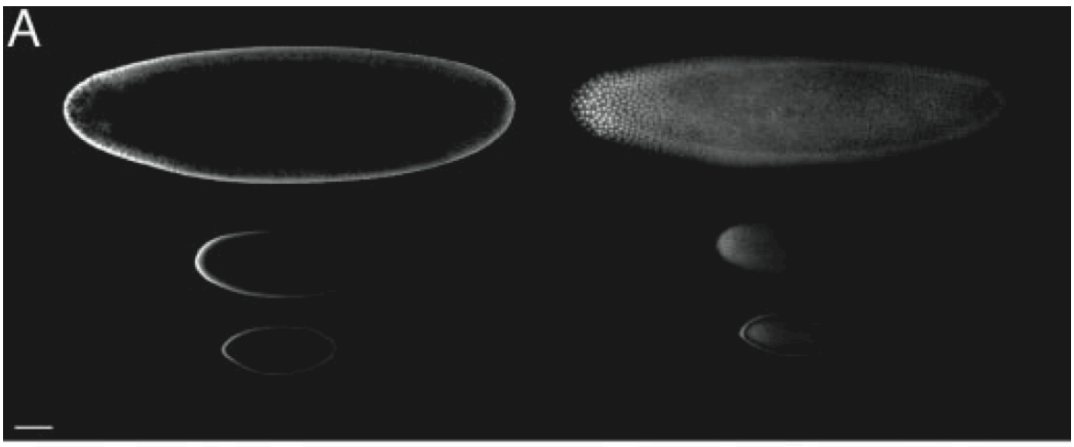

Fig. 1.13 Confocal images of Bcd gradient (immunofluorescence staining) for *Lucilia sericata* (top), *Drosophila melanogaster* (middle) and *Drosophila busckii* (bottom) taken from Ref. [46]. The focal plane is at mid-embryo and top-embryo in the left and right columns, respectively. Scale bar: 100 μm.

Scaling of a morphogen gradient in a developing embryo

Examples of the robustness of functional patterns in multicellular system can be found in morphogen gradients in developing embryos [9, 116]. Morphogen gradient is a widely used paradigm by which a developing tissue provides its cells with positional information. The molecule, i.e., the morphogen, is secreted by a localized group of cells to a larger field where a concentration gradient of the molecule is established. Cells in the field respond to the morphogen in a concentration dependent manner. Interestingly, it has been shown that the morphogen gradient often scales with the size of the field and therefore the proportion within and between tissues is precisely kept. In other words, the morphogen gradients in the developing embryo are robust to size variations. For example, the gradient of Bicoid (figure 1.13), a transcription factor patterning early dipteran embryo [33, 32], was shown to be scaled with the size of the embryo [46, 48, 49] (figure 1.14). The concentration of Bicoid was quantified in embryos from different dipteran species varying by fivefold in size. In all species examined, the Bicoid gradient was shown to be scaled with the size of embryo. The mechanism of the scaling is still under intense discussion [9].

Robustness to variations in cell density in *Dictyostelium* development

The self-organized spatio-temporal pattern of cAMP in *Dictyostelium* development plays a key role in orchestrating cellular behaviors. With regard to temporal pattern of cAMP, periodic increase and decrease of it induces several genes that are required for the cells to differentiate [82]. As to the spatial pattern of cAMP, the core of the spiral-shaped cAMP wave works as an aggregation center to which tens of thousands of cells collect to form a multicellular system. Of particular note is that these pattern formations have to be achieved in natural environments, where various environmental parameters would not be controllable for the cells. This entails that the pattern has

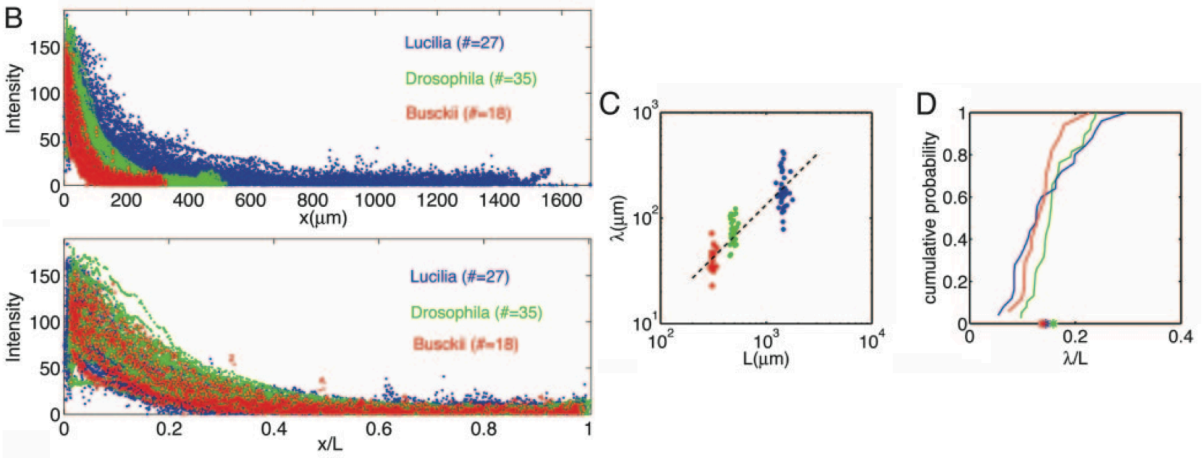

Fig. 1.14 Scaling of Bcd profiles with egg length taken from Ref. [46] (B) Intensity profiles of Bcd fluorescence. The x-axis in upper is absolute the x-axis in lower is relative to egg length. (C) Length constants λ defined as $c(x) \propto \exp(-x/\lambda)$ as a function of egg length for *L.sericata* (blue), *D.melanogaster* (red) and *D.busckii* (green). (D) Cumulative probability distributions of menthe constants λ for *L.sericata* (blue), *D.melanogaster* (red) and *D.busckii* (green). Asterisks indicate the means of the three distributions.

to be robust to variation in environmental parameters.

One of the key parameters that determines the success of the development is initial cell density. It has been investigated whether and how the development is dependent on the parameter. Naturally, there should be a lower limit of initial cell density for the cells to be able to transmit signals to neighboring cells. This critical cell density has been reported to be 5×10^4 cm^{-2}, which corresponds to a few-hundredth monolayer (ML) [50, 41]. This can be explained by supposing that the cells can only detect the signaling molecules in a finite range of concentration [62] and therefore cAMP molecules secreted by a cell has a finite range beyond which the molecule cannot be detected by the neighboring cells [18].

On the other hand, a striking feature in *Dictyostelium* development is that the cells are able to accomplish the development over a huge range of initial cell densities (well more than two orders of magnitudes in initial cell density) [50, 41, 86]. To understand the phenomenon, cell-cell signaling at the pre-aggregation stage would be the key because once the cells have aggregated cell density would increase to a high value. In fact, it has been shown that mutant cells that cannot synthesize cAMP (adenylyl cyclase-null cells) but have activated form of PKA (catalytic subunit of PKA), the major down stream effector of intracellular cAMP, lead to near-normal development only at high cell density [113, 92]. This means that the success in the development at low cell density in wild-type cells can be attributed to cAMP-mediated cell-cell signaling[*3]. However, the reason for the robustness remains unanswered.

[*3] Also, the result strongly suggests that all intracellular cAMP signaling is effected through PKA and that signals other than extracellular cAMP coordinate morphogenesis in the later stage of *Dictyostelium* development.

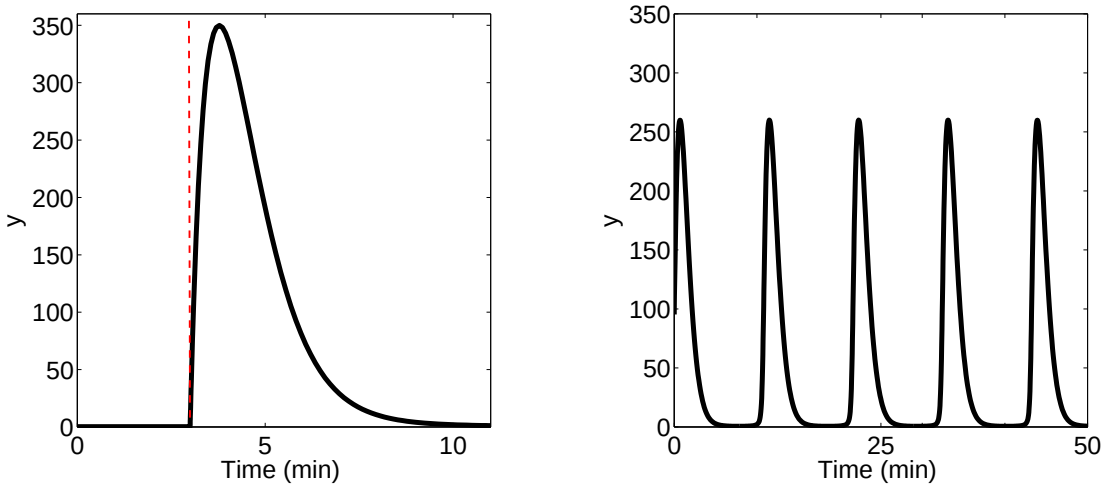

Fig. 1.15 Representative time courses obtained by numerical calculations of the equations 1.2. (Left) Here the variable representing extracellular cAMP, z, is used as a control parameter to mimic the step-like input stimulus. At the time indicated by the dotted red line, the system is subjected to an increase in extracellular cAMP, z, from 0 to 10. (Right) When all the three variables, x, y and z are governed by the equations 1.2, the system exhibits a oscillation. The parameter values used here are the same as in [73]: $k_1 = 0.036$, $k_2 = 0.666$, $L_1 = 10$, $L_2 = 0.005$, $c = 10$, $\alpha = 3$, $\lambda = 0.01$, $\theta = 0.01$, $\epsilon = 1$, $q = 4000$, $\sigma = 0.6$, $k_i = 1.7$, $k_t = 0.9$, $\rho = 0.2$ and $\gamma = 5.4$.

Emergence of cAMP oscillation

Before we discuss the origin of the robustness to variations in initial cell density in cAMP oscillation, we explain the reason why the cells exhibit the oscillation at the early stage of the development. The dynamic properties of cAMP signaling response and cAMP oscillation have been described by a mathematical model originally proposed by Martiel and Goldbeter in 1987 (M&G model) [73]. The model is composed of two-variable ODE equations describing cellular state and one ODE kinetic equation for the extracellular environment. It assumes spatial uniformity, where the cells are supposed to be placed in a well-stirred suspension or in a perfusion chamber. The model has succeeded in reproducing two key features in the dynamics of cAMP signaling: adaptation in cAMP signaling response and cAMP oscillation at the population level in a semi-quantitative way (figure 1.15) [*4].

The equations of the model are

[*4] With a slight modifications of the model, it has been shown that the model can explain several other features observed in *Dictyostelium* development [44]. Among others, the model has reproduced the spatial patterns of cAMP, such as target pattern and spiral pattern, during *Dictyostelium* development by diffusively-coupling the model [110, 111, 67]. Even nowadays the model is still under intense investigation (for example Ref. [38]) to understand the origin of the spatio-temporal patterns in the development.

$$\begin{aligned}\dot{x} &= -f_1(z)x + f_2(z)(1-x)\\ \dot{y} &= q\sigma\phi(x,z) - (k_i + k_t)y\\ \dot{z} &= \rho k_t y - \gamma z,\end{aligned} \tag{1.2}$$

where:

$$\begin{aligned}f_1(z) &= \frac{k_1 + k_2 z}{1+z},\\ f_2(z) &= \frac{k_1 L_1 + k_2 L_2 c z}{1+cz},\\ \phi(x,z) &= \frac{\alpha(\lambda\theta + \epsilon Y^2)}{1 + \alpha\theta + \epsilon Y^2(1+\alpha)},\\ Y &= \frac{xz}{1+z}.\end{aligned}$$

The variables in the model x, y and z represent a regulatory variable within the cell (which was supposed to be the activity of cAMP receptor[*5]), the concentration of intracellular cAMP and the concentration of extracellular cAMP respectively. Most of the parameters in the model are physiologically relevant and its values are collected from experimental studies.

Although the model is composed of a set of rather complicated non-linear ordinary equations, a topological representation may help understand the reason why the model are able to show adaptation and oscillation. In figure 1.16, normal arrows indicate activation effects and blunt edge denotes inhibiting effect. The AND in the diagram represents the way $\phi(x,z)$ works in the model; the function $\phi(x,z)$ take high values only when both x and z are large as is shown in figure 1.17.

First we consider a situation where z is viewed as a control parameter and the system is governed only by the two equations for x and y. Such a situation is achievable in the perfusion chamber if the cell density is sufficiently low and the flow rate is sufficiently high (cf. equation 1.1). In this case a step-like increase in z makes a transient increase in y because the activation of y by z is faster than the inhibiting process of x by z. That is to say the output variable y exhibits adaptation as is shown in the left panel in figure 1.15. The mechanism of adaptation is essentially based on a network topology called incoherent feedforward loop, one of the recurring interaction patterns in biological systems [3]. In the network topology, an input variable activates both an output variable and a repressive process of the output variable.

Then we consider another situation where z is also governed by the equations 1.2. This means that the system's output y are fed back to itself through activation of z

[*5] The assumption itself is now being considered to be wrong from a detailed study of the states of the receptor [59]. In the study, it was shown that the adaptation in cAMP signaling response is achieved downstream of the receptor. However, one can think of the regulatory variable x as an another unknown internal entity that is responsible for adaptation in cAMP signaling response. In that case the model remain valid, in that the model's predictions in terms of the behavior of other 'observable' variables, y and z, essentially agree with experimental results.

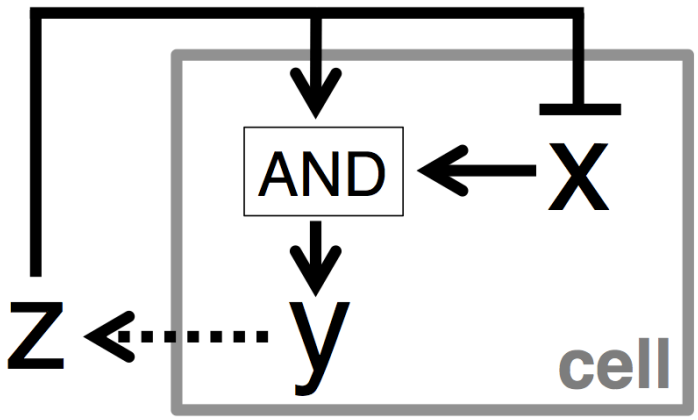

Fig. 1.16 Topological representation of M&G model. The variables x, y and z represent a regulatory variable, the concentration of intracellular cAMP and the concentration of extracellular cAMP. Normal arrows indicate activation effects and blunt edges denote inhibiting effect. The functions of $\phi(x, z)$ is represented by "AND" as is explained in figure 1.17.

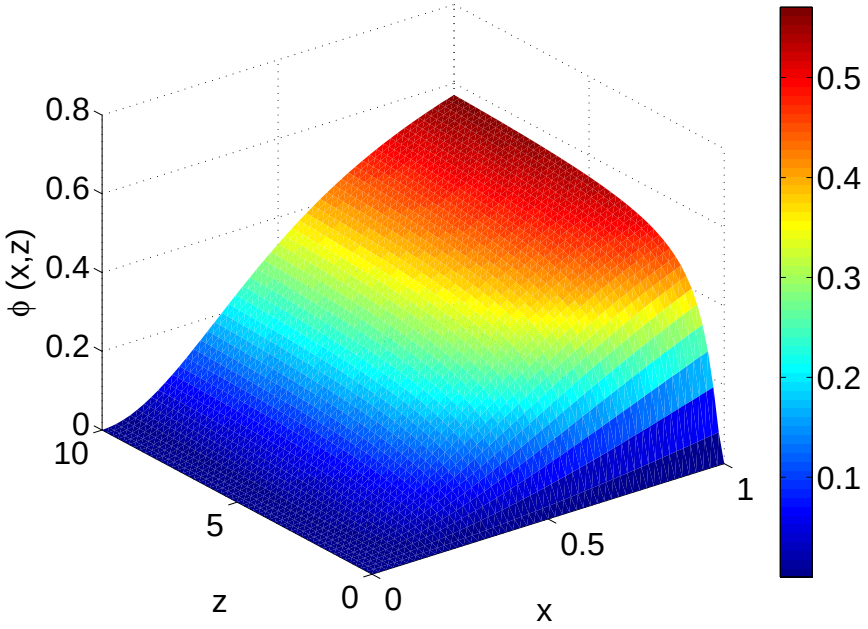

Fig. 1.17 A graph of $\phi(x, z)$ in the model equations 1.2. The function $\phi(x, z)$ can be think of an "AND circuit" because it takes high values only when both x and z are large.

by y (This corresponds to cell's secretion of cAMP, which is represented by a dotted arrow in figure 1.16). Note that the strength of the feedback is dependent on cell density ρ. In a high-cell-density condition, this feedback makes the system unstable and therefore the concentrations of cAMP (i.e., y and z) tend to increase. On the other hand, because of the adaptive property of the cell resulting from an inhibitory process from z to x, the elevated cAMP level tends to decrease, leading to oscillation. In terms of network topology, the system has both a positive feedback loop ($z \to y \to z$) and a negative feedback loop ($z \to x \to y \to z$), which is one of the conditions for a system to be able to oscillate [85].

It has been shown that adaptation can be achieved either by an incoherent feedforward loop or by a negative feedback loop [72]. This suggests that either of the network topology is exploited by the cells to exhibit adaptation. Although an incoherent feedforward loop was adopted in M&G model, the above discussion can also apply to the case in which a negative feedback loop is exploited. In both cases, it can be shown that the system include one positive feedback loop (consisting of synthesis and secretion of a signaling molecule, z) and one negative feedback loop in it and therefore the system can show oscillation. To conclude the reason why a population of *Dictyostelium* cells shows oscillation is that (i) the cells show adaptation and (ii) there is the positive feedback loop resulting from secretion of cAMP.

Robustness of cAMP oscillation in the perfusion system

The above argument explains the *emergence* of the oscillation. However, the *robustness* of the oscillation to variations in cell density remains to be answered. Roughly speaking, one can think of two possible ways to achieve the robustness. One possibility is that the cells finely control the extracellular environment. This might be possible, for example, by controlling the amount of extracellular phosphodiesterase (PDE) concentration [6, 86]. Another possibility is that a response property of cAMP signaling response mainly contributes to the robustness while the control of extracellular cAMP is crude. This may be related to the adaptive property of cAMP signaling response.

Recently Gregor et al. observed populations of cells by using a perfusion system and showed that the cells exhibit cAMP oscillation even in the perfusion chamber. According to equation 1.1, the key parameters in determining the cellular environment and resultant population-level behavior are cell density ρ and dilution rate γ. In the study, the population of cells are shown to exhibit two qualitatively different states depending on the two parameter values (figure 1.18); (a) In regions where cell density is high and flow rate is low and therefore cell-cell interaction is strong, the population of cells exhibited cAMP oscillation (red regions of the phase diagram in figure 1.18) with a constant, approximately six-minutes, periodicity (figure 1.19 left panel). The periodicity is nearly identical to that in a natural condition. (b) In regions where cell-density is low and flow rate is high and therefore cell-cell interaction is weak, the cells exhibited sporadic firing or remained quiet (lower right of the phase diagram in figure 1.18 and figure 1.19 right panel). In the intermediate regions between (a) and (b), sharp transitions from quiet state to oscillatory state were observed.

The existence of the two qualitatively different states *per se* would be explained relatively easily by assuming a finite dynamic range of cAMP receptor. If cell density

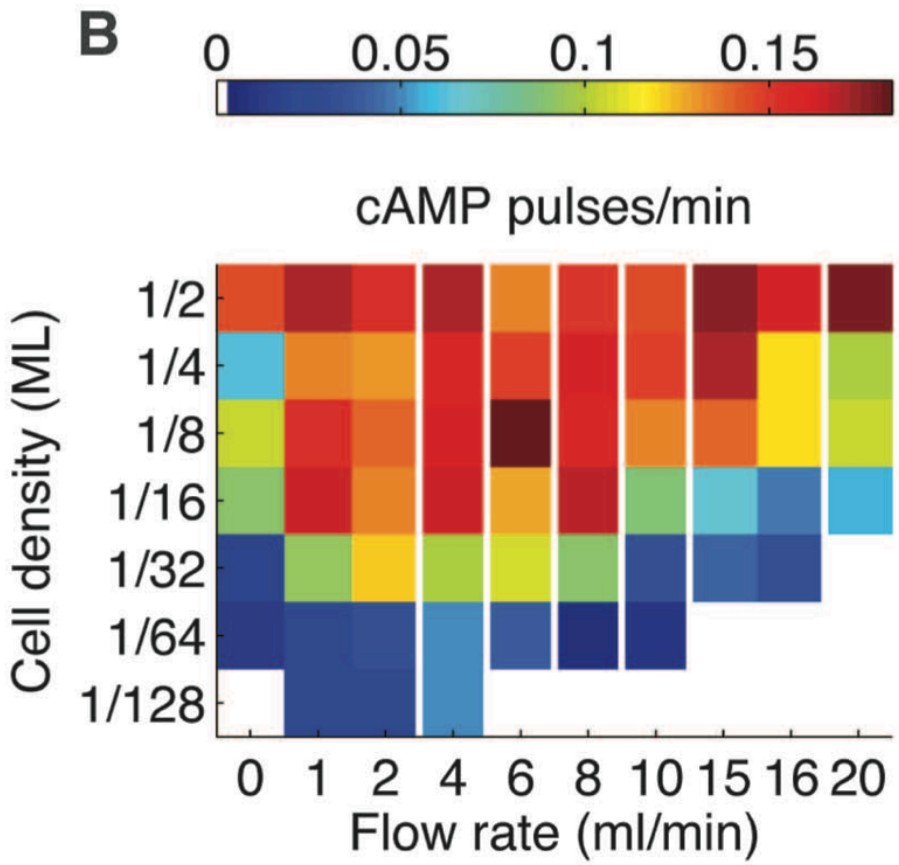

Fig. 1.18 A phase diagram that show fairing rate as a function of cell density and flow rate taken from Ref. [47]. The mean firing rate (min^{-1}) is represented in color. Red regions represents high frequency of the firing rate (period of 6 min) whereas blue (or white) regions represents sporadic firing.

is high and flow rate is low, the concentration of extracellular cAMP would be high enough and the molecule will be detected by the cells and vice versa. Instead, what is important here is that the oscillation is observed more than one order of magnitude in cell density. In other words, cAMP oscillation is robust to variations in cell density even in the perfusion chamber. Note that it is not possible to address maximum cell density where cell population can show oscillation in the experimental system[*6]. Therefore, the range over which the oscillation is observed is underestimated.

As discussed above, we can think of two possible ways to achieve the robustness of cAMP oscillation; a fine control of extracellular environment or a adaptive property in cAMP signaling response. However, it is impossible for the cells to precisely control the amount of PDE and other extracellular proteins because such molecule will be

[*6] In a natural habitat of *Dictyostelium* cells, it is conceivable that the cells are distributed in a three dimensional space in the soil. In such a condition, it would be possible that cell density gets higher than 1 ML, which is defined in two dimensional space. In the perfusion chamber, we can only address cell densities less than 1 ML because the cells are more frequently swept away by shear forces coming from perfusion when the cell density gets higher.

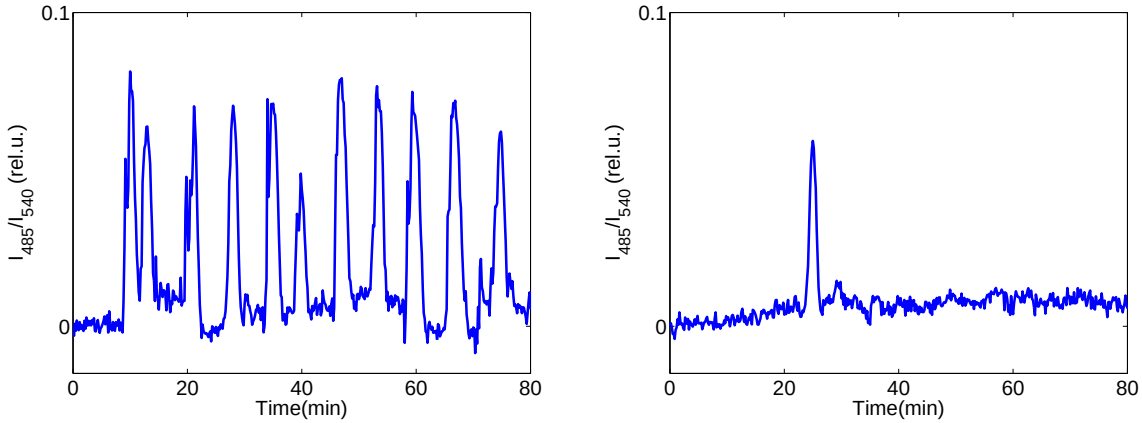

Fig. 1.19 Representative time courses of cAMP oscillation in the perfusion chamber. (Left) In conditions corresponding to the red regions of the phase diagram in figure 1.18 (strong cell-cell interaction), the population of cells exhibits periodic firing of intracellular cAMP. The condition of the data is: flow rate 4 ml/min and cell density 1/16 ML. (Right) In conditions corresponding to blue (or white) regions of the phase diagram (weak cell-cell interaction), the population of cells exhibits sporadic or no firing. The condition of the data is: flow rate 2 ml/min and cell density 1/64 ML.

immediately[*7] washed out by perfusion. Therefore, the robust oscillation observed in the perfusion chamber strongly suggests that the property can be attributed not to an extracellular control but to an intracellular mechanism.

The necessity of fine tuning of parameters in a well-accepted model of cAMP oscillation

One might ask how difficult it is to explain the robust oscillation in the perfusion chamber. As mentioned above, M&G model has succeeded in reproducing various aspects of cAMP signaling often quantitatively. Here we ask whether M&G model can reproduce the phase diagram shown in figure 1.18. Note that the equations for z describing the kinetics of extracellular cAMP in M&G model has the same form as that in the perfusion chamber discussed above (equation 1.1). Therefore we can examine how the oscillation of the model depends on the two parameters; cell density, ρ and degradation rate, γ. Figure 1.20 is the phase diagram that shows parameter regions where oscillation is observed (red) and where oscillation is not observed (blue) obtained from M&G model. It is clear from the figure that M&G model requires fine tuning of the parameter values and therefore the oscillatory regions are narrower than the experimental result. This indicates that it is not trivial to explain the robustness. In other words, a model that can explain the emergence of oscillation does not necessarily explain the robustness of it.

[*7] The buffer in the perfusion chamber is exchanged rapidly (within a few minutes) compared to the timescale for the expression of proteins (∼1 hr).

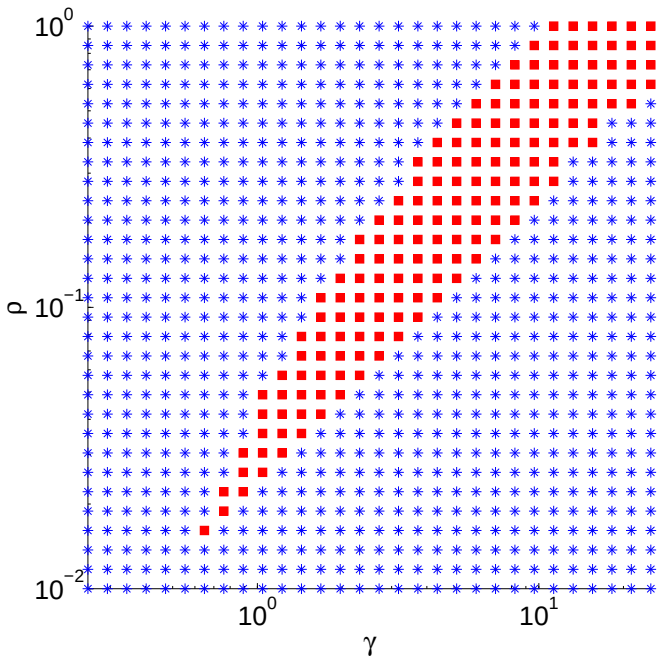

Fig. 1.20 A phase diagram that show existence and non-existence of oscillatory solution in M & G model in a phase plane of γ and ρ. Red and blue regions represents oscillatory and non-oscillatory (fixed point) region respectively. The parameter values are the same as in [73]: $k_1 = 0.036$, $k_2 = 0.666$, $L_1 = 10$, $L_2 = 0.005$, $c = 10$, $\alpha = 3$, $\lambda = 0.01$, $\theta = 0.01$, $\epsilon = 1$, $q = 4000$, $\sigma = 0.6$, $k_i = 1.7$ and $k_t = 0.9$.

1.5 Outline of the thesis

In this chapter, we have discussed the property of cAMP signaling in *Dictyostelium* cells in terms of three different but interrelated point of view, i.e, cellular information processing, cell-cell signaling and pattern formation in development. Exploiting *Dictyostelium* cells as a model system can be advantageous in these fields because (i) we can analyze the dynamics of cellular responses at the single-cell level, (ii) the rule governing cell-cell interaction is relatively simple and (iii) nevertheless, the collective behavior cAMP oscillation has ubiquitous feature in multicellular systems; emergence of a functional pattern and its robustness. Moreover, it is now clear that (a) adaptation in cAMP signaling response is not characterized sufficiently especially in its response-rescaling property and (b) the origin of the robust cAMP oscillation is not yet understood.

With these backgrounds in mind, we investigate the dynamic property of cAMP signaling system at the single cell level and discuss its functional aspect in the fol-

lowing chapters. After introducing experimental systems in chapter 2, we show the results of single-cell analysis of cAMP signaling response in chapter 3. The response is shown to follow fold-change detection (FCD). This is the first direct evidence of FCD in eukaryotic signaling system. Also, the FCD property is shown to be robust to cell-cell variability, meaning that the property is insensitive to the precise values of the biological parameters. Considering the role that cAMP signaling response plays in intercellular communication in *Dictyostelium* development, the results raise a question about the function of FCD in cell-cell signaling. In chapter 4, we develop a mathematical model describing cells capable of FCD communicating with each other. Analysis of the model reveals that the equations have a symmetric property, in that the equations remain invariant to a transformation of variables. The symmetry can be interpreted as a system's robustness to variations in cell density. This strongly suggests that the robustness of cAMP oscillation can be attributed to the FCD property of the constituent cells. To further support the idea, in chapter 5, we test the model's prediction by studying cAMP oscillation in the perfusion chamber. There, we show that the key properties in the model are also observed in the real system. Thus, these data strongly suggest that cAMP oscillation is robust to variations in cell density because each cell has the FCD property in cAMP signaling response. To gain insights as to the molecular mechanisms in cAMP signaling response, in chapter 6, we investigate the dynamics of a signaling molecule PIP_3 which is upstream of ACA in the signal transduction system. We show that the temporal behavior of PIP_3 also follows FCD. This result suggests that the PI3K pathway that governs the dynamics of PIP_3 is the origin of FCD in cAMP signaling response. In chapter 7, we explore the possibility that the relation between FCD and the robustness is generalized to biological system other than *Dictyostelium* cells in the perfusion chamber. By using general form of equation, we show that FCD ensures the robustness to variations in cell density in various conditions. Lastly, in chapter 8, we summarize the results and discuss the outlook of this study in a broader context.

Chapter 2

Materials and Methods

2.1 Cell preparation and measurements

2.1.1 Strain and cell culture

Dictyostelium AX4 cells were used for all experiments. Cell lines used included AX4 cells expressing Epac1camps (Epac1camps/AX4) and PH_{Crac}-RFP (PH domain of Crac fused to monomeric red fluorescent protein (mRFP)) (PH_{Crac}-RFP/AX4).

Epac1camps/AX4

The cell line Epac1camps/AX4 was made in the preceding study [47] by transforming AX4 cells with a expression vector pA15Epac1camps by electroporation [52]. The vector pA15Epac1camps allows constitutive expression of the cAMP sensor Epac1camps [84] under the *act15* promoter.

PH_{Crac}-RFP/AX4

The cell line PH_{Crac}-RFP/AX4 was made in the preceding study [106] by transforming AX4 cells with a vector by electroporation. The expression vector was a generous gift from R. Firtel (University of California, San Diego, CA) and carries a hygromycin resistance cassette and PH domain of CRAC fused to mRFP1. The victor allows constitutive expression of PH_{Crac}-RFP under the *act15* promoter.

Cultivation and starvation of the cells

The cells were selected and grown axenically at 22°C in PS-medium [51] (1% Special Peptone (LP0072; Oxoid), 0.7% Yeast extract (LP0021; Oxoid), 1.5% D-glucose, 0.14% KH_2PO_4, 0.012% $Na_2HPO_4{\cdot}7H_2O$, 40 ng/mL vitamin B_{12}, 80 ng/mL folic acid and 1x antibiotic-antimycotic mix (100X, 15240-112; Gibco), which contains streptomycin, amphotericin B and penicillin, with 10 μg G418 for Epac1camps/AX4 and with 60 μg/ml hygromycin B for PH_{Crac}-RFP; PH 6.5). During the cultivation, 30-ml cell suspensions in PS-medium were shaken in a Erlenmeyer flask (250 ml; Bellco) at a constant speed of 155 rpm, where the cell density was kept below $\sim 2\times10^6$ cells. Before experiments, cells were washed twice with developmental buffer (DB; 10 mM K/Na_2 phosphate buffer, 1 mM $CaCl_2$, 2 mM $MgCl_2$; pH 6.5) by centrifugation of the cells in a centrifuge tube (15ml, 430766; Corning) for 3 minutes at 700 G. The

washed cells were re-suspended in ∼1-ml DB in the centrifuge tube and shaken at $\sim 2 \times 10^7$ cells/mL at a constant speed of 155 rpm for 4 to 5 h.

2.1.2 Live cell microscopy

Starved cells were plated on a perfusion chamber at a density below 1×10^3 cells/cm^2 and perfused with flow rate 4 to 8 ml/min unless otherwise described. Fluorescence images were obtained at 22°C.

Imaging of Epac1camps/AX4

The cell line of Epac1camps/AX4 was observed under inverted microscope (IX-81; Olympus) equipped with a motorized microscope stage (BIOS-215T; Sigma Koki) and filter wheels (99A354 and 99A357; Ludl Electronic Products) through oil immersion objectives (60× PlanApo N, N.A. 1.42, or 20× UPlanSApo N, N.A. 0.85; Olympus) (figure 2.1). The stage and the filter wheels were controlled by a stage controller (FC-101G; Shiguma Koki) and the MAC5000 system (Ludl Electronic Products) respectively. Microscope device control and data acquisition were conducted by using Metamorph software (Molecular Devices). As a light source, we used a xenon lamp (UXL-75XB; Ushio) in a 75W xenon lamp housing (U-LH75XE; Olympus). For FRET analysis, the image of the cells were taken through CFP channel (CFP excitation filter and CFP emission filter) and FRET channel (CFP excitation filter and YFP emission filter). In both channel, the cells were excited with 435-nm light (BP425-445HQ; Olympus) with 50 % and 12% neutral density filters and 30 msec exposure time. The emission from the cells was separated from the excitation by a dichroic mirror (DM450; Olympus) and was passed through an emission filter 460-510 nm (BA460-510HQ; Olympus) for CFP channel and 515-560 nm (BA515-560HQ; Olympus) for FRET channel. Images were taken at 10 to 15 s intervals for total duration of ∼0.5 to 2 hr. CFP and FRET images were taken in succession at ∼ 200 ms interval. We also used YFP channel (YFP excitation filter and YFP emission filter) only once right before each experiment to obtains data which is needed to correct for cross-excitation (see below), where cells were excited with 495-nm light (BP490-500HQ; Olympus) with 50 % and 12% neutral density filters and 30 msec exposure time and the emission was separated from the excitation by a dichroic mirror (DM505; Olympus). The images were captured with a depth of 16 bit by a 512×512 pixels by an EMCCD camera (Cascade II:1024; Photometrics). Data were stored in Tagged Image File Format (TIFF) files.

Imaging of PH_{Crac}-RFP/AX4

The cell line of PH_{Crac}-RFP/AX4 was observed under inverted microscope (IX-81; Olympus) equipped with an automated stage (BIOS-215T; Sigma Koki), a confocal unit (CSU-X1; Yokogawa) and optical shutters (LS6ZM2; Uniblitz Electronics) through an oil immersion objectives (60× PlanApo N, N.A. 1.42; Olympus). The stage and the shutters were controlled by a stage controller (FC-101G; Shiguma Koki) and a shutter driver (VMM-D3; Uniblitz Electronic) respectively. Microscope device control and data acquisition were conducted by using Metamorph software (Molecular Devices). As a light source, we used a diode-pumped solid-state (DPSS) laser

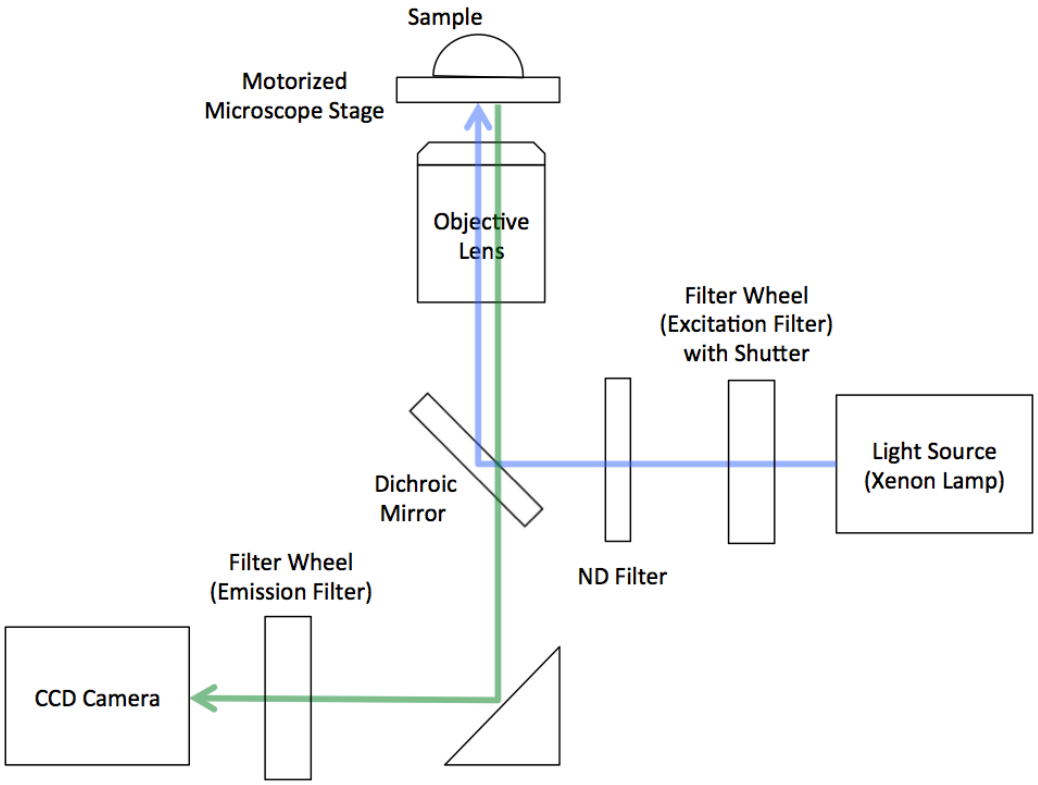

Fig. 2.1 A schematic diagram of the setup for FRET measurement.

(561 nm, 25mW; Melles Griot). PH_{Crac}-RFP were excited with 50 % neutral density filters and 30 msec exposure time and the emission was passed through an emission filter (BA575IF; Olympus). Images were taken at 3 s interval. The images were captured with a depth of 16 bit by a 512×512 pixels by an EMCCD camera (Evolve:512; Photometrics). Data were stored in Tagged Image File Format (TIFF) files.

2.1.3 Perfusion and cAMP stimulation

A chamber insert (RC-37F; Warner instruments) was mounted onto a glass bottom culture dish (35 mm petri dish, 14 mm micro well, No. 0 coverglass; MatTek) using silicone grease (high vacuum grease; Dow Corning) and the device was used as a perfusion chamber. The inlet of the perfusion chamber was attached to syringes filled with cAMP-containing buffer and the outlet was attached to a suction pump (MV-6005V; ASONE) (figure 2.3). To provide a constant influx of cAMP-containing buffer, syringe pumps (NE-1000X dual, New Era Pump Systems Inc.) were used, each of which holds a 50-ml syringe (SS-50LZ; TERMO). The flow rate become controllable by the syringe pumps while the average fluid volume in the perfusion chamber is almost stable at ∼250 μl. To connect the inlet of the perfusion chamber to the syringe pumps and the outlet of the perfusion chamber to the suction pump, tubes of a few meters in total (Polyethlene tubing size 5; Hibiki, Tygon R-3603 (AAC0002); Saint-Gobain and Laboran Silicon tube 1×2; HAGI) connected by tubing connectors (64-0164; Werner instruments) were used. During perfusion, the flow rate was kept

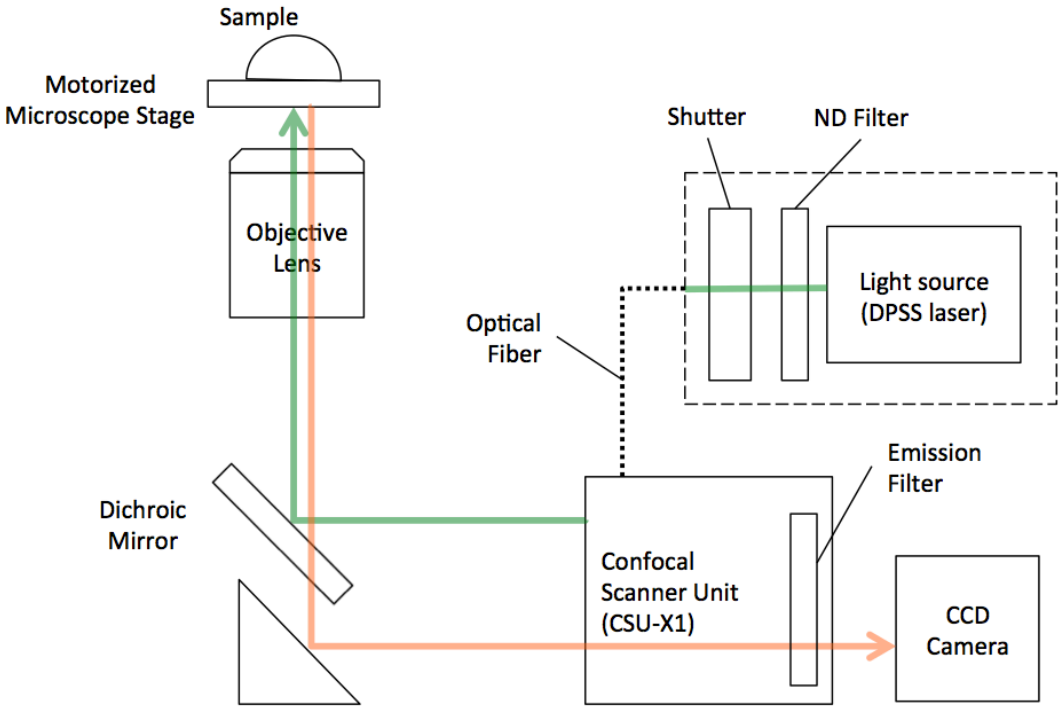

Fig. 2.2 A schematic diagram of the setup for confocal measurement.

at 8 ml/min at least for a minute before and after changing the concentration of extracellular cAMP, which results in step-like changes (within ∼10 s) in the stimulus level (figure 2.4) while the flow rate was reduced to 4 ml/min when there is no need to change stimulus level.

2.2 Image processing and analysis

The following image processing and analysis were performed using MATLAB (MathWorks). The source code central to these analyses are shown in the Appendix.

2.2.1 FRET analysis

Simple ratiometry (i.e., the ratio of fluorescence intensities of donor channel and FRET channel) is a convenient way to analyze FRET data. However it is known that such simple FRET ratio suffers from several sources of distortion such as spectral bleed through, cross-excitation and photobleaching[*1]. To obtain a good indicator of FRET efficiency, which is supposed to accurately reflects the concentration of cAMP, such factors in raw data have to be corrected in a proper way [45, 117, 14]. Such fully-corrected FRET index is more reliable, in that it is independent of the expression level of cAMP sensor Epac1camps and therefore enables us to compare the values of index among different cells. Here we describe how the correction was conducted in our

[*1] In our experimental system, the effect of photobleaching is negligible

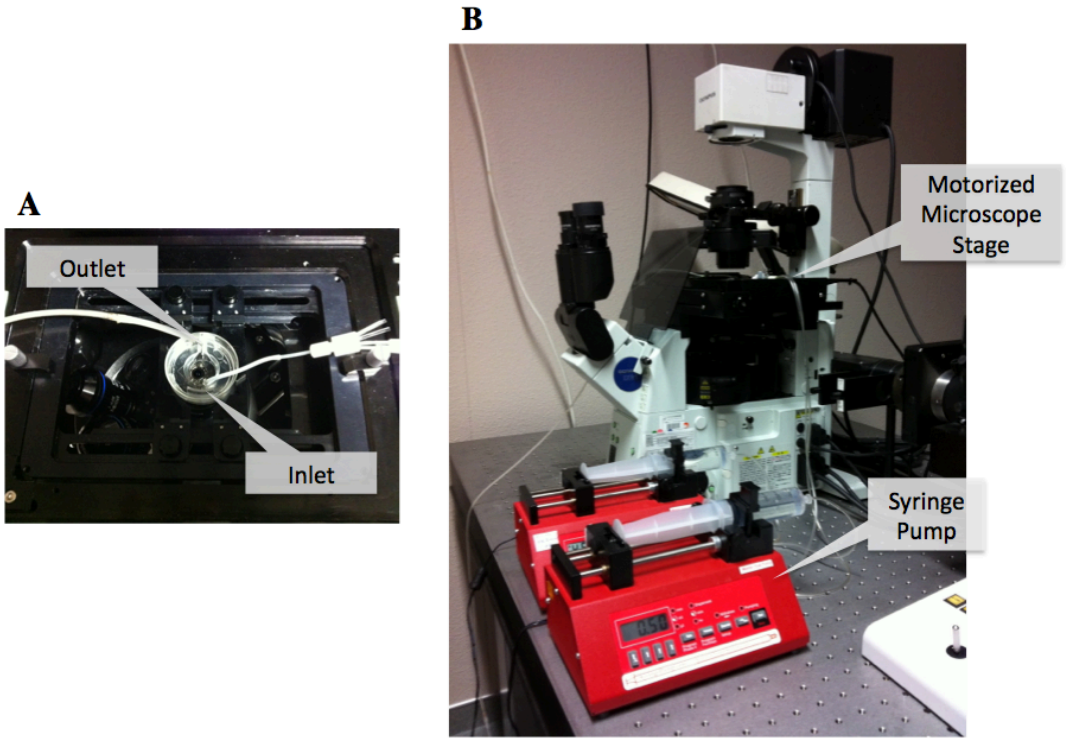

Fig. 2.3 The perfusion system. (A) The perfusion chamber mounted onto a mortared microscope stage. (B) Syringe pumps and a microscope.

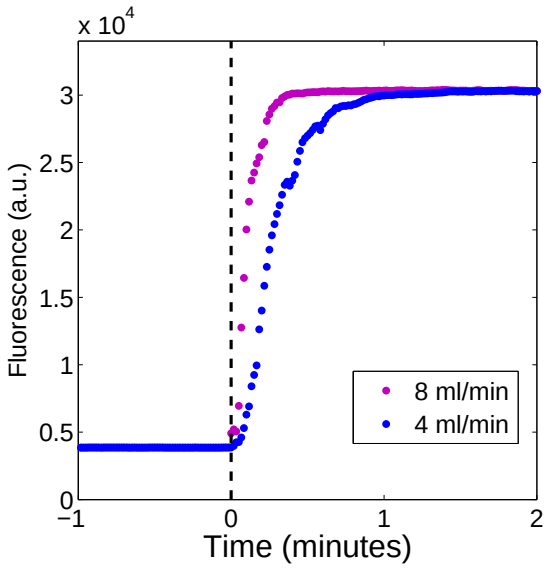

Fig. 2.4 Representative time courses showing exchange rates of fluid in the perfusion chamber. Buffer containing fluorescence was perfused and observed under the microscope.

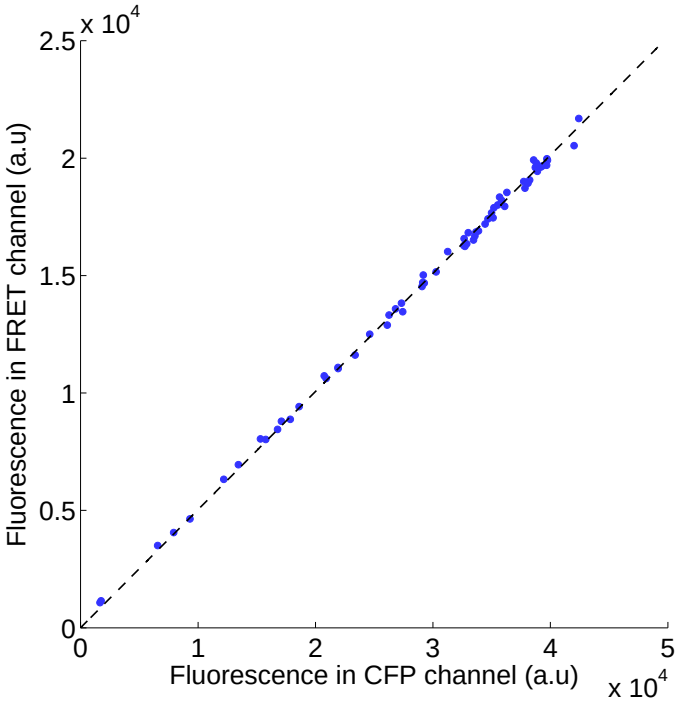

Fig. 2.5 Determining the correction coefficient for bleedthrough. The cells that express only CFP were excited with 435-nm light and fluorescence in CFP and FRET channel with a background correction was measured (65 cells). The least squares regression line is represented by the dotted line ($y = 0.50x$).

FRET experiment.

First, we determined the coefficient for spectral bleedthrough, α. Spectral bleedthrough, or cross-talk, results from the fact that the emission spectrum of CFP overlaps with YFP emission spectrum[*2]. This means that a part of fluorescence in the FRET channel is comimg from the fluorescence emitted by CFP. To determine the correction coefficient for bleedthrough in our system, we excited the cells expressing only CFP with 435-nm light and recorded fluorescence with a background correction in CFP and FRET channels. The ratio of the two fluorescence, α = FRET/CFP, represents the effect of the spectral bleedthrough between the CFP and FRET channel (figure 2.5).

Then, we evaluated the coefficient for cross-excitation, β. Cross-excitation refers to the fact that YFP can also be directly excited by the 435-nm light. To estimate the correction coefficient for cross-excitation in our system, we excited the cells that express only YFP first with 435-nm light (to record the FRET channel emission intensity) and then with 500-nm light (to record the YFP channel emission intensity). The ratio of the two fluorescence, β = FRET/YFP, represents the degree of direct acceptor excitation by 435-nm light (figure 2.6).

Using those coefficients, we corrected FRET channel intensities as follows. At the

[*2] The opposite bleedthrough, i.e., YFP emission bleeding into CFP channel, is negligible.

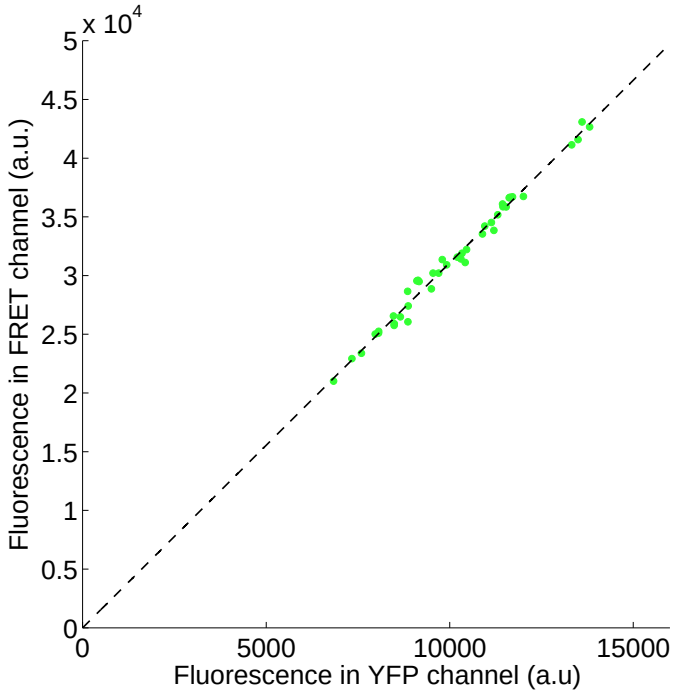

Fig. 2.6 Determining the correction coefficient for cross-excitation. The cells that express only YFP were excited with 435-nm light for FRET channel and 500-nm light for YFP channel and fluorescence in both channels with a background correction was measured (42 cells).The least squares regression line is represented by the dotted line ($y = 3.1x$).

beginning of each FRET experiment, we obtained the acceptor intensity $I_{YFP-dir}$ measured on direct YFP excitation with 500-nm light. From the images of the cells from CFP and FRET channel, we obtained fluorescence of the cells with a background correction (I_{CFP} and I_{FRET} respectively). We then obtained the corrected FRET channel intensity ($I_{FRET-corr}$) as

$$I_{FRET-corr} = I_{FRET} - \alpha \times I_{CFP} - \beta \times I_{YFP-dir}.$$

Finally, we obtained the FRET index as

$$\text{FRETindex} = \frac{\text{I}_{\text{CFP}}}{\text{I}_{\text{FRET}-\text{corr}}}.$$

2.2.2 Quantifying the responses of PH_{Crac}-RFP/AX4

In evaluating the dynamics of PIP_3 response in PH_{Crac}-RFP/AX4, we analyzed the images of the cells in essentially the same way as that developed by Postma et al [90]. To accurately evaluate the dynamics of translocation of PH_{Crac}-RFP, which reflects the amount of synthesized PIP_3 at the membrane, one have to obtain relative fluorescence intensity in the cytosolic region. This requires three processes: (i)

discrimination between cytosolic region and other fluorescent and nonfluorescent region resulting from organella and (ii) normalization of the fluorescence intensities (iii) correction of photobleaching.

Selecting regions of interest.
First, to select regions of interest, i.e., cytosolic regions, from the images, we omitted non-cytosolic regions from raw data by using the techniques of image analysis[*3](figure 2.7). The regions to be eliminated include the boundary (the membrane) of the cells, fluorescent region such as nucleus and vesicles and nonfluorescent region such as vacuoles. Briefly speaking, we selected spatially-clustered high-intensity or low-intensity regions of the images by using both median filtering with a proper window size and binalization technique. As shown in figure 2.7, this method enables to detect non-cytosolic regions stably, regardless of whether the cell is responding to a stimulus (cytosolic intensities are high) or not (cytosolic intensities are low).

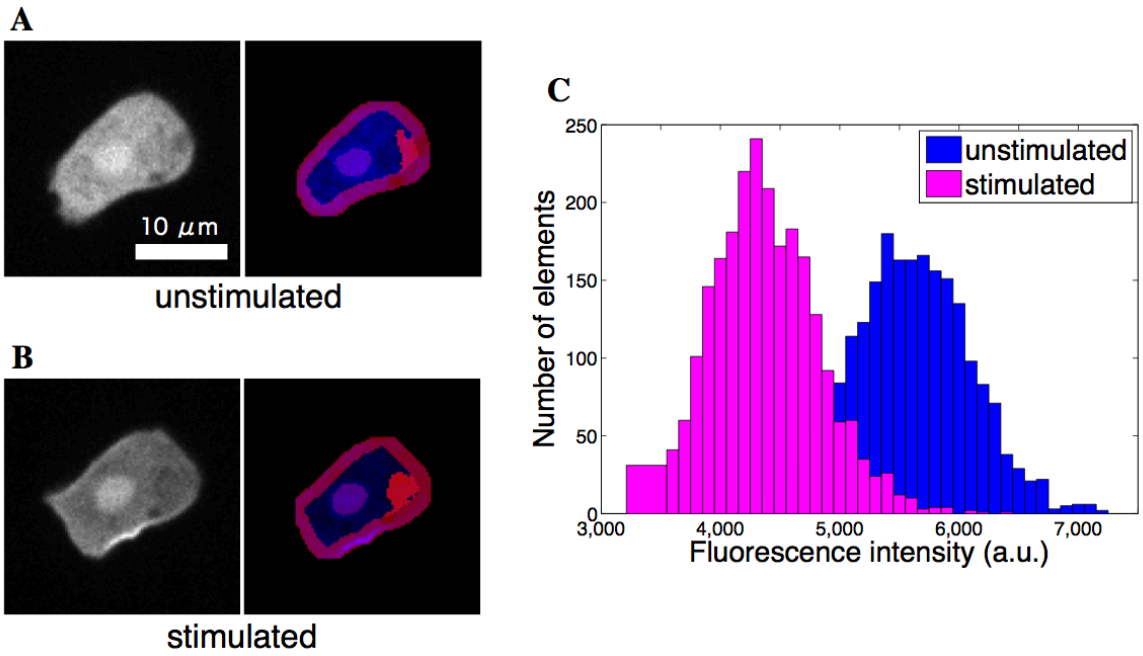

Fig. 2.7 Quantification of fluorescence intensity in the cytosol. Representative images of the cells before (A left) and after (B left) stimulation with 1 μM cAMP are shown. Areas of cytosol (blue area in the right images of panels A and B) were selected by omitting the plasma membrane and strongly fluorescent and nonfluorescent objects (red, purple and magenta area in the right images of panels A and B). The histograms (panel C) show the distribution of fluorescence intensities in the cytosol of the cell shown in panels A and B respectively.

After selecting the region of interest, a median and a standard deviation of the fluorescence intensities of the regions were obtained at each time. The left panel in

[*3] In the preceding work [90], the selection of the region of interest was performed manually but we developed a fully-automatic method.

fig.2.8 shows a representative time course of fluorescence intensity. The SD values of the time series data are relatively constant, which means the cytosolic fluorescence intensity is properly estimated. Otherwise the SD values would fluctuate significantly because the organella are so dynamic that they come and go on the focal plane even within this short-time observation.

Normalization of fluorescence intensity of PH_{Crac}-RFP in the cytosol.
Next, we normalized the time series of the fluorescence intensity. This is required because the expression levels of PH_{Crac}-RFP and therefore the cytosolic fluorescence intensities are variable between cells. Normalized fluorescence intensity $\hat{I}_C$ was calculated as follows:

$$\hat{I}_C = \frac{I_C - I_B}{I_{C0} - I_B}, \tag{2.1}$$

where I_C and I_B is a median value of the fluorescence intensity in the cytosol and the background fluorescence intensity outside the cell respectively. I_{C0} was defined as the average value of I_C in five images just before cAMP stimulation. Representative time courses are shown in the right panel of fig.2.8.

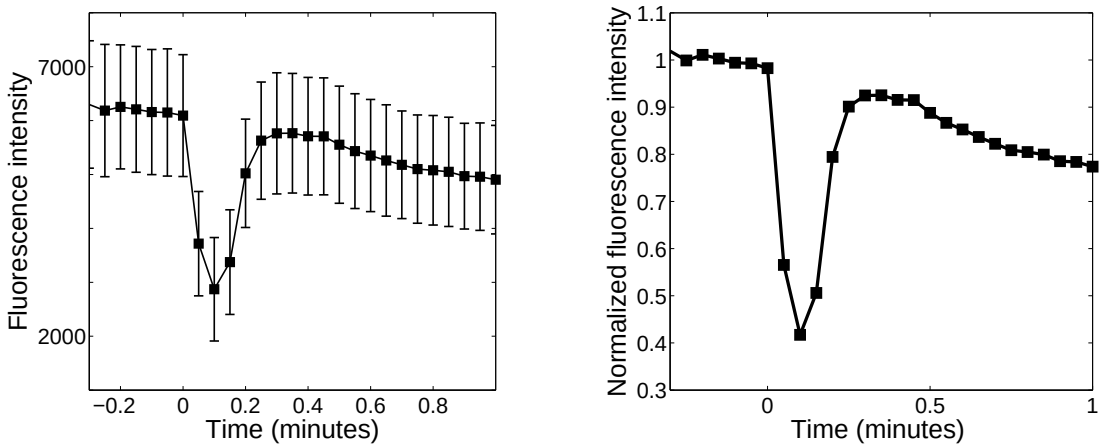

Fig. 2.8 Representative time courses of PIP_3 response. In both figures, the cell, the raw images of which are shown in fig.6.1, was stimulated with 1 μM cAMP at $t = 0$ s. (Left) The results shown are the median and the SD of the fluorescence intensity in the cytosol. Note the relative constancy of the SD values. This is because the cytosolic fluorescence intensity is properly estimated by omitting the fluorescent and nonfluorescent objects (fig.2.7). (Right) Normalized fluorescence intensity defined as eq.2.1.

Correction for RFP photobleaching.
Finally, we corrected the effect of photobleaching. We correct the data by using an estimated rate at which the fluorescence intensity decrease. Specifically, we first obtained confocal images of unstimulated cells (figure 2.9). By fitting these data with a linear equation $y = ax+1$, we obtained the photobleaching rate in this experimental condition (16 % per minute). Using the value of photobleaching rate, we corrected the normalized cytosolic fluorescence (figure 2.10).

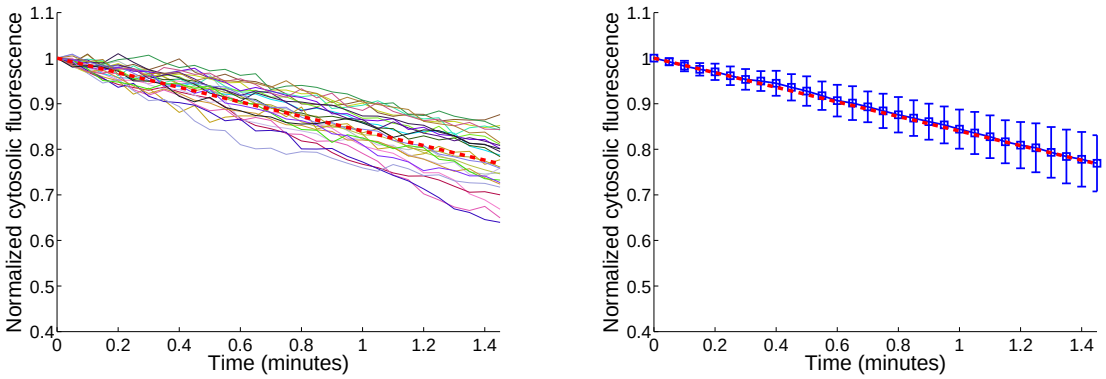

Fig. 2.9 Estimating the rate at which the fluorescence intensity decrease by photobleaching. Confocal images of 27 unstimulated cells were obtained. Each normalized florescence intensities (left) and mean and SD (right) are plotted respectively. The red dotted lines in both figures are least-square fit representing $y = -0.16x + 1$.

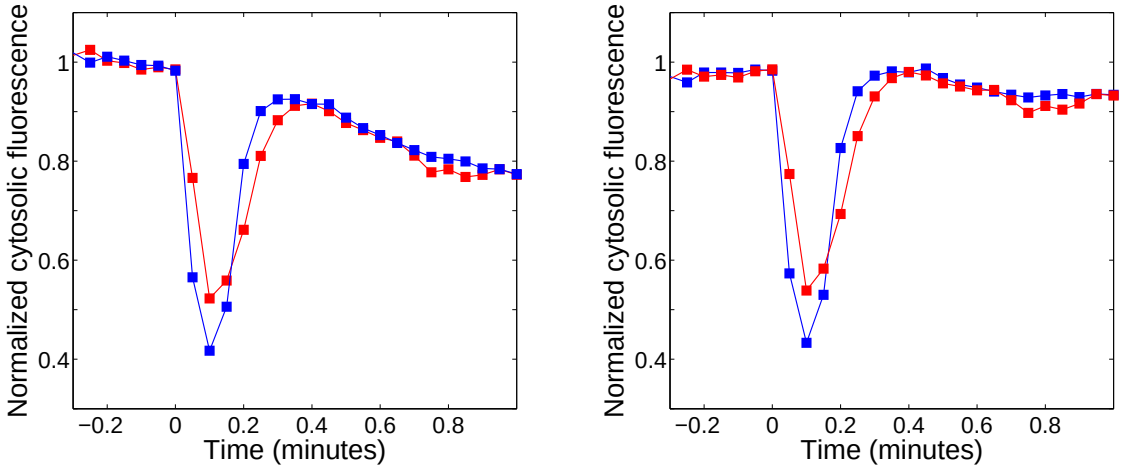

Fig. 2.10 Correction of photobleaching. The normalized cytosolic fluorescence (left) was corrected (right) using the estimated rate of decrease in fluorescence intensity (figure 2.6). Two cells are represented by different colors.

Chapter 3

Characterization of cAMP signaling response at the single-cell level

3.1 Introduction

In *Dictyostelium* cells, binding of extracellular cAMP to the receptor on the membrane elicits synthesis and secretion of intracellular cAMP. The response called cAMP signaling response underlies cell-cell signaling and its resultant cAMP oscillation during *Dictyostelium* development. Recent advantage in FRET-based cAMP sensor has enabled us to observe cAMP signaling response at the single cell level. In preceding studies, the response has been shown to be adaptive, meaning the synthesis of cAMP occurs only transiently even in a persistent input [29, 47]. As discussed in chapter 1, however, the response property remains to be fully elucidated. In particular, a key feature in characterizing an adaptive system, a response-rescaling property, has not been investigated. Here, we address the issue by a single-cell analysis of cAMP signaling response.

Brief summary of the experimental system

In this chapter, input-output relations in cAMP signaling response are investigated in a quantitative way. To do this we used FRET-based cAMP sensor, Epac1-camps [84], and a perfusion system. The cAMP sensor expressed in a transformed cell (Epac1-camps/AX4) provides a real-time readout of a FRET index. The FRET index corresponds to the concentration of intracellular cAMP. Importantly we corrected cell-cell variation in the expression level of the sensor protein and therefore the value of the FRET index can be comparable between cells. The perfusion system enabled us to control extracellular environment. By employing a pair of syringe pumps, well-defined time-varying input signal (i.e., extracellular cAMP) was delivered to the perfusion chamber. Representative time courses are shown in figure 3.1. Further information on the experimental system can be found in chapter 2.

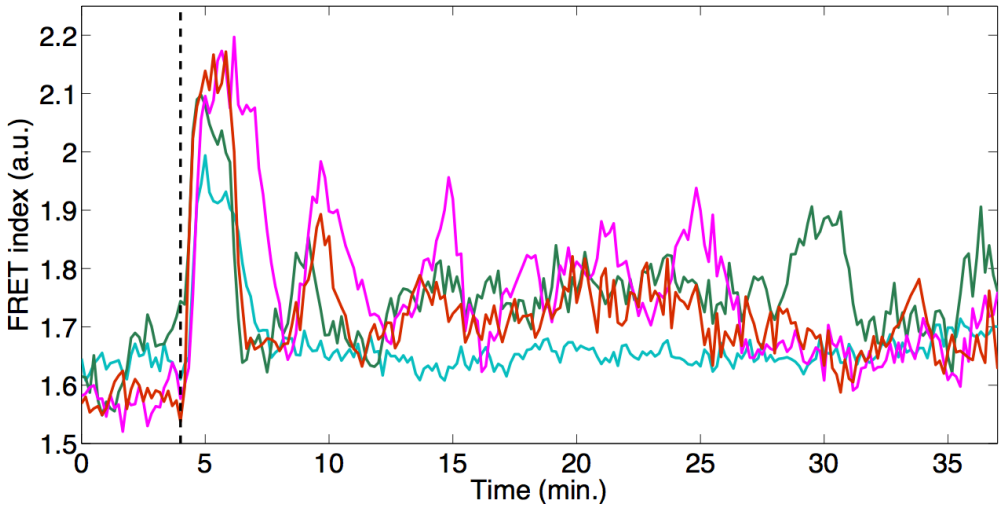

Fig. 3.1 Representative time courses of adaptive cAMP signaling response obtained by full correction of FRET ratio (FRET index; see chapter 2). Four cells are represented by different colors. 3 nM cAMP was applied at the dotted line.

3.2 Results and discussions

3.2.1 Adaptation in cAMP signaling response in low concentrations of extracellular cAMP

In a preceding study [47], it was shown that the level of intracellular cAMP rises transiently and peaks within 2 to 3 minutes upon step stimulus of extracellular cAMP (figure 3.1). The initial peak was shown to be followed by several peaks and the subsequent peaks sustain in a higher concentration of extracellular cAMP, meaning the timescale of adaptation depends on the stimulus level. To investigate the timescale of adaptation and the range over which the response is able to adapt, we exposed the cells to step stimuli with 0-M basal level (figure 3.2). To minimize photo damage to the cells and avoid defocusing resulting from relatively long-time measurement, we observed the cells only in a limited time window; 5-minutes measurement every 10 minutes. Figure 3.3 and 3.4 show representative time courses.

Figure 3.5 shows how amplitude of the response decreases depending on the stimulus level. Here amplitude is defined as the maximum value of FRET index within each 5-minutes time window. As reported in the preceding work [47], 1 nM or higher extracellular cAMP evoked the increase in the concentration of intracellular cAMP right after the step change in the input[*1]. The figure also shows that the amplitude of the response gradually decreases in a dose-dependent manner; the higher the stimulus

[*1] It was demonstrated that the cells exhibit pulsatile, stochastic synthesis of intracellular cAMP in a sub-nanomolar concentration [47], although the level of stimuli don't evoke such deterministic responses as 1 nM or higher cAMP do.

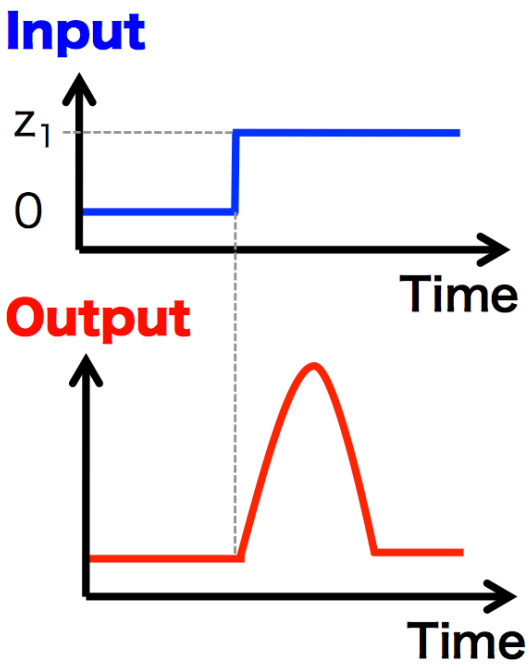

Fig. 3.2 A schematic of the experimental setup. In this experiment, the cells in a cAMP-free environment was stimulated with various concentrations of extracellular cAMP in a step-like manner.

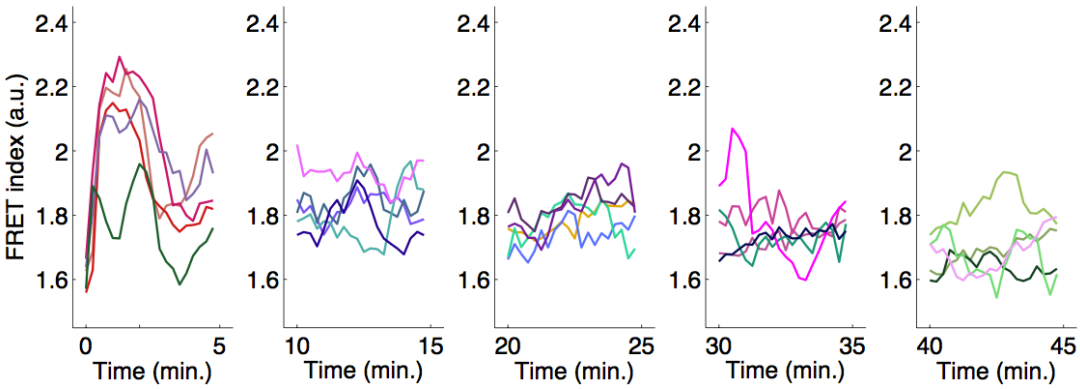

Fig. 3.3 Representative time courses of cAMP signaling response to 10 nM extracellular cAMP. Five cells are represented by different colors. The time lapsed after the stimulation is indicated in x-axis. Observation was made for 5 minutes every10 minutes after stimulation at $t = 0$.

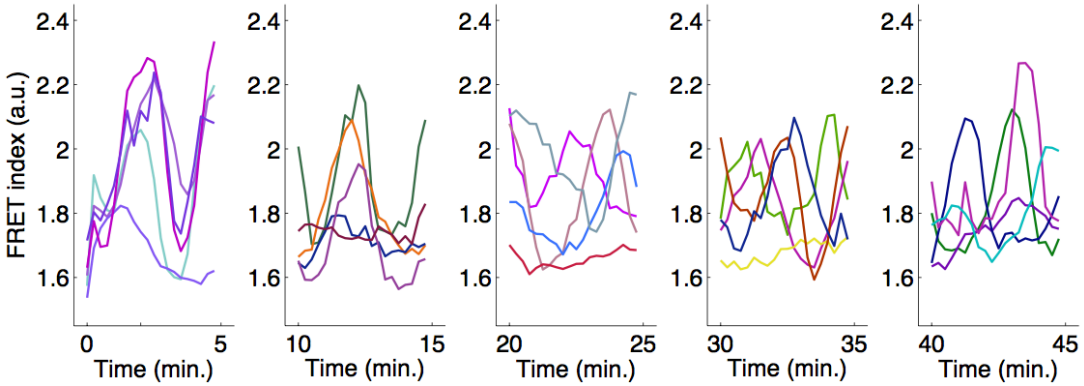

Fig. 3.4 Representative time courses of cAMP signaling response to 1 uM extracellular cAMP. Five cells are represented by different colors.

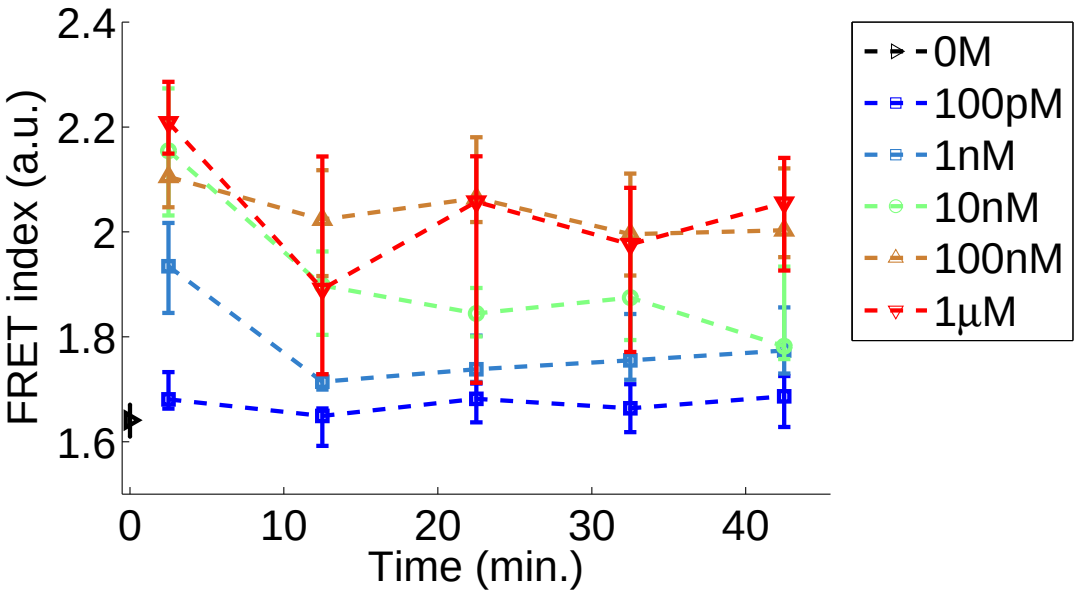

Fig. 3.5 Response intensities as a function of time after the change in the level of cAMP form 0 M. Response intensities were evaluated as a maximum FRET index within 5-minutes time windows. Median and quartile are shown.

level is the longer the response sustains. At steady state (specifically, 40-minutes after stimulation), qualitatively different two modes of responses are observed (figure 3.6); at 10-nM cAMP or lower, the response adapts to the stimulation while, at 100-nM cAMP or higher, the response tends to sustain.

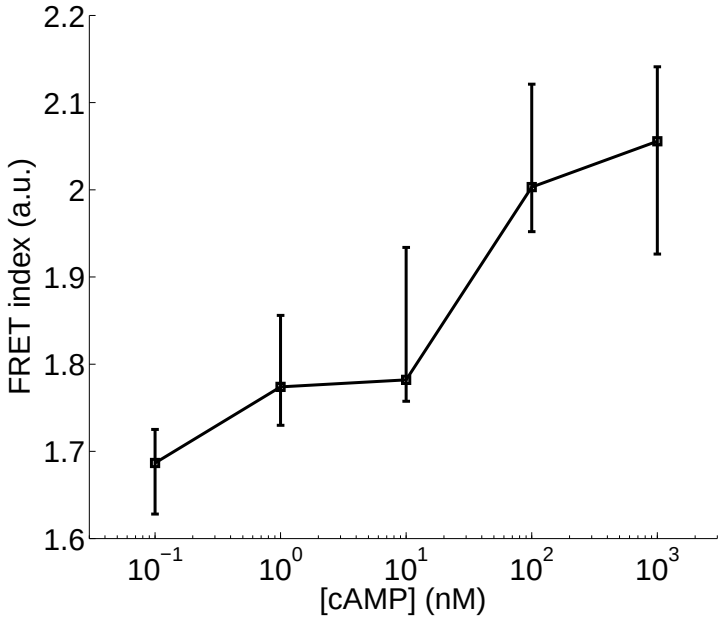

Fig. 3.6 Response intensities 40 minutes after the change in the level of cAMP. In ∼10 nM or below cAMP, the response almost reset to the pre-stimulated level, whereas, in ∼100 nM or above cAMP, it shows prolonged response. Median and quartile are shown.

3.3 cAMP signaling response to relative changes in the level of input stimulus

3.3.1 Weber's law in cAMP signaling response

To investigate the response to relative increase in input stimulus, we exposed the cells to step stimuli with nonzero basal level (Fig.3.7). Specifically, the cells were first pretreated with a pre-stimulation (z_0 in figure 3.7, z_0 = 10 nM or less) and allowed to adapt to it (it takes less than 40 minutes). After that the stimulation was changed to a level of post-stimulation (z_1 in figure 3.7) in a step-like manner.

Representative time courses are shown in figure 3.8. We found that the response intensity, which we define as maximum value of the FRET index after step change in the input, does not necessarily increase even when the difference between pre-stimulus level and post-stimulus level increases; the cells adapted to 100 pM cAMP respond to 1-nM stimulus with relatively high amplitudes (900-pM increase; left panel in figure 3.8) whereas the cells in 1 nM cAMP respond to 3-nM stimulus with small amplitudes (2-nM increase, right panel in figure 3.8). These results suggest that the response intensity is not determined by the absolute change of the input stimulus.

Figure 3.9 shows the response intensities as a function of fold-change in the stimulus level. As the three curves obtained from different pre-stimulus condition (100 pM, 1 nM, 3 nM) overlap significantly, the result shows that the response intensity is

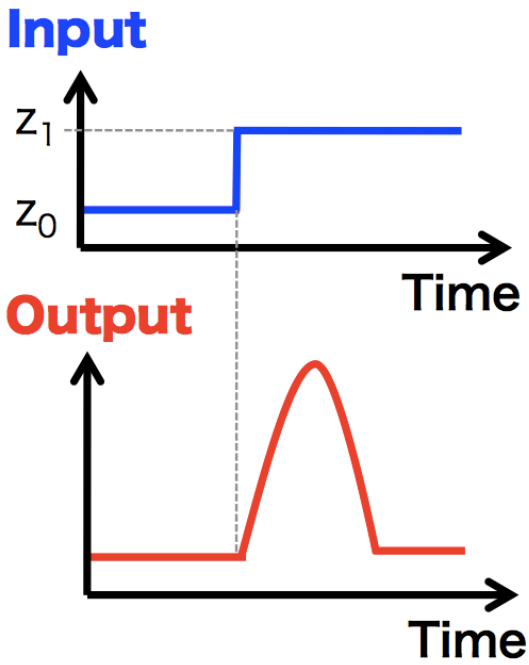

Fig. 3.7 A schematic of the experimental setup. Here the cells are initially exposed to a pre-stimulus level (z_0) of extracellular cAMP for less than 40 minutes and allowed to adapt to the stimulus. Then the extracellular cAMP is elevated to a post-stimulus level $z_1 (> z_0)$ in a step-like manner.

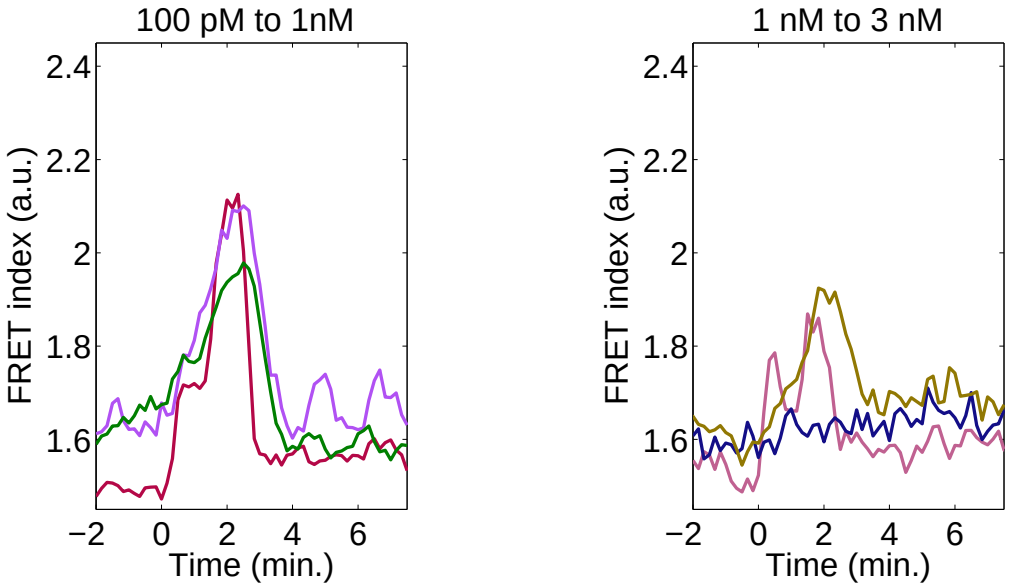

Fig. 3.8 Representative time courses of cAMP signaling responses to relative input changes. In each panel, three different cells are represented by different colors. The stimulus levels were changed at $t = 0$.

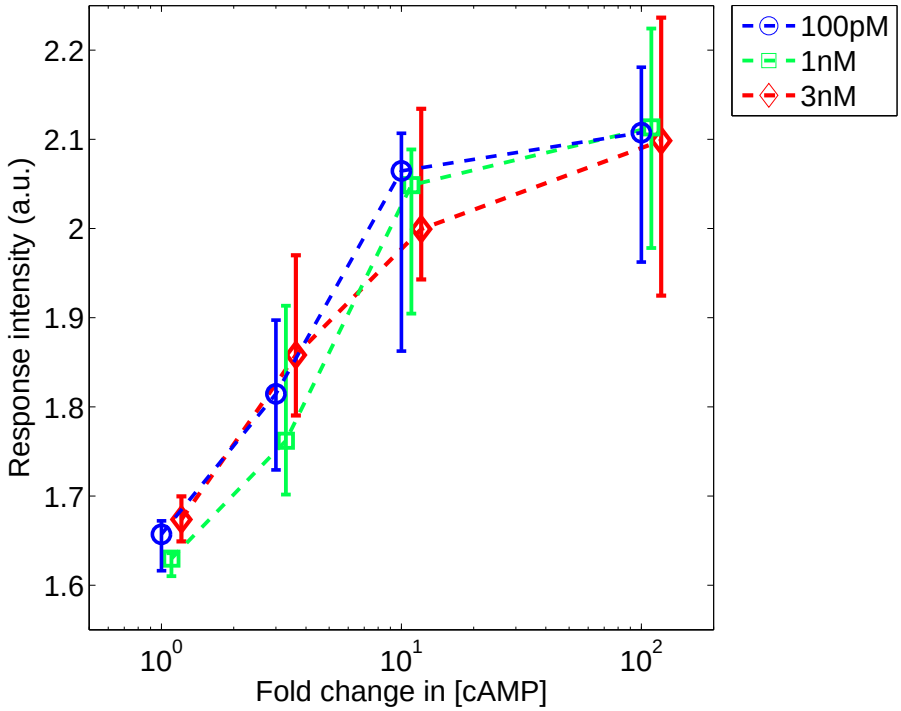

Fig. 3.9 Dose response curves of cAMP signaling response. The response intensity is dictated by fold-change of the stimulus level (z_1/z_0), in that the curves considerably overlaps irrespective of more than 10-fold difference in pre-stimulus levels. The response intensity is defined as the maximum FRET index (amplitude) within 5 minutes after the change in input stimuli. Median and quartile are shown.

dictated by the fold-change of the stimulus level (z_1/z_0) (Fig.3.9). The result means that cAMP signaling response follows Weber's law – a common feature observed in many sensory systems such as vision. Weber's law refers to an I/O relation in which the maximal response to a change in input signal is dictated by the fold-change of the signal (see figure 1.7) [97].

3.3.2 A FCD property in the initial peak of cAMP signaling response

Then we asked whether cAMP signaling response follows fold-change detection (FCD) as well as Weber's law. FCD refers to a response whose entire shape, including its amplitude and duration, depends only on fold change in input stimulus (see figure 1.7). By comparing time series data, we found that the entire shape of cAMP signaling response does not follow FCD (figure 3.8 and 3.11); the second or later peaks following the initial peak in the response become more prominent as the absolute level of the stimulus increases. For example, the responses to a step change from 1 nM to 10 nM (left panel in figure 3.11) shows more prominent second peak than the responses to a step change from 100 pM to 1 nM (left panel in figure 3.8). As mentioned above, the cells shows sustained response at ∼100-nM extracellular cAMP or higher (figure 3.5 also [47]). Consistent with these observation, sustained responses were observed when

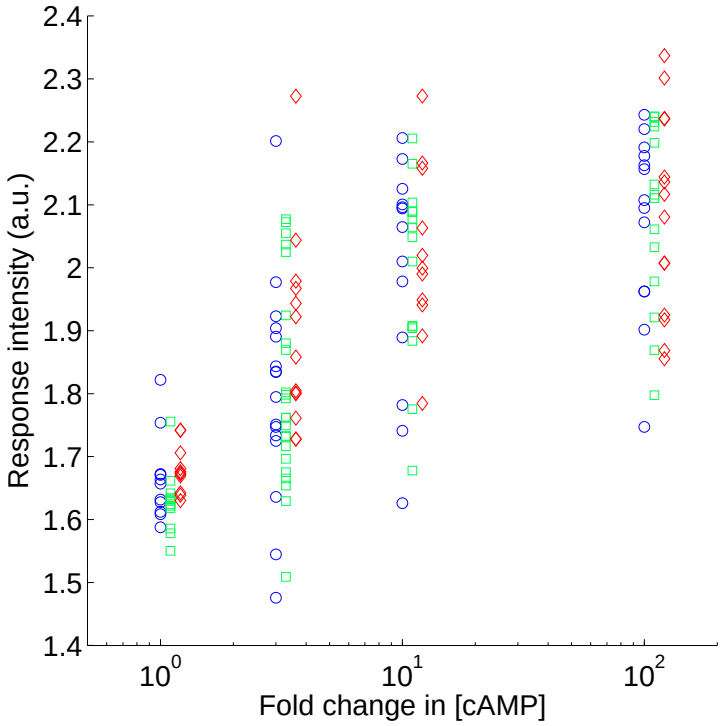

Fig. 3.10 Raw data used in figure 3.9. Blue, green and red represents data for 100 pM, 1nM and 3 nM respectively.

the cells are exposed to a relative increase in the input (right panel in figure 3.11). Thus, the absolute level of input stimulus is reflected in the amplitudes of second or later peaks and therefore the entire shape of the response does not follow FCD.

However, as far as cAMP oscillation is considered, the step inputs (figure 3.7) we have used so far are not realistic: during cAMP oscillation, the concentration of extracellular cAMP oscillates with a period of 6 minutes. Therefore, developmentally-relevant properties of the response should be investigated by using periodic stimuli (figure 3.12). Moreover, periodic stimuli, as well as step stimuli, is important in characterizing an adaptive system in general. In fact adaptive systems such as the osmo-response pathway of *Saccharomyces cerevisiae* and the chemotactic pathway of *Escherichia coli* show deferent responsiveness depending on the frequencies of periodic stimuli [76, 80, 12, 95]. In other words, such periodic inputs can reveal a characteristic time constant of a system.

To observe cAMP signaling response in a physiological condition, we exposed the cells to rectangular stimuli with a period of 6 minutes. Figure 3.13 shows representative time courses. We found that the intracellular cAMP level increases only during up-phases of the input (double-headed arrows in the figure). That is, the second or later peaks after the initial peak are suppressed in the down phases of the stimuli while the initial peak is prominent in each up-phase. The initial peaks showed no refractoriness; the amplitude of the response did not decrease in successive 6-minutes periodic inputs. Furthermore, the amplitude of the initial peak is dictated by the fold change of the input as was the case in the responses to step stimuli. In fact, as shown

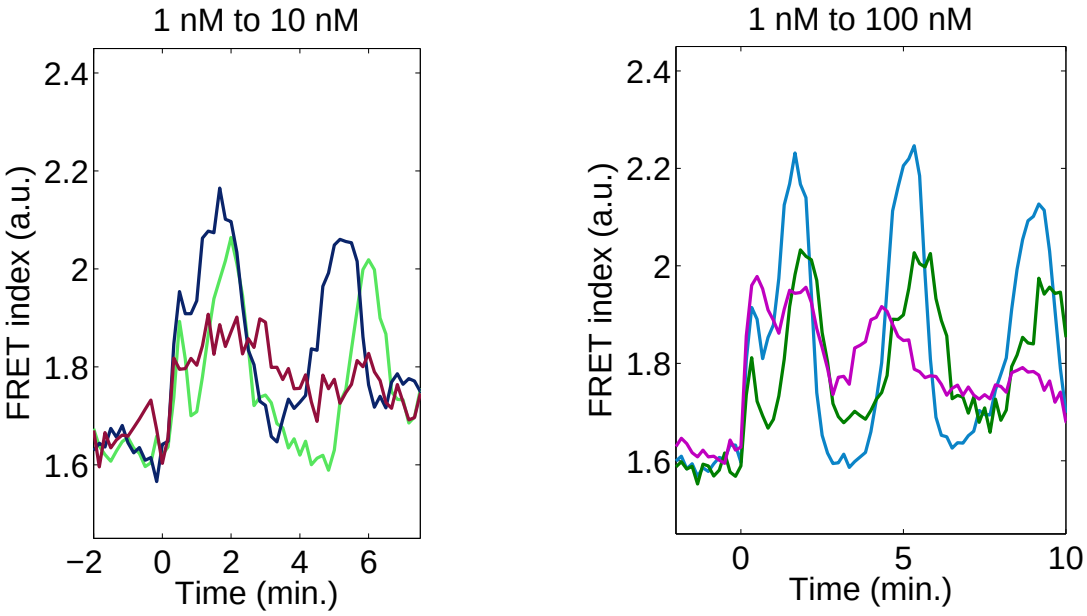

Fig. 3.11 Representative time courses of cAMP signaling responses to relative input changes. In each panel, three different cells are represented by different colors. The stimulus levels were changed at $t = 0$.

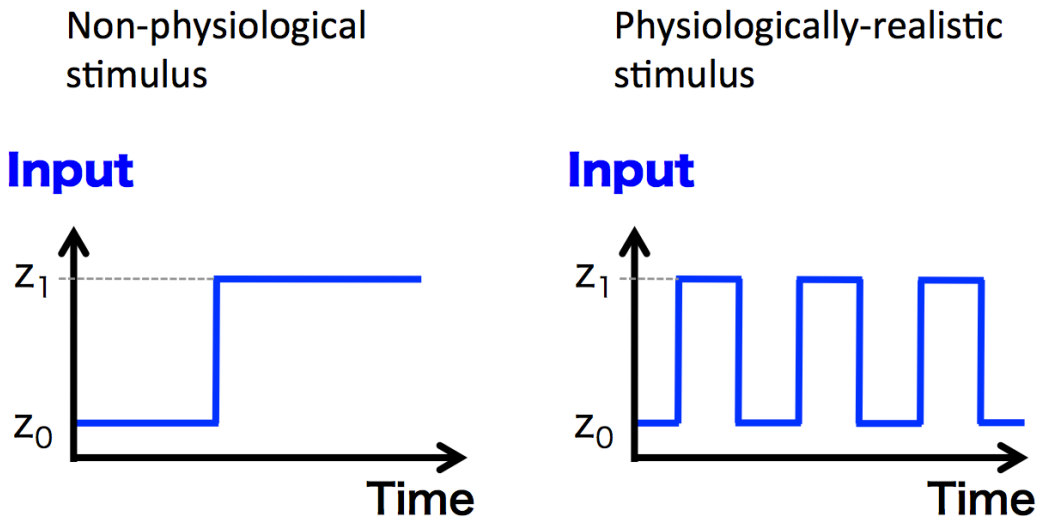

Fig. 3.12 The step inputs we have used so far are not realistic but periodic inputs are more developmentally related as far as we consider cAMP oscillation in *Dictyostelium* development.

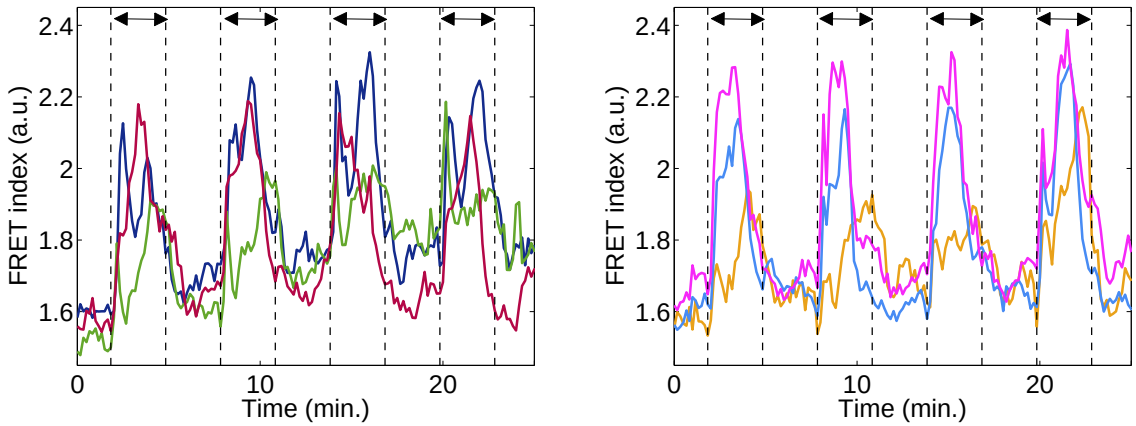

Fig. 3.13 Representative time courses of cAMP signaling response to stimuli with a period of 6 minutes . In the left panel, the stimulus level was elevated from 100 pM to 3 nM during the time windows denoted by double-headed arrows. In the right panel, it was elevated from 1 nM to 30 nM. Each cell is represented by different colors.

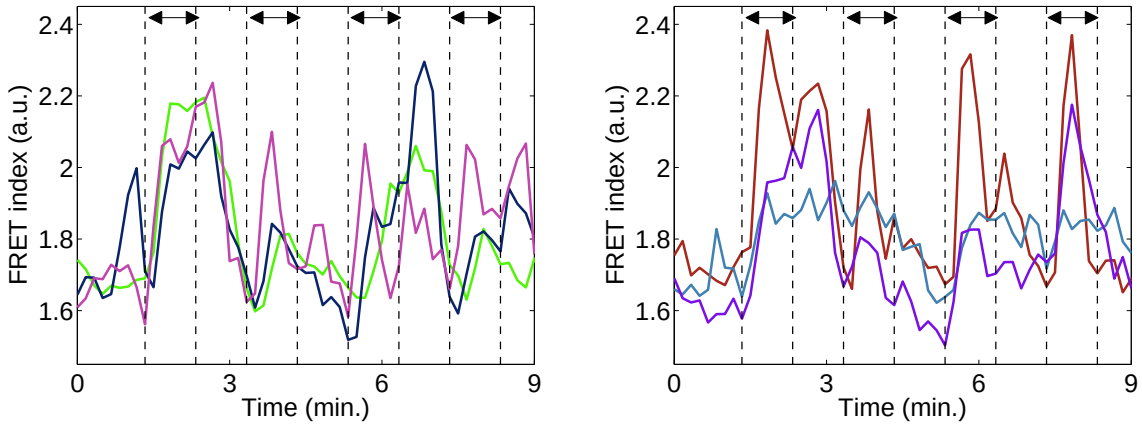

Fig. 3.14 Representative time courses of cAMP signaling response to stimuli with a period of 2 minutes. In the left panel, the stimulus level was elevated from 100 pM to 3 nM during the time windows denoted by double-headed arrows. In the right panel, it was elevated from 1 nM to 30 nM. Each cell is represented by different colors.

in figure 3.13, two periodic inputs with the same fold change but different absolute level evoked similar outputs . When the period of inputs become significantly shorter than 6 minutes, the initial peaks showed refractoriness and did not follow the up-phases of the inputs (figure 3.14). These data suggest that the initial peak in cAMP signaling response is responsible for the rise in the level of intracellular cAMP during cAMP oscillation. Also, note that the duration of the initial peak seems independent of the absolute level of the input. Specifically, it is approximately 3 to 4 minutes regardless of whether the input is step-like one or periodic one. Thus, we conclude that the initial peak in cAMP signaling response follows FCD.

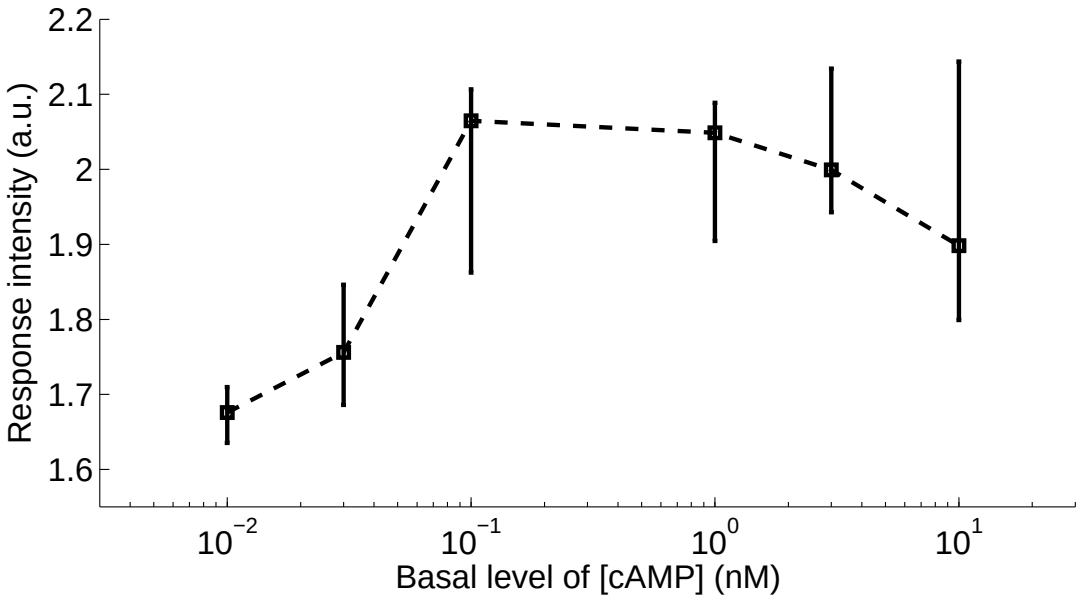

Fig. 3.15 The range over which the FCD property holds. Response intensities to 10-fold change in input stimuli from indicated basal levels are shown. Median and quartile are shown.

3.3.3 The dynamic range of the relative response

To probe the dynamic range over which the FCD property holds, we studied the response amplitudes to 10-fold change at different pre-stimulation levels. Figure 3.15 summarizes the result. The cells begin to respond to 10-fold increase in the stimulus level at ∼100 pM pre-stimulation level. The responsiveness remains almost constant until pre-stimulation level reach ∼10 nM, which is nearly maximum concentration that the response adapt. Thus, we conclude that the cells are capable of FCD over approximately 2 orders of magnitude in pre-stimulation level.

3.3.4 Robustness of the FCD property in cAMP signaling response

As can be seen in the time series data of cAMP signaling response (e.g. figure 3.8 or figure 3.11), the shapes of the initial peaks are highly variable between cells. In general, most biochemical parameters of living cells such as cell size and protein concentrations often vary significantly between cells due to stochastic effect, even if the cells are genetically identical [36]. Nevertheless some properties in cell signaling systems have been shown to be robust to cell-cell variation [5, 19]. Such robustness is often achieved by a special type of connectivity, or network topology, between constituent proteins of the signaling system [8, 118, 77]. Knowing which property is robust, therefore, can constrain potential mechanisms of the system [5, 72, 78]. Furthermore, such robustness would suggest that the property may be biologically important because a functional property would be required to be stable [5, 19].

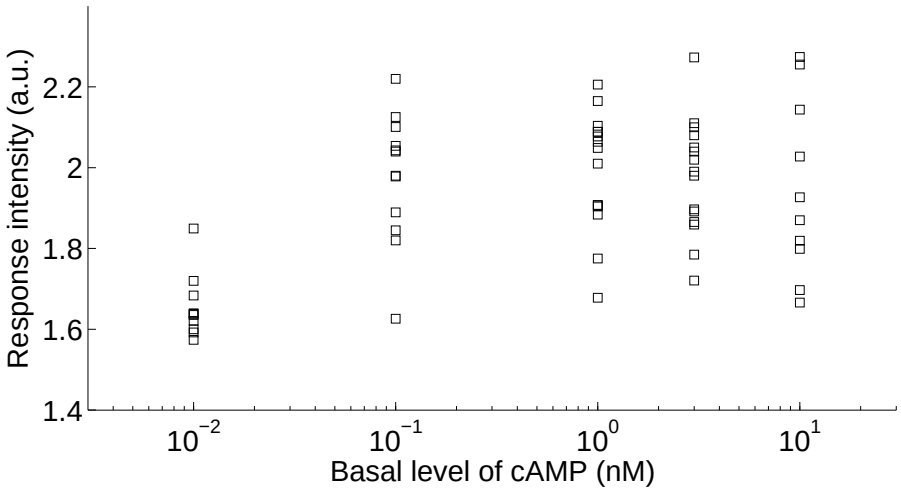

Fig. 3.16 Raw data used in figure 3.15.

Here we ask whether the FCD property in cAMP signaling response is a robust property or not. What we mean by robustness of the FCD property is as follows. Imagine two cells that have identical biochemical parameters and the cells are stimulated with step inputs with identical fold-change but different absolute level. If both cells are capable of FCD, by definition, such stimulations would yield outputs whose entire shapes are equal to each other. Assume that we can somehow change biochemical parameters of the cells just a little from its original state to another state simultaneously in both cells. Then we ask what happens when the cells are again stimulated as before. The responses of the cells in the new states would, in general, be different from the previous ones because of the alteration in their biochemical parameters. Suppose if the FCD property requires fine-tuning of the parameters, then the FCD property no longer holds in the new condition; the entire shape of the responses are not identical to each other. On the other hand, if the FCD property does not depend on the precise values of their biochemical parameters, i.e., if FCD is a robust property, then the shape of the responses remain equal to each other. Although preparing two biochemically-identical cells is unattainable because of the individuality of the cells, we would be able to assume that each individual cells have nearly identical biochemical parameter values for a brief period of time. This assumption enables us to interpret the following experiments as a similar experiment discussed above: that is, we expose each individual cell to two successive step inputs with identical fold change but different absolute level (figure 3.17) to test whether the FCD property is robust or not.

Representative time courses of the responses to such inputs are shown in figure 3.18, where the cells are exposed to two successive 5-fold increase in extracellular cAMP. To evaluate the similarity between the two successive responses, we analyzed the correlation between the amplitudes of the two. Figure 3.19 shows a scatter plot, which represents the amplitude to the 1st step change (300 pM to 1.5 nM) and that to the 2nd step change (1.5 nM to 7.5 nM). The figure clearly shows that, although amplitude itself is highly variable between cells, the amplitudes of two successive

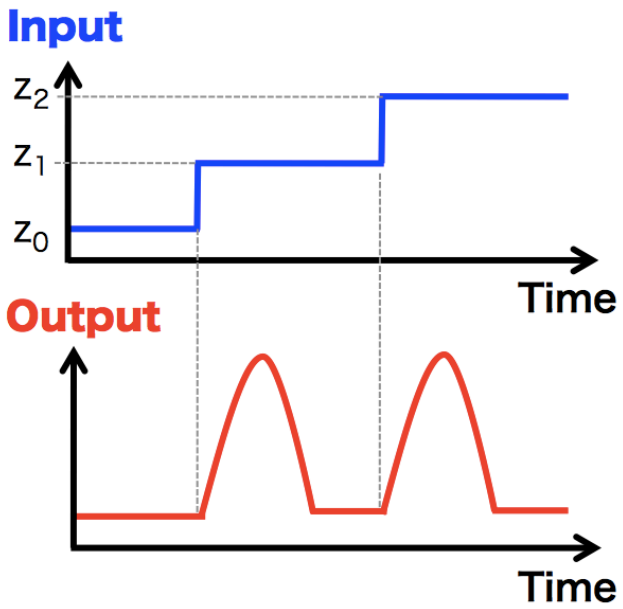

Fig. 3.17 Schematic of the experimental setup to test whether the FCD property is robust or not.

responses are highly correlated with each other (correlation coefficient: 0.81). This means that the cells tend to respond with a relatively constant amplitude to a certain ratio of increase in input stimuli in spite of the difference in its absolute level. This suggests that the FCD property is less sensitive to the precise values of the biochemical parameters of the cell than the amplitude of the response.

3.4 Some comments on the two modes of oscillation in cAMP signaling

We have assumed that the initial peak of cAMP signaling response is primarily relevant to cAMP oscillation but the following peaks of the response, or its oscillatory behavior, are not. One might think that the oscillatory behavior in cAMP signaling response observed at the single cell level directly explains cAMP oscillation at the population level, but it's not. Here we summarize observations that support our assumption and explain how the two oscillations observed at the single-cell level and at the population level are different.

Single-cell level oscillatory dynamics in cAMP signaling response

The necessity to discriminate between the two modes of oscillation in cAMP signaling has emerged only recently because the multiple peaks in cAMP signaling response have been observed for the first time in 2010 at the single-cell level by using FRET-based cAMP sensor [47]. This was in contrast to the previous measurements on populations of cells, in which cAMP signaling response were shown to consist of a unimodal peak [26, 25]. The reason for the discrepancy between the two observation can be

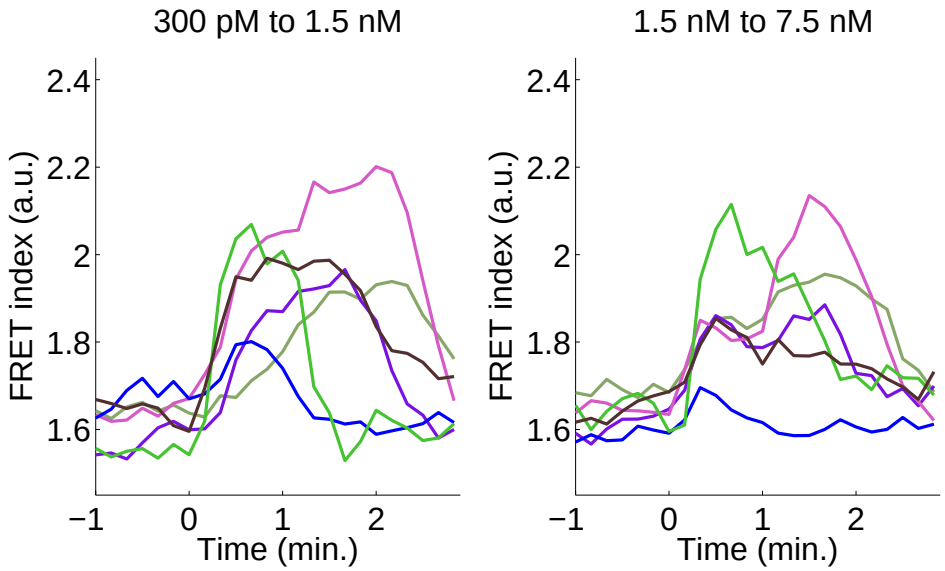

Fig. 3.18 Representative time courses of cAMP signaling response to two successive step inputs with identical fold-change. Six cells are represented by different colors and data obtained from the same cell is represented by the same color in the both panel. Here cells are first exposed to 300 pM cAMP and then 1.5 nM cAMP for 15 minutes and then 7.5 nM cAMP.

understood as follows. Suppose that each individual cells exhibit oscillation but the phases of the oscillations are not well synchronized between the cells. If the output of the system was observed only at the population level, the output would look non-oscillatory because of averaging effect [63, 81] (fig.3.20). Thus, the oscillatory property have been revealed by the virtue of single-cell analysis.

Two different oscillations observed in two different conditions; subcellular oscillation and cAMP oscillation

The observation of the oscillation at the single-cell level raised a question as to its relation to the collective behavior of cAMP oscillation. However, the two oscillations can be observed in two different experimental setup respectively (figure 3.21). The oscillation in cAMP signaling response is observed in a condition where the cells are isolated from other cells and stimulated with a *fixed* concentration of extracellular cAMP. On the other hand, cAMP oscillation is observed in a condition in which the cells are placed at a sufficiently high density and therefore are allowed to communicate with each other through secreted cAMP. As a result of secretion of cAMP, the concentration of extracellular cAMP also oscillates in cAMP oscillation. Note that the temporal properties of the input stimuli that the cells experience are totally different in the two conditions.

We name the former oscillation *subcellular oscillation*, whereas we call the latter

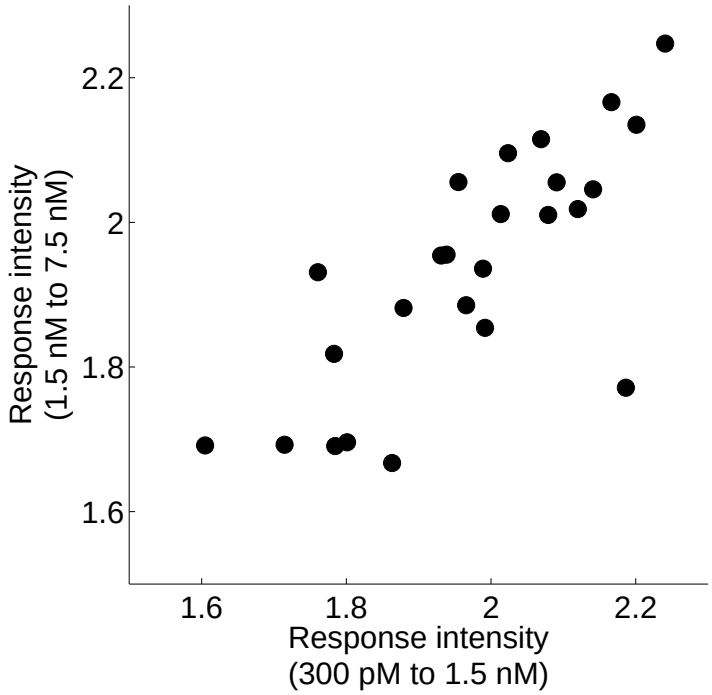

Fig. 3.19 A scatter plot that shows correlation of two amplitudes of the responses to two successive step inputs with identical fold-change. Each dot is a measurement obtained from an individual cell ($R = 0.68$).

cAMP oscillation as customary. Note that we call it *subcellular* oscillation because the oscillation can be observed even in a constant level of extracellular cAMP, that is to say, the molecular mechanism responsible for the oscillation exists within the intracellular, or subcellular, space (left panel in figure 3.21). On the other hand, cAMP oscillation requires the concentration of extracellular cAMP to oscillate (right panel in figure 3.21). In fact, externally-applied extracellular cAMP perturbs the oscillation significantly (as more fully discussed in chapter 5), meaning that the molecular circuit responsible for cAMP oscillation contains the concentration of extracellular cAMP. Also, as shown in figure 3.13, a periodic stimuli evoke only initial peaks at the up-phase of the stimuli but no following peaks. Thus, we conclude that the two modes of oscillations are different in their dependence on extracellular condition and therefore in their mechanisms.

The periodicity of the oscillations are different.

As discussed, some experimental evidences show that the two oscillations are different in their mechanisms. In addition to that, the periods of the two oscillations are different. As mentioned in chapter 1, the periodicity of cAMP oscillation is ∼6 minutes both in vivo and in the perfusion chamber (figure 1.18). However the periodicity of cAMP signaling response is significantly faster than that of cAMP oscillation. To quantify the periodicity of the spikes in cAMP signaling response, we conducted autocorrelation analysis. Figure 3.22 shows the results where the cells are stimulated with 10 nM and 1 μM cAMP. Although the sustainability of the oscillation depends on

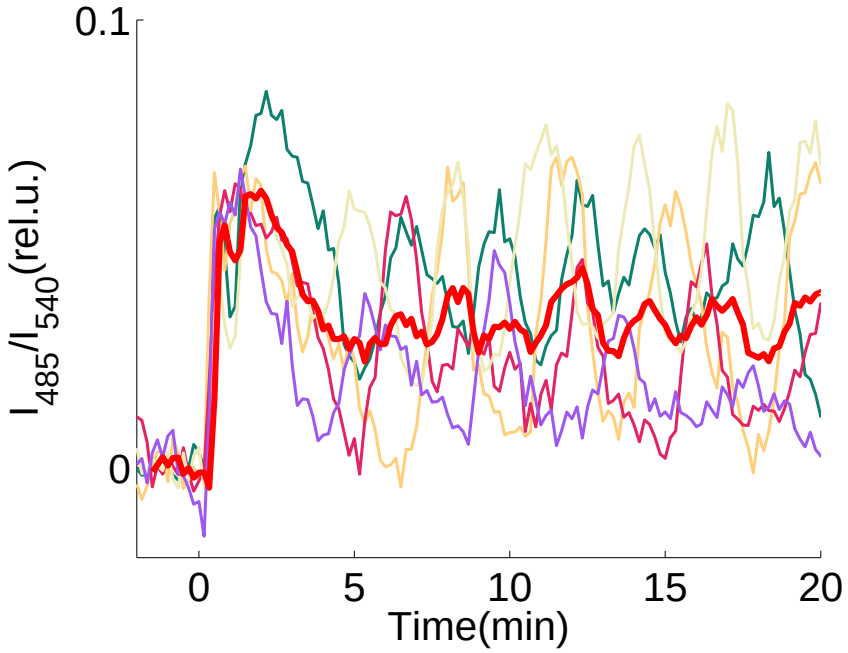

Fig. 3.20 Comparison of individual and averaged cAMP response. Cells are exposed to a constant flow of buffer with or without cAMP. Thin lines indicate response in five cells to 1 μM extracellular cAMP applied at time zero. The red line in bold is the group average. Peaks after the initial spike are not clearly visible in the averaged signal.

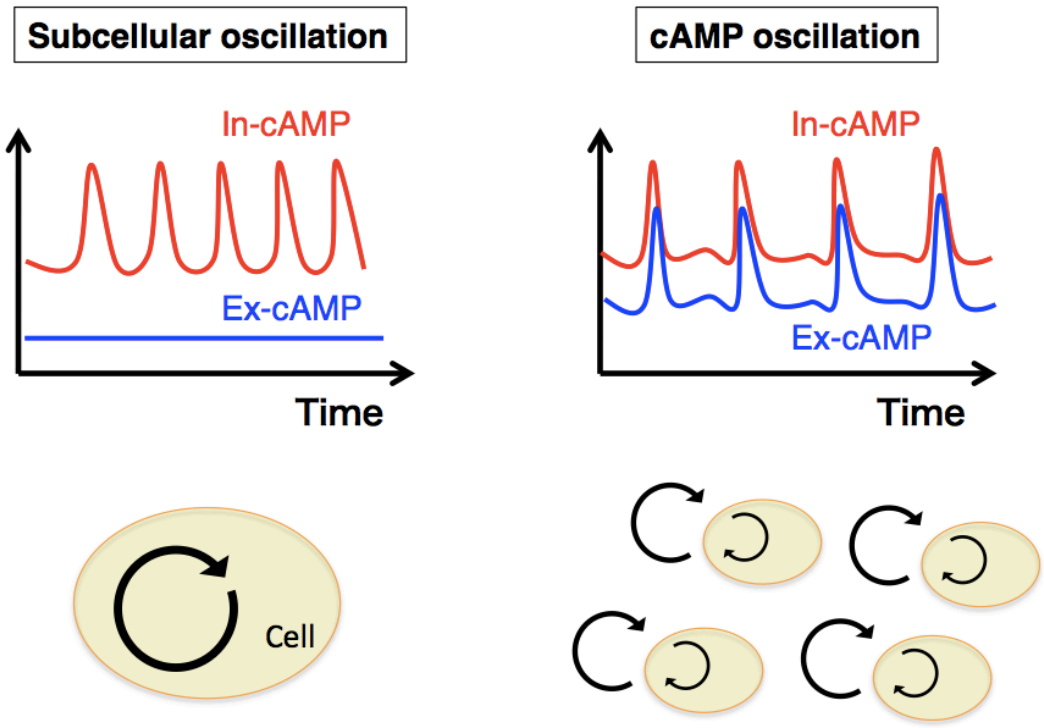

Fig. 3.21 Two modes of oscillation in cAMP signaling system.

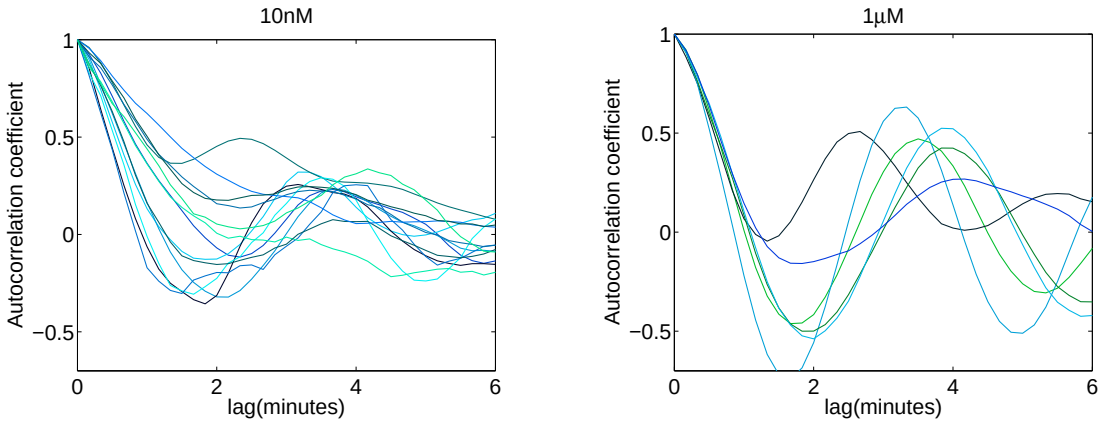

Fig. 3.22 Autocorrelation function of cAMP signaling response defined as $\phi(\tau) = E\{(Y(t) - E\{Y(t)\})(Y(t-\tau) - E\{Y(t)\})\}$, where $Y(t)$ represents time series of cAMP signaling response and $E\{\ \}$ represents expectation operator.

the concentration of extracellular cMAP as discussed in section 3.2.1, the periodicity seems to be independent of the concentration and is constant at approximately 3 to 4 minutes.

Thus, it is now clear that the oscillatory property in cAMP signaling response can not explain cAMP oscillation by itself. This raise a question as to the biological importance of the oscillation in cAMP signaling response. It is conceivable that the fast oscillation is functioning at the later stage of *Dictyostelium* development. In fact, it has been reported that the frequency of cAMP oscillation increases at the aggregation or mound stage [30, 31]. It would be interesting to investigate the relation between the single-cell level oscillation and the collective behavior observed in the later development in the future.

Chapter 4

A possible function of fold-change detection in cell-cell signaling

4.1 Introduction

In the previous chapter, it has been demonstrated that the initial peak of cAMP signaling response follows fold-change detection (FCD). One of the prominent features in cAMP signaling response is that the output of the response, i.e., intracellular cAMP, is secreted to extracellular space and therefore it can feed back to the cell. As briefly discussed in section 1.4, the positive feedback loop resulting from the secretion of cAMP is the reason for cAMP oscillation during development: Adaptability of cAMP signaling response suggests that there exists a suppressive interaction between molecular species within the cell. The suppressive interaction essentially composes an incoherent feedforward loop (left panel in figure 4.1) or a negative feedback loop (right panel in figure 4.1) [72]. Because of the secretion of cAMP (dotted line in figure 4.1), both system have one positive feedback loop and one negative feedback loop in it. Such a network topology is capable of oscillation [85]. This is intuitively explained as follows. The positive feedback loop consisting of secretion of cAMP and detection of the molecule make quiescent state unstable and leads to higher concentration of cAMP. However, the process of the increase of cAMP is interrupted at a certain point as the suppressive effect resulting from adaptability of the cell become stronger and therefore the concentration of cAMP begin to decrease. The newly-achieved low-concentration state is again unstable and therefore the system proceeds to oscillate.

Then, how could the FCD property in *Dictyostelium* cells be advantageous in this cAMP-mediated cell-cell signaling? To answer the question, in this chapter, we try to understand the function of FCD by using a mathematical description of communicating cells capable of FCD. Through the analysis of the model, we propose the hypothesis that the FCD property of *Dictyostelium* cells enables cAMP oscillation to be robust to cell density. The explanatory power of the models are partially discussed by reproducing a feature of the phase diagram (figure 1.18), which has been obtained from measurements on the cell populations in the perfusion chamber [47]. The model is further corroborated in the next chapter by more closely investigating the property of cAMP oscillation in the perfusion chamber.

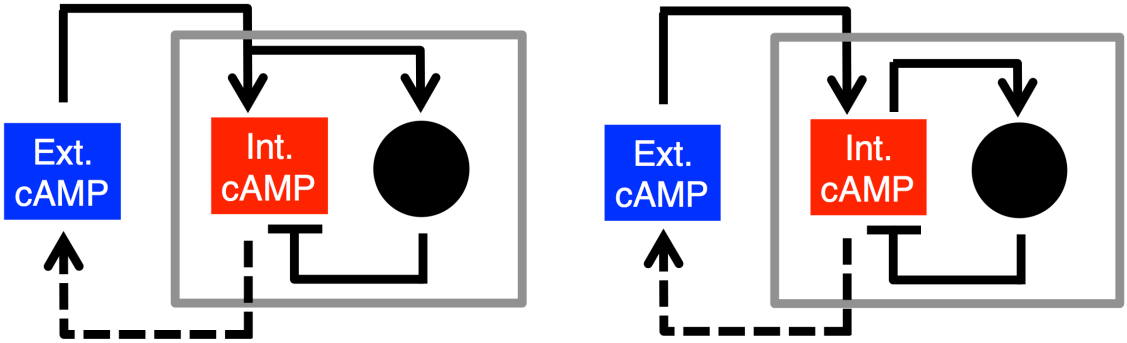

Fig. 4.1 Network topologies describing cAMP-mediated cell-cell signaling in *Dictyostelium* cells.

4.2 Results and discussions

4.2.1 Robustness to cell density in cell-cell signaling enabled by the FCD property of the cells: a mathematical formulation

Consider a cell described by a set of ordinary differential equations, with internal variable x, output y and input z. The dynamics of these variables are

$$\begin{aligned} \dot{x} &= f(x, y, z) \\ \dot{y} &= g(x, y, z). \end{aligned} \tag{4.1}$$

FCD is defined as follows. Consider a system that is initially at steady state. FCD means that the output $y(t)$ is exactly the same for any two inputs $z_1(t)$ and $z_2(t)$ that are proportional to each other, $z_2(t) = pz_1(t)$, for any $p > 0$ and $z_1(t) > 0$. By definition, a system capable of FCD yields precisely the same temporal output to, for example, two step inputs with the same fold change but different absolute level (cf. figure 1.7).

It has been shown that FCD holds if the system is stable[*1], shows exact adaptation[*2], and g and f satisfy the following condition for any $p > 0$ with an appropriate

[*1] The system is stable, under a constant input, if every trajectories approaches a fixed point of which value is dependent on the input strength in general.

[*2] The system exactly adapts, under a constant input, if there exists a fixed point of which value is independent of the input strength. Note that the notion of *perfect adaptation* used in biology corresponds to a system's property where the system is *stable* and capable of *exact adaptation* [97] because the mathematical definition of exact adaptation does not refer to the stability of the fixed point.

function ϕ [97] (proof shown in Appendix 4.3.1)[*3]:

$$f(\phi(p,x),y,pz) = \frac{\partial\phi(p,x)}{\partial x} f(x,y,z) \tag{4.2}$$

$$g(\phi(p,x),y,pz) = g(x,y,z). \tag{4.3}$$

As mentioned in section 1.3, in a perfusion chamber with a large number of cells in it, the concentration of extracellular cAMP is governed by the equation $\frac{d[cAMP]_{ext}(t)}{dt} = \rho k_t [cAMP]_{int}(t) - \gamma [cAMP]_{ext}(t)$ (equation 1.1). Here $[cAMP]_{ext}$ can be seen as input (z) and $[cAMP]_{int}$ as output (y) and therefore the equation can be written as

$$\dot{z} = \rho k_t y - \gamma z, \tag{4.4}$$

using the same notation as in equation 4.1. Combining equations 4.1 and equation 4.4, the whole system, i.e., cells communicating with each other in the perfusion chamber, can be described as

$$\begin{aligned} \dot{x} &= f(x,y,z) \\ \dot{y} &= g(x,y,z) \\ \dot{z} &= \rho k_t y - \gamma z. \end{aligned} \tag{4.5}$$

where f, g satisfy the condition 4.2, 4.3 respectively. Note that here we consider a situation where the extracellular cellular environment is spatially uniform and therefore the state of each individual cells, which would be specified by x_i and y_i, are all synchronized and hence represented by x and y.

Here we show that the system 4.5 is invariant under the transformation

$$\begin{aligned} x &\to \phi(p,X) \\ z &\to pZ \\ \rho &\to p\rho. \end{aligned} \tag{4.6}$$

This yields that

$$\begin{aligned} \dot{X} &= \frac{1}{\frac{\partial\phi}{\partial X}} f(\phi(p,X),y,pZ) \\ &= f(X,y,Z), \end{aligned}$$

using the condition 4.2 and

$$\begin{aligned} \dot{y} &= g(\phi(p,X),y,pZ) \\ &= g(X,y,Z), \end{aligned}$$

using the condition 4.3. The equation for z is transformed to

$$\begin{aligned} p\dot{Z} &= p\rho k_t y - \gamma pZ \\ \iff Z &= \rho k_t y - \gamma Z. \end{aligned}$$

[*3] This condition is not only sufficient but necessary for a system to be able to exhibit FCD if the system is controllable and observable in the sense of control theory [97].

Therefore the whole equations become

$$\begin{aligned} \dot{X} &= f(X, y, Z) \\ \dot{y} &= g(X, y, Z) \\ \dot{Z} &= \rho k_t y - \gamma Z. \end{aligned} \tag{4.7}$$

The invariance of equations 7.2.1 to the transformation 4.6 means that the system's output $y(t)$ is independent of the parameter ρ. As the parameter ρ represents cell density, we conclude that the output of the system 7.2.1 is robust to variations in cell density. Also, it is obvious from the proof that the reason why the robustness emerged in the system is that the cells, i.e., the subsystem consisting of x and y, exhibit FCD.

4.2.2 Phenomenological models capable of robust oscillation by means of fold-change detection

In the previous subsection, we have shown that the equations 4.5 that describes communicating cells capable of FCD in the perfusion chamber is invariant under the transformation. This leads us to hypothesize that the robustness of cAMP oscillation to cell density in the perfusion chamber also based on the FCD property at the single-cell level. As a first step towards corroboration of the hypothesis, here we develop phenomenological models whose outputs are independent of cell density and capable of oscillation. Predictions of these models are compared with experimental results later.

Two-node three-link circuits capable of FCD.

In the preceding works, it was demonstrated that a type of incoherent feedforward loop [43] and several types of negative feedback loops [97] are able to show FCD. Importantly, these ODE models are equipped with circuits as simple as two-node three-link network topology. In the models, one node represents the output of the system, another node plays a regulatory role in a topology-dependent manner, and both of the nodes can be affected by input signal. Two-node three-link network topology is the simplest framework for FCD because the topology is required for a system to be able to exhibit perfect adaptation, which is a prerequisite for FCD.

Here we propose four networks as the simplest models capable of robust FCD (figure 4.2 and 4.3) based on the preceding works [43, 97]. What we mean by robust here is that the property of FCD of the models are independent of the precise parameter values. The network topologies of the four networks are either a incoherent feedforward loop (figure 4.2 for model (a) and (b)) or a negative feedback loop (figure 4.3 for model (c) and (d))[*4]. Those networks exhibit FCD because all models satisfy the conditions for FCD: $f(\phi(p,x), y, pz) = \frac{\partial \phi(p,x)}{\partial x} f(x, y, z)$, $g(\phi(p,x), y, pz) = g(x, y, z)$ (equations 4.2 and 4.3) by choosing $\phi(p, x) = px$ for network (a), (c) and (d), and

[*4] Either of the topologies would be required for FCD because it has been shown by a computational search that either of them is necessary for a system to exhibit adaptation [72].

$\phi(p, x) = x/p$ for network (b)[*5] [*6].

The FCD models with an additional positive feedback loop can have oscillatory solutions. Now that we have obtained several two-variable models capable of FCD, we examine whether the models can exhibit oscillatory output when input variable z obey the equation $\dot{z} = \rho k_t y - \gamma z$ (equation 4.4). We recall adding the equation to the FCD models is a mathematical representation of cell-cell signaling; the cells are allowed to communicate with each other by secretion and recognition of the signaling molecule z. In other words, adding equation 4.4 to the models means to introduce a positive feedback loop through extracellular space (figure 4.4).

In addition to that, in order for an ODE system to exhibit limit cycle oscillation, it is required that there is sufficient nonlineality in the equations [85]. To introduce such nonlinearlity into the models we substitute the term that represents activation of output variable y by input z (i.e., z/x for (a), (b) and (c) , zx for (b)) by Michaelis-Menten equation as $z/x \rightarrow z^n/(z^n + (Kx)^n)$ or $zx \rightarrow (zx)^n/((zx)^n + K^n)$. Note this substitution introduces a saturation effect of input stimuli z when it is sufficiently large while it does not change the FCD property, i.e., the conditions for FCD (eq.4.2 and 4.3) still hold. With these modifications, all the three-variable models are capable of oscillation (figure 4.5 and 4.6).

The three-variable models exhibit robust oscillation to cell density
From the previous discussion (subsubsection 4.2.1), it is obvious that the equations are invariant under the transformation 4.6. That is, the oscillatory outputs, $y(t)$, of

[*5] One can also think of FCD models based on negative feedback loops which satisfy the condition for FCD (equations 4.2 and 4.3) by choosing $\phi(p, x) = x/p$ instead of $\phi(p, x) = px$. However such models can be obtained by a transformation of variable, $x = 1/\xi$, of the model (c) and (d) and therefore we here confine our interest only to model (c) and (d).

[*6] A more intuitive way to show the FCD property of the models is as follows. Here we consider the case of the model (a) in figure 4.2 but similar considerations are applicable to other models. The model (a) can be written as

$$\begin{aligned} \dot{x} &= az - bx \\ \dot{y} &= c\frac{z}{x} - dy. \end{aligned} \tag{4.8}$$

Let us define the following dimensionless variables,

$$\begin{aligned} X &= \frac{x}{(a/b)z_0} \\ Y &= \frac{y}{cb/ad}, \end{aligned}$$

in which the variables x and y are normalized by the steady-state solutions for $z = z_0$. Then the equations 4.8 become

$$\begin{aligned} \frac{1}{b}\dot{X} &= z/z_0 - X \\ \frac{1}{d}\dot{Y} &= \frac{(z/z_0)}{X} - Y. \end{aligned}$$

Observe in the equations the dynamics of X and Y (and therefore y) only depends on fold-change in z, which is the FCD property.

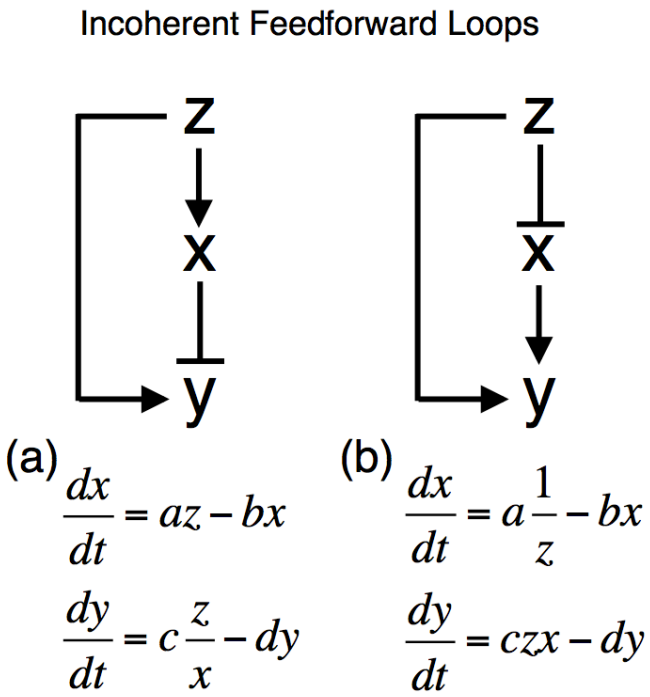

Fig. 4.2 The simplest models capable of FCD based on incoherent feed-forward loop (IFFL). Normal arrows indicate activation effects and blunt edges denote inhibitory effects. The network (a) has already been reported in the preceding work[97].

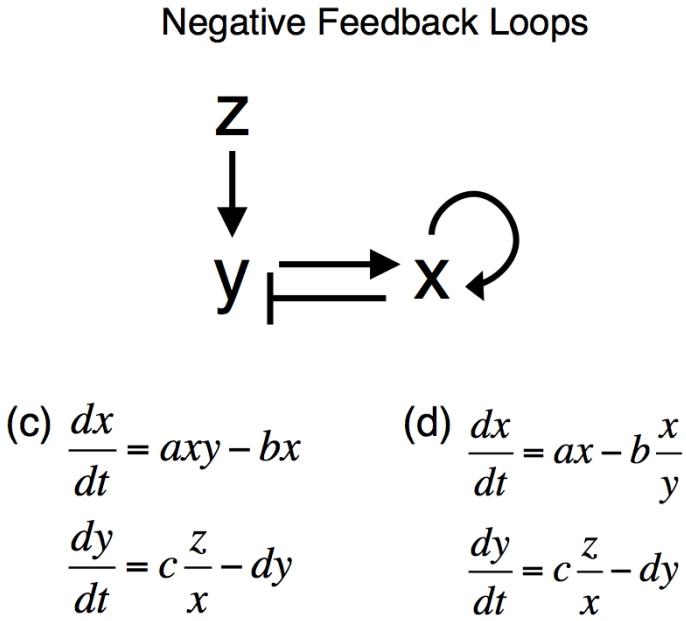

Fig. 4.3 The simplest models capable of FCD based on negative feedback loop. Normal arrows indicate activation effects and blunt edges denote inhibitory effects. The network (c) has already been reported in the preceding work[97].

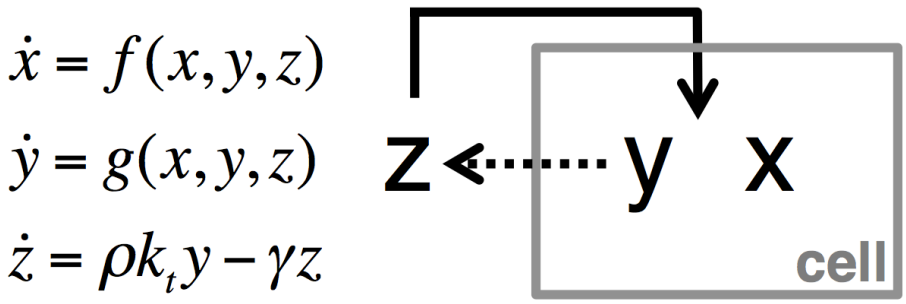

Fig. 4.4 Introducing the equation for z, which corresponds to the concentration of extracellular signaling molecule, can be interpreted as adding a positive feedback loop to the system consisting of secretion of signaling molecules (dotted arrow) and recognition of the molecules (normal arrow).

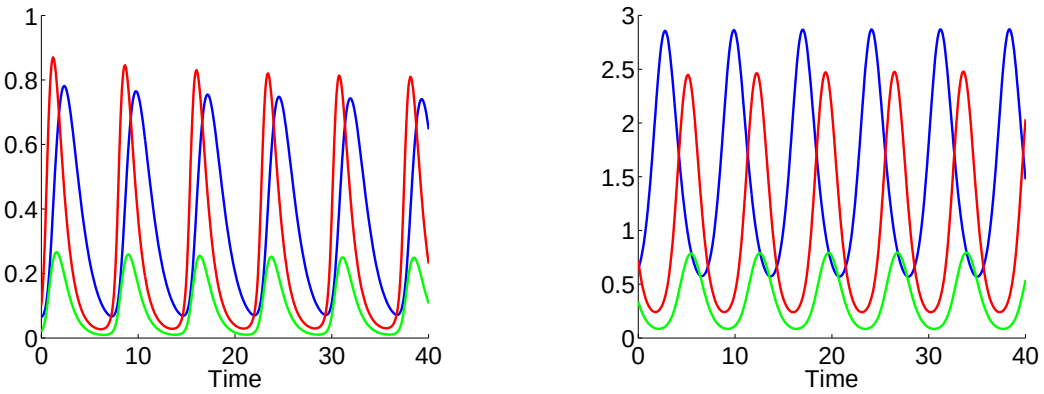

Fig. 4.5 Representative time courses of oscillatory solutions of the models based on incoherent feedforward loops (figure 4.2). Blue, red and green lines represent x, y and z respectively. Left panel is the modified version of model (a): $\dot{x} = az - bx$, $\dot{y} = cz^n/(z^n + (Kx)^n) - dy$, $\dot{z} = \rho k_t y - \gamma z$ where $a = 4$, $b = 1$, $c = 5$, $d = 1.5$, $n = 2$, $K = 1$, $\rho k_t = 1$ and $\gamma = 3$. Right panel is the modified version of model (b): $\dot{x} = a/z - bx$, $\dot{y} = c(zx)^n/((zx)^n + K^n) - dy$, $\dot{z} = \rho k_t y - \gamma z$ where $a = 0.3$, $b = 1$, $c = 12$, $d = 1.7$, $n = 2$, $K = 1$, $\rho k_t = 1$ and $\gamma = 3$.

the models are invariant to variations in cell density ρ. Just to show specific example, we demonstrate the invariance by using our models introduced above. Here we take a model (a) (with a positive feedback loop and nonlineality in input function) as an example but the same is true for other models. The equation of the model (a) can be written as

$$\begin{aligned} \dot{x} &= f(x,y) = az - bx \\ \dot{y} &= g(x,y) = c\frac{z^n}{z^n + (Kx)^n} - dy \\ \dot{z} &= \rho k_t y - \gamma z. \end{aligned} \tag{4.9}$$

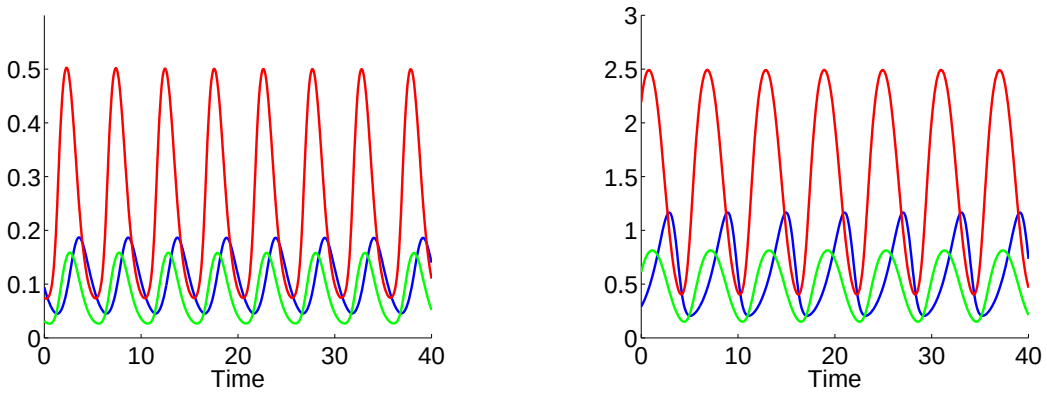

Fig. 4.6 Representative time courses of oscillatory solutions of the models based on negative feedback loops (figure 4.3). Blue, red and green lines represent x, y and z respectively. Left panel corresponded to the modified version of model (c) : $\dot{x} = axy - bx$, $\dot{y} = c(z^n)/(z^n + (Kx)^n) - dy$, $\dot{z} = \rho k_t y - \gamma z$ where $a = 4$, $b = 1$, $c = 2$, $d = 3$, $n = 2$, $K = 1$, $\rho k_t = 1$ and $\gamma = 3$. Right panel corresponded to the modified version of model (d): $\dot{x} = ax - b(x/y)$, $\dot{y} = czx^n/(zx^n + (K)^n) - dy$, $\dot{z} = \rho k_t y - \gamma z$ where $a = 1$, $b = 1$, $c = 5$, $d = 1.5$, $n = 2$, $K = 1$, $\rho k_t = 1$ and $\gamma = 3$.

The subsystem x, y of this equation satisfies the FCD condition (equations 4.2 and 4.3) if we take ϕ as $\phi(p, x) = px$. Therefore we transform the variables as (in the same way as equations 4.6)

$$\begin{aligned} x &\to px \\ z &\to pz \\ \rho &\to p\rho. \end{aligned} \tag{4.10}$$

This yields

$$\begin{aligned} \dot{X} &= aZ - bX \\ \dot{y} &= c\frac{Z^n}{Z^n + (KX)^n} - dy \\ \dot{Z} &= \rho k_t y - \gamma Z. \end{aligned}$$

That is, the equations are invariant under the transformation of 4.10, meaning the output variable, $y(t)$, is invariant to variations in cell density. Figure 4.7 shows a representative time courses of the model 4.9 and its dependence on cell density ρ. As is obvious from equations 4.10, x and z is linearly dependent on ρ whereas the output variable y is independent of ρ.

The models reproduce the robust property of cAMP oscillation in the perfusion chamber. In section 1.4, we introduced an experimental result reported by Gregor et al. [47] where they examined the dependence of cAMP oscillation on cell density (ρ) and flow rate (γ) by using a perfusion chamber (figure 1.18). As mentioned there, there are

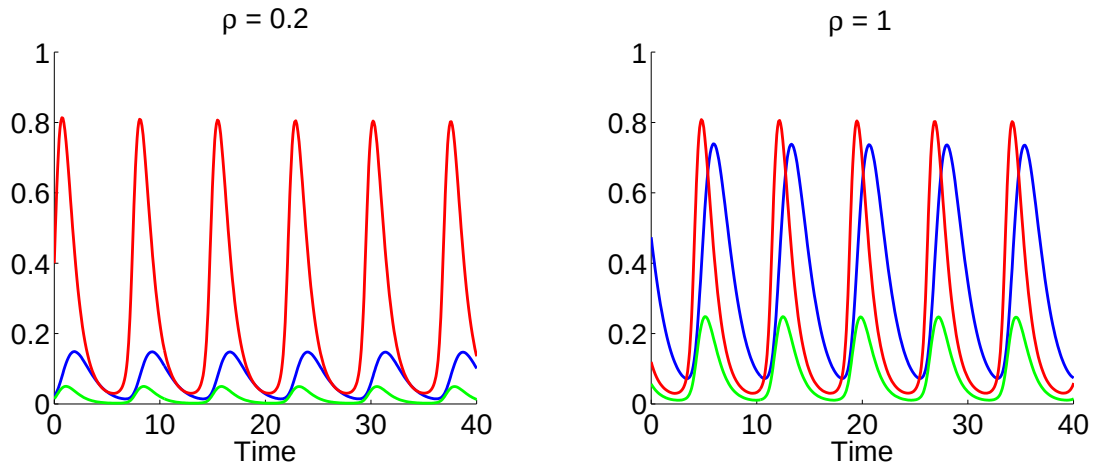

Fig. 4.7 Independence and dependence of the model 4.9 on cell density ρ. Blue, red and green lines represent x, y and z respectively. Left panel represents time courses when cell density is low ($\rho = 0.2$). Right panel represents time courses when cell density is high ($\rho = 1$). It is clearly shown that the variables x and z are dependent on cell density ρ but the output variable y is independent of the parameter. Parameter values are $a = 4$, $b = 1$, $c = 5$, $d = 1.5$, $n = 2$, $K = 1$, $k_t = 1$ and $\gamma = 3$.

oscillatory and non-oscillatory regions and the oscillatory regions have a characteristic triangular shape in the γ-ρ phase plane. There we suggested that the existence of the non-oscillatory region in high-γ and low-ρ regions can be understood by counting the lower detection limit of cAMP receptors.

Here, to include lower detection limit of input signal, we make a slight modification to the FCD models developed above and test if the models can reproduce the feature of the phase diagram. Again, we take the model (a) as an example. The model can now be written as

$$\begin{aligned} \dot{x} &= axy - bx \\ \dot{y} &= c\frac{(z+\delta)^n}{(z+\delta)^n + (Kx)^n} - dy \\ \dot{z} &= \rho k_t y - \gamma z, \end{aligned} \tag{4.11}$$

where, in the equation for y, z is substituted by $z+\delta$[*7] to introduce a lower detection limit of z to the model. Note that the cells, i.e., the subsystem x and y, no longer exhibit the FCD property in a precise sense because of the new term δ. However, when the level of input stimuli z is sufficiently high, the effect of δ would become

[*7] One can choose other function forms to introduce the lower detection limit: $c\frac{z^n}{z^n+K(x+\alpha)^n}$ or $c\frac{(z+\delta)^n}{(z+\delta)^n+K(x+\alpha)^n}$, both of which are compatible with the one described in the main text. In fact, qualitative feature of the phase diagram is independent of the choices (data not shown).

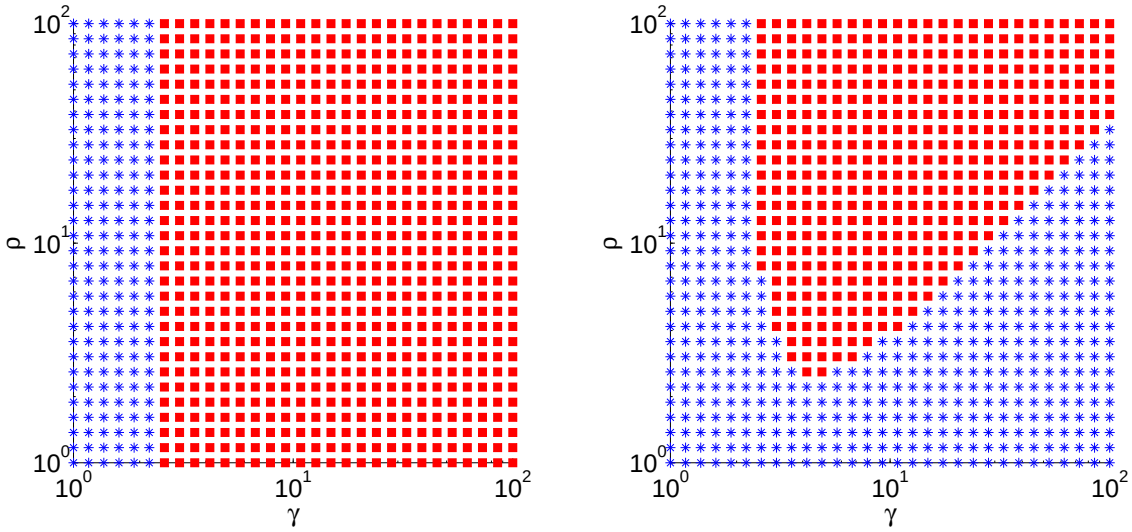

Fig. 4.8 A phase diagram that show existence and non-existence of oscillatory solution of the model 4.11. Red and blue regions represents oscillatory and non-oscillatory (equilibrium state) region respectively. Left panel represent the results calculated from the perfect FCD model ($\delta = 0$). Right panel is from the approximate FCD model ($\delta = 0.01$). The parameter values are $a = 4$, $b = 1$, $c = 5$, $d = 1.5$, $n = 2$ and $K = 1$.

negligible as the relative magnitude of z and x would become sufficiently large.

As shown in figure 4.8, the model without lower detection limit (a perfect FCD model, i.e., $\delta = 0$ in equations 4.11) exhibits oscillation even in a infinitesimally small cell density (figure 4.8 left panel). On the other hand, the model with a lower detection limit successfully reproduced the triangular shape of oscillatory region in the phase diagram (figure 4.8 right panel). This can be interpreted as follows: Because the model with lower detection limit is no longer a perfect FCD model, the system no longer exhibits oscillation at small cell-density regions in which the average level of input stimuli z is small. On the other hand, at high cell-density and low flow-rate regions, the average input level z (and therefore x) is high enough and therefore the effect of lower detection limit (i.e., the effect of δ) is negligible and therefore the cells show nearly perfect FCD. This feature of the phase diagram is also successfully reproduced with other FCD models by introducing lower detection limit of input stimuli (figure 4.9). Therefore we conclude that the robustness and triangular shape of the phase diagram results from the FCD property of each individual cells and the lower detection limit instead of the detailed structures of the system such as network topologies of the signaling system.

FCD is required for cell-cell signaling in the perfusion chamber to be robust to variations in cell density.

It has been suggested that FCD is one of the sensible strategies for a population of cells to achieve the robustness in a perfusion chamber. However, it remains unanswered whether the strategy based on FCD is the only way to achieve the robustness.

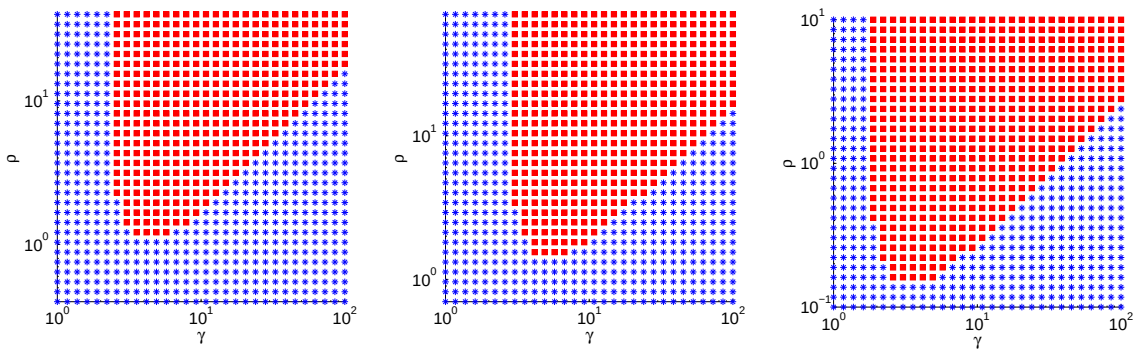

Fig. 4.9 Phase diagrams that show existence and non-existence of oscillatory solution of approximate FCD models based on model (B) (left), model (C) (middle) and model (D) (right). Red and blue regions represents oscillatory and non-oscillatory (equilibrium state) region respectively. The parameter values are (B): $a = 0.3$, $b = 1$, $c = 8$, $d = 1.7$, $n = 2$, $K = 1$ and $\delta = 0.01$, (C) : $a = 4$, $b = 1$, $c = 2$, $d = 3$, $n = 2$, $K = 1$ and $\delta = 0.01$, (D): $a = 1$, $b = 1$, $c = 5$, $d = 1.5$, $n = 2$, $K = 1$ and $\delta = 0.01$.

We consider a system written as

$$\begin{aligned} \dot{x} &= f(x, y, z) \\ \dot{y} &= g(x, y, z) \\ \dot{z} &= \rho k_t y - \gamma z, \end{aligned} \tag{4.12}$$

We denote the trajectory of a variable i $(= x,\ y,\ z)$ of the system with an initial condition μ when the cell density is ρ as:

$$\Psi_i(t, \mu, \rho),$$

and the trajectory of a variable i $(= x,\ y)$ of the subsystem composed of x and y with an initial condition ν when the input is $z(t)$ as:

$$\psi_i(t, \nu, z).$$

The robustness of the system 4.12 to cell density means that the output variable y remain invariant to any multiplication of cell density ρ. That is, there exists a initial condition μ_0' that satisfies the following condition for any p[*8]:

$$\Psi_y(t, \mu_0, \rho) = \Psi_y(t, \mu_0', p\rho). \tag{4.13}$$

Given the robustness, it is obvious that the following statement is true from the linearity of the equation for z in terms of the variable z: there exists an initial condition μ_1' that satisfies the following condition for any p:

$$\Psi_z(t, \mu_1', p\rho) = p\Psi_z(t, \mu_1, \rho). \tag{4.14}$$

[*8] Although this condition is rather strict if the initial condition μ_0 are allowed to take any value, here we assume μ_0 take values within attractors of the solutions of the system.

Given 4.13 and 4.14, the output of the subsystem composed of x and y must be invariant to any multiplication of input z. That is, there exists an initial condition ν_0' that satisfies the following condition for any p:

$$\psi_y(t, \nu_0, z(t)) = \psi_y(t, \nu_0', pz(t)). \tag{4.15}$$

This means that the system responds to only relative changes of the input, i.e., a property that characterizes systems capable of FCD[*9].

Although we showed that M&G model cannot reproduce the phase diagram (section 1.4), one might think that it may be possible to increase the robustness to cell density by choosing more appropriate parameter values. However, the discussion above strongly suggests that improving M&G model so that it can show the robustness to cell density is no more than to make the constituent cell (i.e, the subsystem (x, y)) capable of FCD. In other words, the result suggests that FCD is the only way to achieve the robustness to cell density.

4.3 Technical notes

4.3.1 A sufficient condition for FCD.

This proof is essentially the same as the one described in [97] except that here we explicitly consider a general condition for FCD instead of a special condition of which proof is described in [97].

Here we consider a system whose dynamics is

$$\dot{x} = f(x, y, z)$$
$$\dot{y} = g(x, y, z)$$

and shows stability and exact adaptation. Here, we show that if

$$f(\phi(p, x), y, pz) = \frac{\partial \phi(p, x)}{\partial x} f(x, y, z) \tag{4.16}$$
$$g(\phi(p, x), y, pz) = g(x, y, z), \tag{4.17}$$

then FCD holds. We compare the output y of the system to two different inputs: $z_1(t)$ and $z_2(t)$ with a constant ratio $p > 0$ between them, $z_2(t) = pz_1(t)$. That is, we compare the outputs y_1 and y_2 of the systems

$$\dot{x_1} = f(x_1, y_1, z_1)$$
$$\dot{y_1} = g(x_1, y_1, z_1)$$

and

$$\dot{x_2} = f(x_2, y_2, z_2)$$
$$\dot{y_2} = g(x_2, y_2, z_2).$$

[*9] It remains as a future work to show strictly whether the FCD is necessary for the robustness because the equation 4.15 is not equivalent to the definition of FCD (cf. subsection 4.2.1).

At time 0, the system is at a steady-state output y_0 in constant inputs $z_1(0) = z_1^0$ and $z_2(0) = z_2^0$. Thus, the following equations hold:

$$\begin{aligned} f(x_1^0, y_0, z_1^0) &= 0 \\ g(x_1^0, y_0, z_1^0) &= 0 \end{aligned}$$

$$\begin{aligned} f(x_2^0, y_0, z_2^0) &= 0 \\ g(x_2^0, y_0, z_2^0) &= 0 \end{aligned}$$

Using the condition 4.16 we have that

$$x_2^0 = \phi(p, x_1^0), \tag{4.18}$$

because $f(x_2^0, y_0, z_2^0) = f(x_2^0, y_0, pz_1^0) = 0$ holds and there is only one value for x that yields $f = 0$ at a given input z at steady state.

Consider the coordinate transformation for x_2 and z_2:

$$\begin{aligned} \phi(p, \tilde{x}_2) &= x_2 \\ \tilde{z}_2 &= \frac{z_2}{p}. \end{aligned}$$

By this transformation and the condition 4.16, we have that

$$\begin{aligned} \dot{x}_2 &= \frac{\partial \phi(p, \tilde{x}_2)}{\partial t} \\ &= \dot{\tilde{x}}_2 \frac{\partial \phi(p, \tilde{x}_2)}{\partial \tilde{x}_2} \end{aligned}$$

and

$$\begin{aligned} f(x_2, y_2, z_2) &= f(\phi(p, \tilde{x}_2), y_2, p\tilde{z}_2) \\ &= \frac{\partial \phi(p, \tilde{x}_2)}{\partial \tilde{x}_2} f(\tilde{x}_2, y_2, \tilde{z}_2) \\ &= \frac{\partial \phi(p, \tilde{x}_2)}{\partial \tilde{x}_2} f(\tilde{x}_2, y_2, z_1). \end{aligned}$$

Note that here we used the relation $\tilde{z}_2 = z_2/p = z_1$. Thus, the new variable $\tilde{x}_2$ follows the equation:

$$\dot{\tilde{x}}_2 = f(\tilde{x}_2, y_2, z_1).$$

On the other hand, the equation that govern the output y_2 can be written as

$$\begin{aligned} \dot{y}_2 &= g(\phi(p, \tilde{x}_2), y_2, p\tilde{z}_2) \\ &= g(\tilde{x}_2, y_2, \tilde{z}_2) \\ &= g(\tilde{x}_2, y_2, z_1), \end{aligned}$$

using the condition 4.17. The initial condition for y_2 is equal to that for y_1 $(= y_0)$ because of exact adaptation. The initial condition for $\tilde{x}_2$ $(= \tilde{x}_2^0)$ is equal to that for x_1 $(= x_1^0)$ because the following equation holds:

$$\phi(p, \tilde{x}_2^0) = x_2^0 = \phi(p, x_1^0),$$

where the equality 4.18 was used. Thus, because the initial condition for x and y are equal and their time derivatives are equal the relations, $x_1(t) = \tilde{x}_2(t)$ and $y_2(t) = y_1(t)$, holds. As the output $y_2(t)$ is identical to $y_1(1)$ despite the input is multiplied by a scalar, this means the system shows the FCD property.

4.3.2 Path inhibition in a FCD model

We used nonlinear terms such as z/x in developing FCD models. Although one might think such a term is unnatural as a biochemical interactions, there are a few conditions in which this type of regulation holds as described below.

- The term z/x can be think of as an approximation of a Michaelis-Menten inhibition term $z/(K + x)$, with $K \ll 1$ [96].
- Consider a system described in figure 4.10. This system can be written as

$$\tau\dot{\xi} = \alpha z - \beta\xi x$$
$$\dot{y} = \gamma\xi - \mu y.$$

  Then we suppose that the kinetics of the variable is sufficiently fast, i.e., the parameter τ is sufficiently small. In such a condition, a quasi-steady-state hypothesis could be justified for ξ, whose kinetic equation would then be reduce to the algebraic relation:

$$\xi = \frac{z}{x}.$$

  Therefore the dynamics of y is now governed by

$$\dot{y} = \gamma\frac{z}{x} - \mu y,$$

  where the ratio z/x contribute to the synthesis of y.

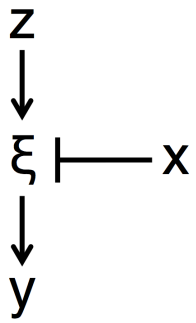

Fig. 4.10 Explicit representation of path inhibition. normal arrows indicate activation effects, and blunt edges denote inhibition.

Chapter 5

Testing the relation between FCD and the robustness to cell density

5.1 Introduction

In the previous chapter, we have developed a mathematical framework by using a set of equations, in which the combination of the FCD property of the cells and the extracellular condition in the perfusion chamber were shown to result in a scale-invariant property of the system. The scale invariance means that the system's output, i.e., intracellular cAMP, is independent of the parameter of cell density. This strongly suggests that the robustness to cell density of cAMP oscillation in the perfusion chamber results from the FCD property at the single-cell level. To deduce some testable predictions from the hypothesis, we have developed some specific phenomenological models and demonstrated that the models reproduce the essential features of the phase diagram of cAMP oscillation in the perfusion chamber. In this chapter, we show some experimental and theoretical results that further support the validity of the relation between FCD and the robustness to cell density.

Experimental tests

First, we test the predictions of the models through a series of experiments using the perfusion system. Generally speaking, it would not be obvious which property of a model should be consistent with a real system especially when discussing a phenomenological toy model: The degree of freedom of our models would be too small to reproduce all the experimental results in a *quantitative* manner. Instead, we investigate a few *qualitative* features that is closely related to the origin of cell-density robustness in the models – features that remain true as long as the constituent cells are capable of FCD. In that sense, the following features, among others, would be the key property: (i) Independence of the temporal behavior of *intracellular* cAMP to cell density in cAMP oscillation. (ii) Increases in the average concentration of *extracellualr* cAMP with cell density. As explained below, these features are closely related to our scenario about the origin of cell-density robustness while they are independent of specific details of the models such as network topology.

First of all, it is obvious that the feature (i), i.e., invariance of the dynamics of the

output variable (y or intracellular cAMP) to cell density, is the key to our discussion because the feature is the requirement for the system to be robust to cell density (figure 4.7). Nevertheless the feature has not yet been directly observed. Therefore we test whether the whole time series of the oscillation essentially remain invariant in different cell-density conditions.

The feature (ii), increases in the average concentration of *extracellualr* cAMP with cell density, results mainly from the assumption in the model's equation for z ($dz/dt = \rho k_t y - \gamma z$). That is to say, we have assumed that secretion of cAMP and its resultant increase in the concentration of extracellular cAMP is dependent on cell density (i.e., $\rho k_t y$) whereas the degradation (or dilution) of it is independent of cell density (i.e., $-\gamma z$) [*1]. The feature would also be a key in testing the relation between FCD and the robustness to cell density: if it were not for such increase in the average concentration of extracellular cAMP with cell density, then the FCD property, i.e., the property to reset sensitivity to stimuli in accordance with its basal stimulus levels, would not be required in achieving the robustness. Rather, it would become more important to understand the mechanism for keeping the average concentration constant irrespective of cell density. However the feature has not yet been addressed experimentally mainly because of the technical difficulty in measuring the concentration of extracellular cAMP in the perfusion system. Here, instead of measuring it directory, we will investigate the extracellular environment by observing the system's response to a perturbation of an externally-applied cAMP stimuli as will be described later.

A theoretical test

In addition to those experimental corroborations, we will ask whether our phenomenological models are capable of *excitation* with a little bit of modification. One of the characteristics observed during *Dictyostelium* development is propagating waves of cAMP over a layer of signaling cells (figure 1.2). It has been realized that the waves have a generic properties of excitable media, in that the waves propagate unidirectionally without damping in amplitude and those waves annihilate when two fronts collide [34]. Both excitability and oscillatory property of the cell population are observed in the course of the development and the way the cells transit between the two states have been considered to be a key to make macroscopic spiral patterns [67]. From the dynamical systems point of view, excitability and oscillation are closely related in that an excitable system often bifurcates and become oscillatory depending on the values of parameters [103]. Therefore it would be fair to say that an oscillatory model capable of bifurcation to excitable state better describes cAMP oscillation than a oscillatory model incapable of bifurcation [44]. Although the FCD-based oscillatory models introduced in the previous chapter do not show excitability by themselves, we show that a bit of modification of the models makes them excitable without changing the FCD property. This result also strongly support the validity of our phenomenological modeling.

[*1] In other words, we have assumed that the decrease in the concentration of extracellular cAMP is not attributed to cell-secreted molecules such as phosphodiesterase. The concentration of the molecule would be dependent on cell density.

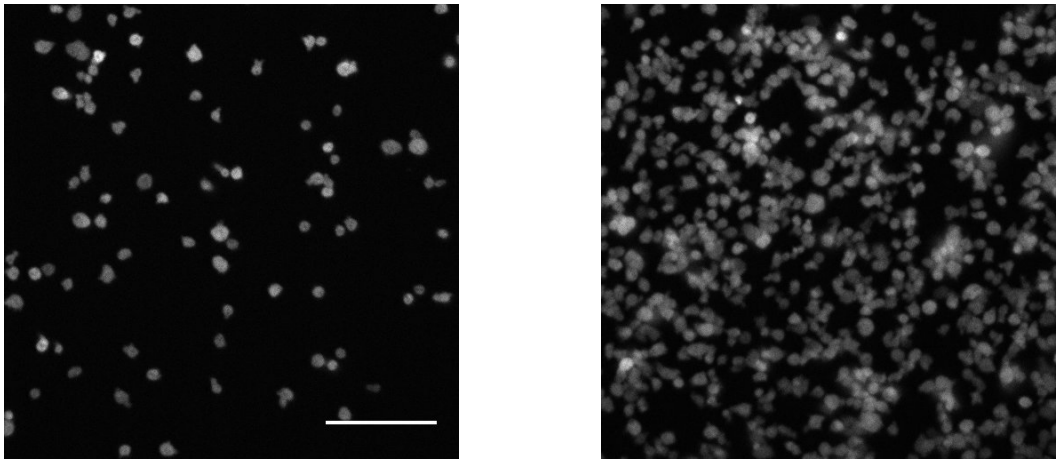

Fig. 5.1 Images of the cells at 1/10 ML (left) and 1/2 ML (right) obtained by the FRET channel (CFP excitation filter and YFP emission filter) through 20x objective lens. The scale bar represents 100 μm. In the experiments at the population level described in this chapter, the flow rate of perfusion was kept 1.5 ml/min in the both conditions unless otherwise noted.

5.2 Results and discussions

5.2.1 Invariance of the temporal behavior of the output variable in different cell-density conditions.

The key feature of the models is that the dynamics of the output variable is independent of cell density (the feature (i)). Here we compare the dynamics of cAMP oscillation between a low-cell-density condition (1/10 ML) and a high-cell-density condition (1/2 ML). We use the corrected FRET ratio (FRET index) which allows us to compare its absolute value of the signal as well as its temporal information as discussed in chapter 2.

Figure 5.1 shows representative images of cell populations at the density of 1/10 ML (left) and 1/2 ML (right) obtained through 20x objective lens. It is clear from these images that the spatial occupancy by the cells are significantly different between these two conditions. Figure 5.2 shows representative time courses of cAMP oscillation in the two different conditions. The FRET index was obtained at the population level, i.e., the averaged intensities with background correction of CFP image and FRET image (and YFP image for correction) were used to obtain the FRET index. In the preceding study [47], it has been demonstrated that the periodicity of the oscillation is nearly constant at 6 minutes over a wide range of cell density on average except at a critical point where transition from quiescence to oscillation occurs [47].

Figure 5.3 shows FRET index values at the top and at the bottom during cAMP oscillation in two different cell-density conditions (i.e., 1/10 ML and 1/2 ML). This clearly shows that, regardless of the five-fold difference in cell density, there is no significant difference between the two in their absolute values of the FRET indexes both

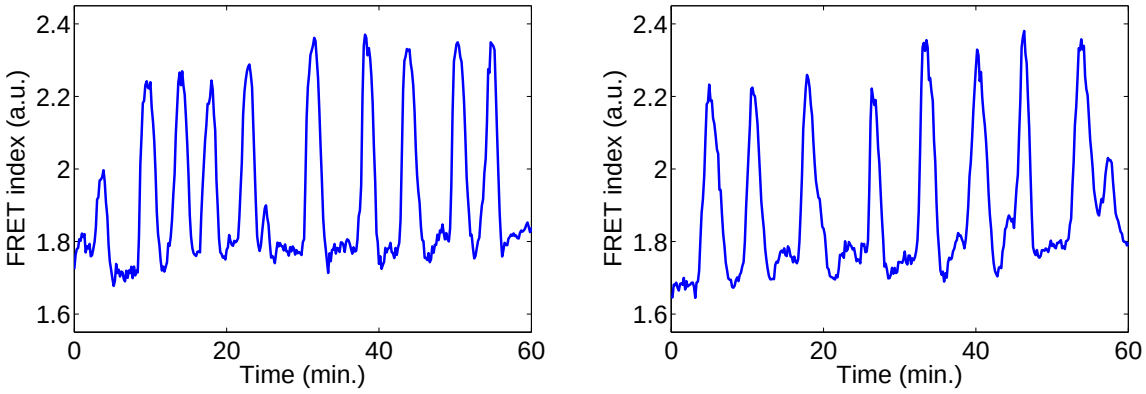

Fig. 5.2 Representative time courses of cAMP oscillation at the population level. Left panel shows cAMP oscillation at the density of 1/10 ML. Right panel shows cAMP oscillation at the density of 1/2 ML.

at the top and the bottom. As the corrected FRET index is a single-valued function of the concentration of intracellular cAMP in a fixed experimental condition[14], the result means that the absolute concentration of intracellular cAMP is not dependent on cell density as well as its average periodicity.

5.2.2 Increase in the average concentration of extracellular cAMP with cell density.

It has been demonstrated that, during cAMP oscillation, the concentration of extracellular cAMP exhibits oscillation [40, 109] as a result of secretion of intracellular cAMP to outer space [27]. In addition, the dynamics of cAMP oscillation is significantly affected by externally-applied cAMP [39], demonstrating extracellular cAMP is one of the key factors consisting of the chemical circuit responsible for the oscillation. Here, by using the perfusion system, we test how the oscillation is perturbed by externally-applied cAMP and whether the effects are dependent on cell density. This experiments would corroborate the prediction of our molds, i.e., the average concentration of extracellular cAMP increases with cell density (the feature (ii)): if it is true in the real system, the oscillation at higher cell density (and therefore higher average concentration of extracellular cAMP) would be more insensitive to a small amount of externally-applied cAMP than the oscillation at lower cell density. This is because the relative magnitude of the perturbation to the average concentration is different between the two conditions[*2]. As a perturbation, we adopted a constant elevation of basal level in extracellular cAMP because such relatively simple interference with the system can be expressed explicitly in the equations of our phenomenological model and therefore it enables us to compare the results between the experimental results

[*2] Here we are assuming that the relative scale of the perturbation is important because the constituent cells detect the relative change of extracellular cAMP.

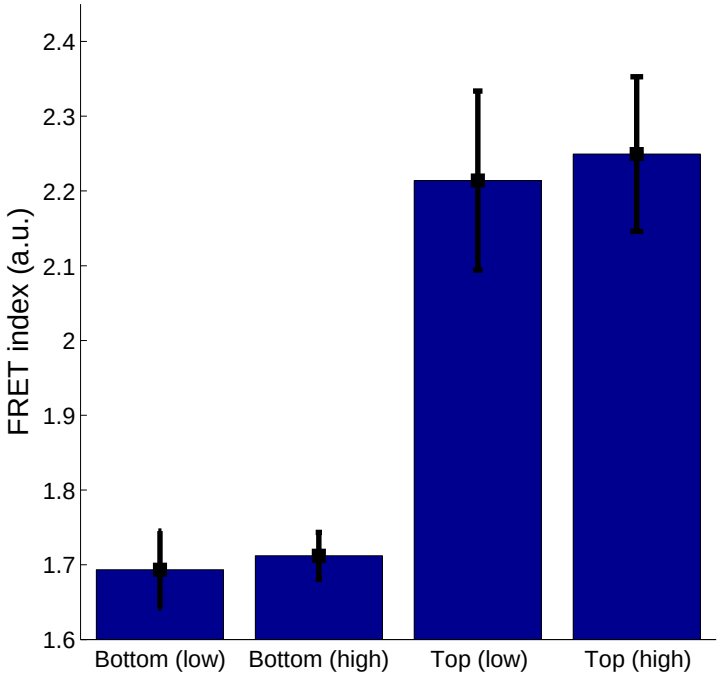

Fig. 5.3 FRET index values at the top and bottom during cAMP oscillation. Two different cell-density conditions are compared (Low: 1/10 ML, High: 1/2 ML). More than 20 points of data are used from two independent time series data for each bar. Mean and standard deviation are shown.

and the phenomenological models.

In this case the system is governed by the equations

$$\begin{aligned} \dot{x} &= f(x, y, z) \\ \dot{y} &= g(x, y, z) \\ \dot{z} &= \rho k_t y - \gamma(z - z_0), \end{aligned} \tag{5.1}$$

where f and g satisfy the FCD condition (equation 4.2 and 4.3). The only difference here is that the new constant parameter z_0 is introduced to represents the concentration of cAMP that is applied externally by the perfusion system.

By using such perturbation, we observed the population of cells in the perfusion chamber. Here, the flow rate was kept at 1.5 ml/min during the observation. In figure 5.4, representative time courses of the FRET indexes are shown in which 0.5 nM of extracellular cAMP is applied to the system at the dotted line. cAMP oscillation at the cell density of 1/10 ML (left panel in figure 5.4) ceased after application of 500-pM cAMP ($N \geq 3$) while the oscillation at the cell density of 1/2 ML (right panel in figure 5.4) is less perturbed ($N \geq 3$). The oscillation at a higher cell density was also significantly perturbed when the level of perturbation is increased as shown in the left panel of figure 5.5, where the oscillation at the cell density of 1/2 ML is disturbed after application of 2.5-nM cAMP ($N \geq 3$). Also we confirmed that the cease of the oscillation is irreversible. The right panel in figure shows that the population of cells at the cell density of 1/2 ML starts to oscillate when externally- applied 2.5 nM

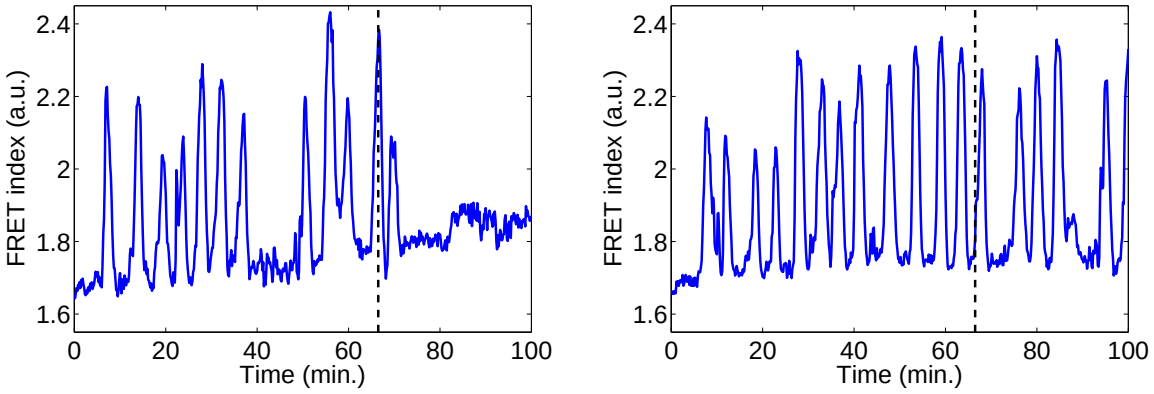

Fig. 5.4 Effects of externally-applied 500 pM cAMP to cAMP oscillation. Y-axis indicates FRET index averaged over the population of cells within a region of interest. (Left) In a relatively low cell density (1/10 ML), the oscillation is strongly perturbed by the basal increase of extracellular cAMP. (Right) On the other hand, in a relatively high cell density (1/2 ML) the same level of perturbation does not affect the oscillation very much.

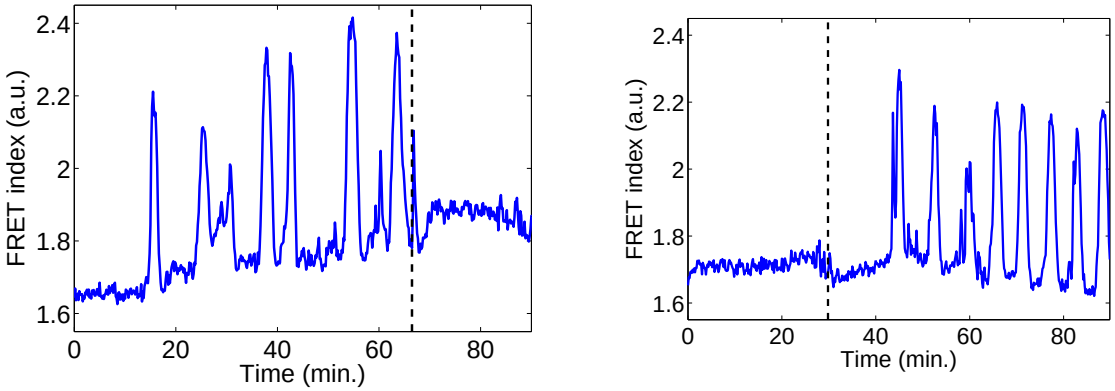

Fig. 5.5 (Left) cAMP oscillation at a high cell density (1/2 ML) can also be disturbed by a sufficiently high level of perturbation. Here 2.5 nM cAMP was applied after the dotted line. (Right) Perturbation effect of externally-applied cAMP is reversible. Here 2.5 nM cAMP was applied to a cell population of 1/2 ML until the dotted line and then removed by perfusing cAMP-free buffer. cAMP oscillation appears after the removal of external perturbation.

cAMP is removed by re-flashing cAMP-free buffer ($N \geq 2$). This result suggests that the disturbance of the oscillation by externally-applied cAMP does not result from some changes in the cellular state.

These results can be summarized as follows: (a) Sufficiently high concentration of extracellular cAMP externally applied to the system can disturb cAMP oscillation significantly. (b) The insensitivity to a certain level of elevation in the concentration of extracellular cAMP increases with cell density. Note that the results eliminate the

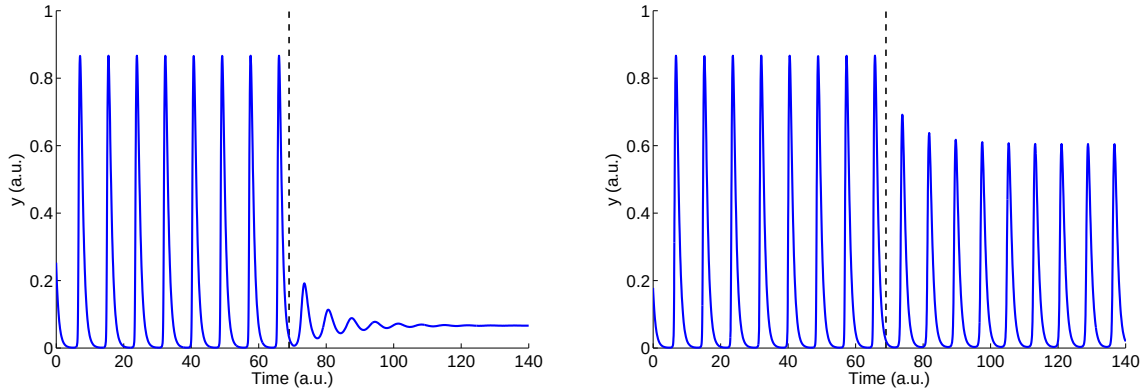

Fig. 5.6 Numerical simulation of equations 5.1 that shows different sensitivities to a perturbation in extracellular cAMP depending on cell density. In left figure cell density is low and in right figure cell density is high while the same level of perturbation is applied after the dotted line. The parameters used are $\rho = 1$ for left figure and $\rho = 20$ for right figure. Other parameters are $a = 7$, $b = 1$, $c = 5$, $d = 1.5$, $n = 2$, $k_t = 1$, K=1 and $z_0 = 0.005$.

possibility that cAMP oscillation in the perfusion chamber is a kind of noise-driven collective oscillation observed in an excitable media [79]: if one think of the system of cAMP oscillation as an excitable media with a certain *fixed* threshold, a constant elevation of extracellular cAMP would increase the probability that the noise elicit the response of cells and hence collective oscillation. Instead, our data suggests that the average concentration of extracellular cAMP are changeable depending on cell density and therefore there is no such fixed threshold for making spikes.

Next, to test whether the experimental results are consistent with the behavior of the model, we numerically calculated the equations 5.1 [*3] and try to understand the results. Figure 5.6 shows representative time courses of output variable y obtained from the simulation. It's revealed that the sensitivity of the system to a constant level of perturbation is different depending on cell density: At low cell density (left panel in figure 5.6), a certain level of perturbation is sufficient to prevent the system from oscillating, while, at high cell density (right panel in figure 5.6), the same level of perturbation does not stop oscillation. With a higher concentration of extracellular cAMP, however, the oscillation ceases even in the high cell-density condition. These results are completely consistent with the experimental results.

These behaviors can be understood as follows: First of all, observe that, with the addition of the new parameter z_0, the equations 5.1 no longer satisfies the invariant

[*3] In this subsection, to obtain specific time courses from the model, we used model A of the four models introduced in the previous chapter with the addition of the perturbation effect z_0:

$$\dot{x} = az - bx$$
$$\dot{y} = c\frac{z^n}{z^n + (Kx)^n} - dy$$
$$\dot{z} = \rho k_t y - \gamma(z - z_0).$$

However, qualitative feature of the results is independent of specific details of the model.

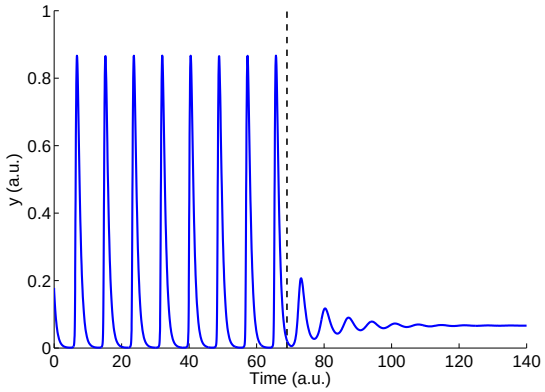

Fig. 5.7 Numerical simulation of equations 5.1 that shows different sensitivities to a perturbation in extracellular cAMP depending on cell density. The parameters values are the same as that in figure 5.6 except $\rho = 20$ and $z_0 = 0.1$

property to the transformation of variables 4.6, i.e., the system's output y is no longer independent of cell density. On the other hand, irrespective of the presence or absence of the term z_0, it is the case that the higher cell density ρ is the higher average extracellular cAMP concentration z is. It is also the case that, because of the FCD property of the cells (i.e., the subsystem consists of x and y), the key factor in eliciting cellular response is not the *absolute* change but the *relative* change in z. The reason why a (sufficiently strong) perturbation in z ceases the oscillation is that a constant increase in the average level of z by a factor, the amount of which is determined by z_0, decreases the relative changes in z (left panel in figure 5.8. Simply put, the ratio, $(z_{max} + \delta)/(z_{min} + \delta)$, decreases with increase in δ). Also the reason why the oscillation in lower cell-density condition is more sensitive to a perturbation is that a certain level of increase in the average level of z decrease the ratio of change in z more significantly than that in high cell-density condition (right panel in figure 5.8. The ratio, $(z_{max} + \delta)/(z_{min} + \delta)$, decreases with decrease in the absolute level of z_{max} and z_{min}).

Discussion: On the absolute concentration of extracellular cAMP during cAMP oscillation. We have observed that external application of 500 pM cAMP significantly disturbs cAMP oscillation at the cell density of 1/10 ML whereas the same level of perturbation does not prevent cAMP oscillation at the cell density of 1/2 ML. Here we show that the results are consistent with earlier works as well as our results obtained from single-cell level experiment by using specific biochemical parameters and the estimated concentration of intracellular cAMP.

First, we recall that we assumed a kinetic equation for extracellular environment in the perfusion chamber:

$$\dot{z} = \rho k_t y - \gamma z,$$

where the variables z and y represent the concentrations of extracellular and intracellular cAMP respectively and the parameters ρ, k_t and γ represent cell density, rate

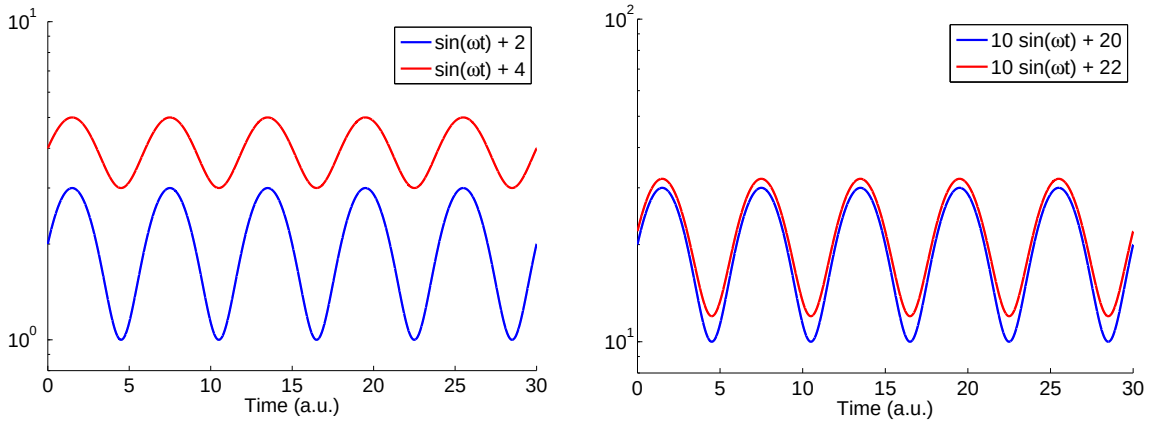

Fig. 5.8 The reasons why the dynamics of cAMP oscillation changes in a perturbation of extracellular cAMP. (Left) Relative change (such as top-to-bottom ratio) of an oscillatory dynamics with a fixed amplitude decreases with the average value of the oscillation. Therefore a constant increase in the average level of extracellular cAMP disturbs cAMP oscillation. (Right) A constant increase in the average level of an oscillation alters its relative change less significantly when the absolute level of the oscillation gets higher (compared to the left panel). Therefore a condition with higher cell density is more insensitive to a perturbation.

of cAMP secretion and rate of dilution respectively.

The parameter k_t has already been determined by an earlier experiment as approximately 0.9 (min^{-1}) [27, 73]. In the perfusion system, absolute values of cell density ρ at the cell density of 1 ML ($= 6.6 \times 10^3$ cells/mm^2) can be evaluated as follows:

$$\begin{aligned} \rho_1 &= \frac{6.6 \times 10^3 \text{ cells/mm}^2 \times \pi r^2|_{r=6.5 \text{ mm}^2} \times \frac{4\pi R^3}{3}|_{R=7.5\mu\text{m}}}{250\ \mu\text{ l}} \\ &\sim 6 \times 10^{-3}, \end{aligned} \tag{5.2}$$

where πr^2 is the glass area where the cells are placed in the perfusion chamber and R is the radius of the cells. Also the dilution rate γ is evaluated as

$$\begin{aligned} \gamma &= \frac{\text{Flow rate}}{\text{Fluid volume in the chamber}} \\ &= \frac{1.5 \text{ ml/min}}{250\ \mu\text{ l}} \\ &= 6 \text{ min}^{-1}. \end{aligned} \tag{5.3}$$

Note that the factor γ determines the time scale of the kinetics of z and that its absolute value (6 min^{-1}) is sufficiently larger than the time scale of the oscillation, which is roughly the reciprocal of the period ($1/(6 \text{ min}) = 0.17 \text{ min}^{-1}$). In such a condition, a quasi-steady-state hypothesis could be justified for z and therefore its

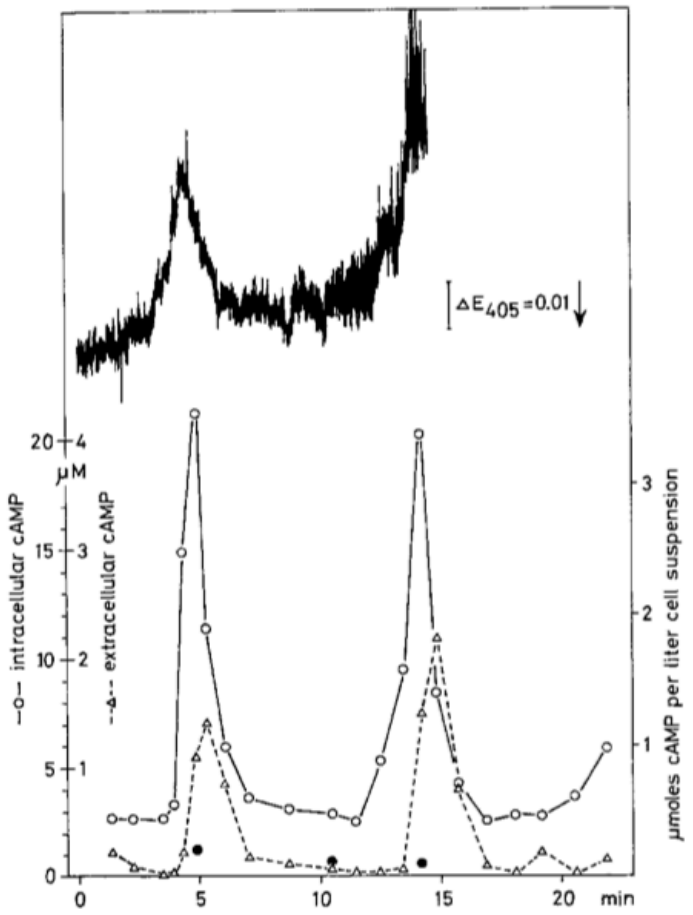

Fig. 5.9 cAMP oscillation in a cell suspension taken from Ref. [40]. The top time series represents light scattering changes in a cell suspension. The bottom two time series represents the concentration of intracellular and extracellular cAMP respectively.

kinetic equation becomes the algebraic relation:

$$z = \frac{\rho k_t}{\gamma} y.$$

In an earlier study [40], the concentration of intracellular cAMP during cAMP oscillation has been evaluated, where it was shown that the basal level of intracellular cAMP is approximately 3 μM and it increases by a factor of about 10 at the peak of cAMP oscillation (figure 5.9). By using those parameters, we can estimate the concentration of extracellular cAMP during cAMP oscillation in the perfusion chamber as follows. At the low-cell-density condition (1/10 ML), the extracellular cAMP concentrations

both at the bottom and at the top would be

$$\begin{aligned} z_{min}|_{\rho=\frac{1}{10}\mathrm{ML}} &= \frac{(1/10)\rho_1 k_t}{\gamma} y\Big|_{y=3\ \mu\mathrm{M}} \\ &= \frac{((1/10)\times 6\times 10^{-3})\times 0.9\ \mathrm{min}^{-1}}{6\ \mathrm{min}^{-1}} \times 3\ \mu\mathrm{M} \\ &\sim 3\times 10^2\ \mathrm{pM}, \end{aligned}$$

and

$$\begin{aligned} z_{max}|_{\rho=\frac{1}{10}\mathrm{ML}} &= \frac{(1/10)\rho_1 k_t}{\gamma} y\Big|_{y=30\ \mu\mathrm{M}} \\ &\sim 3\ \mathrm{nM}, \end{aligned}$$

respectively. Also, at the high-cell-density condition, the concentrations would be

$$\begin{aligned} z_{min}|_{\rho=\frac{1}{2}\mathrm{ML}} &= \frac{(1/2)\rho_1 k_t}{\gamma} y\Big|_{y=3\ \mu\mathrm{M}} \\ &\sim 1.4\ \mathrm{nM} \end{aligned}$$

and

$$\begin{aligned} z_{max}|_{\rho=\frac{1}{2}\mathrm{ML}} &= \frac{(1/2)\rho_1 k_t}{\gamma} y\Big|_{y=30\ \mu\mathrm{M}} \\ &\sim 14\ \mathrm{nM}, \end{aligned}$$

respectively. Note that the estimations are consistent with our single-cell level observation because the estimated basal concentrations are within the range over which the cells are capable of FCD (from $\sim$ 100 pM to $\sim$ 10 nM). As the absolute concentrations of cAMP in these two conditions are different, the effect of the external perturbations would also be different. One simple estimation of the effect would be to calculate the ratio (= fold change) of the maximum to the minimum of extracellular cAMP and to know how it deviates from 10-fold change. For the low-cell-density condition, this is

$$\begin{aligned} \frac{z_{max}|_{\rho=\frac{1}{10}\mathrm{ML}} + 500\ \mathrm{pM}}{z_{min}|_{\rho=\frac{1}{10}\mathrm{ML}} + 500\ \mathrm{pM}} &= \frac{3\ \mathrm{nM} + 500\ \mathrm{pM}}{3\times 10^2\ \mathrm{pM} + 500\ \mathrm{pM}} \\ &\sim 4\ \text{fold change}, \end{aligned}$$

and for the high-cell-density condition, this becomes

$$\begin{aligned} \frac{z_{max}|_{\rho=\frac{1}{2}\mathrm{ML}} + 500\ \mathrm{pM}}{z_{min}|_{\rho=\frac{1}{2}\mathrm{ML}} + 500\ \mathrm{pM}} &= \frac{14\ \mathrm{nM} + 500\ \mathrm{pM}}{1.4\ \mathrm{nM} + 500\ \mathrm{pM}} \\ &\sim 8\ \text{fold change}. \end{aligned}$$

Therefore, the effect of the perturbation is less significant for the oscillation at higher cell density.

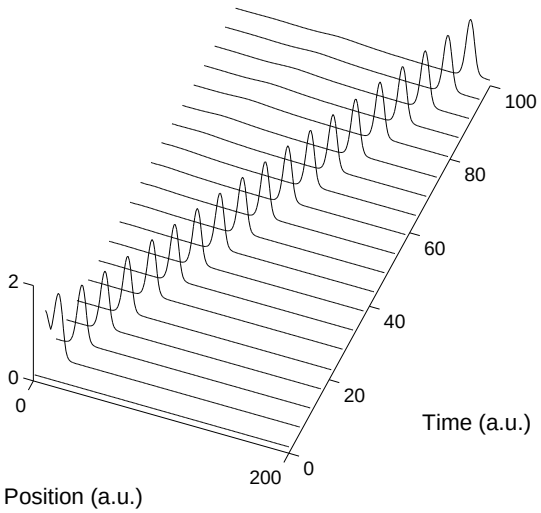

Fig. 5.10 Propagating waves of equations 5.4. Parameter values used here are $a = 0.28$, $b = 0.04$, $c = 5$, $d = 1.5$, $\alpha = 0.1$, $n = 2$, $K = 1$, $\rho = 10$, $\gamma = 15$ and $D = 20$.

5.2.3 The models reproduce the property of excitable media.

As we have introduced in the section 5.1, the models we have developed in the previous section are capable of oscillation but not of excitation. Here we make the models capable of both properties with a little bit of (and biochemically-acceptable) modification. The modified equations of the model (a)[*4] are:

$$\begin{aligned} \dot{x} &= axy - bx \\ \dot{y} &= c\frac{z^n}{z^n + (Kx)^n} - dy + \alpha \\ \dot{z} &= \rho y - \gamma z + D\nabla^2 z, \end{aligned} \tag{5.4}$$

where a constant α is added to the equation for y and an diffusion effect of z is taken into consideration to test the stability of propagating waves. The new term α can be interpreted as a basal activity of ACA by which the output value y become to have nonzero value even when the input is absent. This model can exhibit the property of excitable media, i.e., the model shows a propagating wave without damping in amplitude (figure 5.10), annihilation of the waves in a collision (figure 5.11) and refractoriness to two successive perturbations with short interval (figure 5.12).

Why has it become possible to make the system excitable just by adding a constant term to the equations for y? In figure 5.13, we show nullclines of the equations 5.4

[*4] Here we picked up the FCD model (a) which contains incoherent feedforward loop (equation 4.9), but same modification to models with negative feedback loop also make them excitable.

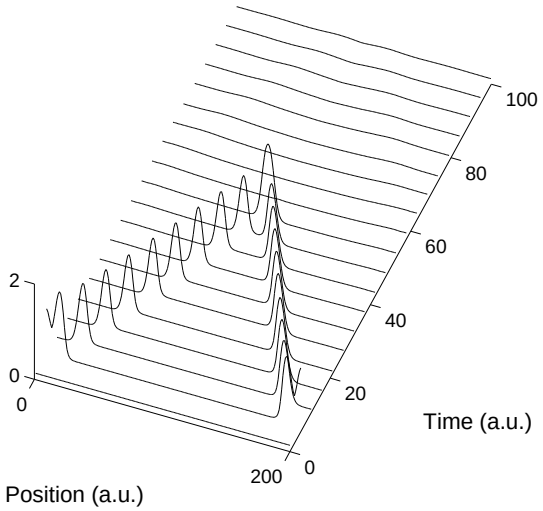

Fig. 5.11 Annihilation of two proper gating waves of equations 5.4. Parameter values are the same as in figure 5.10.

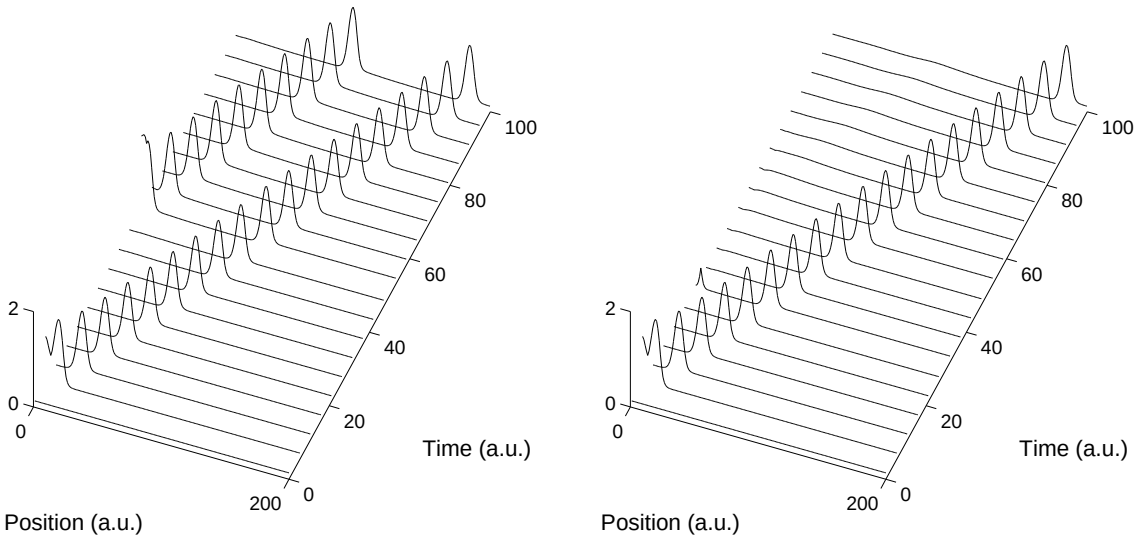

Fig. 5.12 Refractoriness to two successive perturbations of equations 5.4. When the interval between the two perturbations are long, a propagating wave with full amplitude is generated (left panel). On the other hand, when the interval is short the wave is not generated. Parameter values are the same as in figure 5.10.

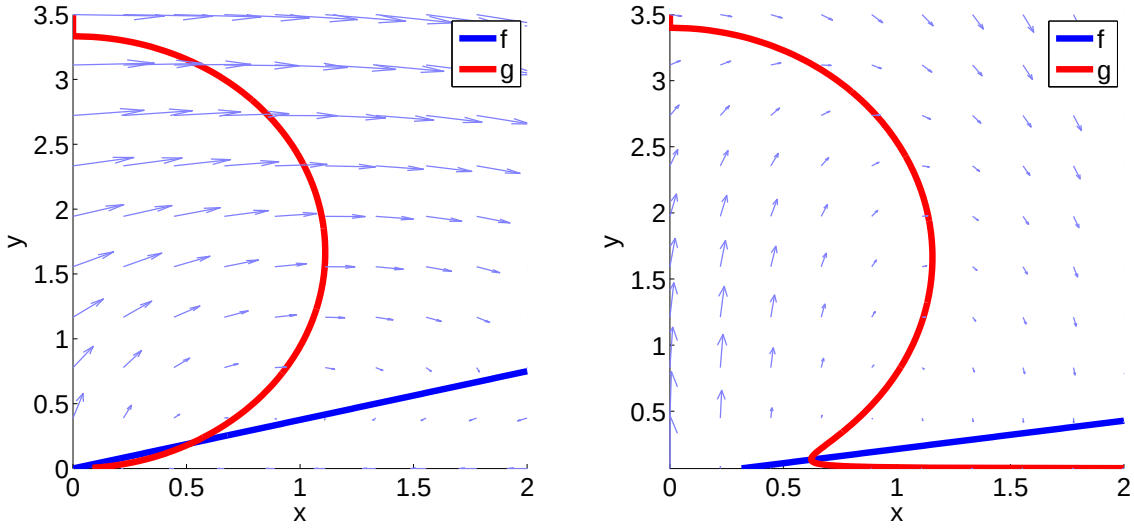

Fig. 5.13 Left: $a = 4$, $b = 1$, $c = 5$, $d = 1.5$ and $alpha = 0$. Right: $a = 0.28$, $b = 0.04$, $c = 5$, $d = 1.5$ and $\alpha = 0.1$.

(without the diffusion term) in which the three-variable system is reduced to two-variable system by assuming that the kinetics of the equation for z is much faster than other variables: the nullclines are

$$\begin{aligned} \dot{x} &= axy - bx = f(x, y) \\ \dot{y} &= c\frac{((\rho/\gamma)y)^n}{((\rho/\gamma)y)^n + (Kx)^n} - dy + \alpha = g(x, y). \end{aligned} \tag{5.5}$$

With a finite value of α in equation 5.5, the equation $g(x, y) = 0$ become N-shaped nullcline on the phase plane, which is a prominent feature of an excitable system [58]. Depending on the slope of the line $0 = f(x, y)$, the system shows bifurcation to an oscillatory mode.

Thus, we succeeded in developing excitable FCD models. Considering the experimental fact that cAMP oscillation is near bifurcation point [44], this strongly suggests that our mathematical descriptions of cAMP oscillation captur the essence of cAMP oscillation in the perfusion chamber.

Chapter 6

Dynamics of the PI3K pathway

6.1 Introduction

6.1.1 The molecular mechanisms for achieving the FCD property in eukaryotic cells remain to be identified.

As mentioned in Chapter 1, some preceding studies suggest that the FCD property is widely observable in signal transduction systems in eukaryotic cells [19, 42]. However, the molecular mechanism responsible for FCD in eukaryotic systems still remains elusive. The main reason for the difficulty in identifying it is that there had been no direct observation of FCD property in a signaling system. Now that we have shown that the initial peak in cAMP signaling response follows FCD not just based on a direct measurement but also at the single-cell level, it would be highly advantageous to investigate the molecular mechanism of FCD by using *Dictyostelium* cells. In fact, the structures of the intracellular signaling pathways responsible for cAMP signaling have been investigated intensely by many researchers [104]. To integrate the accumulating knowledge of the molecular networks of the signaling system, it is required to know the dynamic property of the system at the single-cell level [4, 81]. Here, to understand the molecular origin of FCD in cAMP singling system, we focus our attention to the dynamics of the PI3K pathway that exists upstream of ACA.

6.1.2 PI3K signaling is necessary for the synthesis of cAMP.

In the signal transduction system of *Dictyostelium* cells, one of the key signaling pathway, among others, is the phosphatidylinositol-(3,4,5)-triphosphate(PIP_3)-dependent signaling system called PI3K signaling pathway [54]. Upon stimulation with extracellular cAMP, the signaling molecule PIP_3 transiently translocates to the plasmamembrane [87] (PIP_3 response) resulting from a positive regulation by phosphoinositide 3-kinase (PI3-kinase) and a negative regulation by PI3-phosphatase (PTEN) [53, 56]. The transient accumulation of PIP_3 on the membrane is required for cAMP synthesis since the accumulated PIP_3 confer binding sites for multiple PH domain-containing proteins necessary for cAMP synthesis.

One of the PH domain-containing proteins is cytosolic regulator of adenylyl cyclase (CRAC) [57]. The PH domain of CRAC (PH_{Crac}) fused to fluorescent protein can

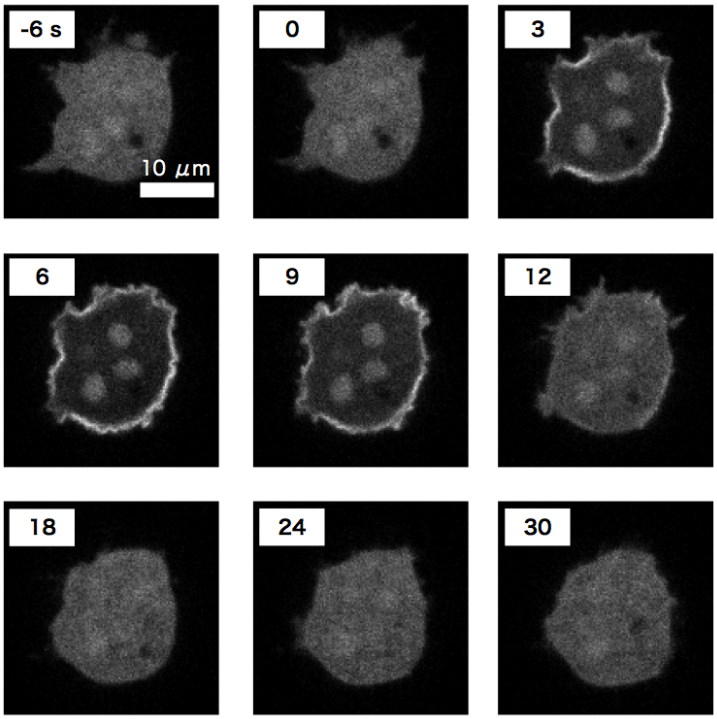

Fig. 6.1 Translocation of PH_{Crac}-RFP upon stimulation with 1 μM extracellular cAMP. Confocal images were taken at the time indicated. Cells were stimulated in a perfusion chamber with a spatially-homogeneous cAMP concentration of 1 μM at $t = 0$ s.

be used as an indicator for PIP_3 synthesis, and therefore PIP_3 response, because the sensor molecules translocate from the cytosol to the plasma membrane by binding to the synthesized PIP_3 [87, 90, 71]. Figure 6.1 shows a series of confocal fluorescence images of a single cell recorded during 6 seconds before and 30 seconds after stimulation with 1 μM cAMP. Before stimulation PH_{Crac}-RFP exists mainly in the cytosol. After addition of extracellular cAMP, a decrease of fluorescence at the cytosolic area and an increase at the boundary, i.e., plasma membrane, become apparent transiently.

PIP_3 response can be observed not only in the perfusion chamber but also during development. Using the fluorescently-labeled PH_{Crac}, Weijer and his colleagues demonstrated that the cells exhibit periodic translocation of fluorescently-labeled PH_{Crac} during the early stage of the developmental [31] (figure 6.2). This is consistent with the fact that the PI3K signaling pathway is necessary for cAMP synthesis as the cells during early stage of the development exhibit oscillatory synthesis of cAMP as explained in chapter 1.

6.1.3 How do the cells reset the sensitivity in the PI3K pathway?

PIP_3 response seems to be tightly coupled with cAMP signaling response not just from biochemical evidences [104] but also temporal behavior during cAMP signaling.

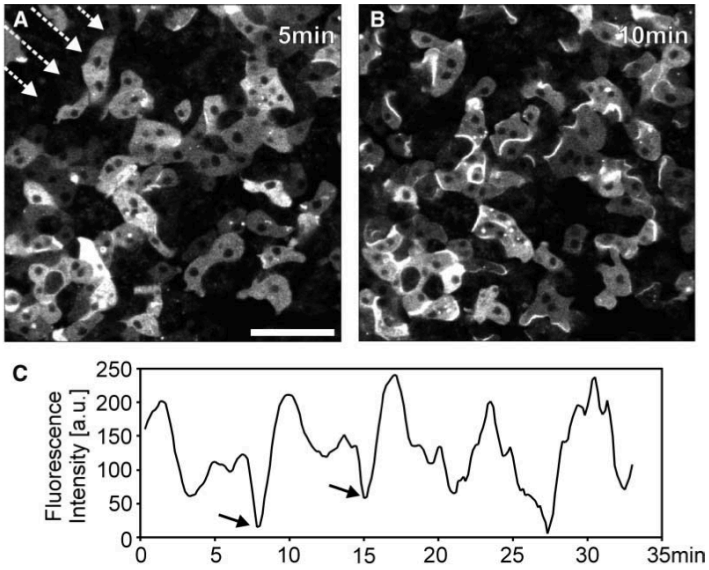

Fig. 6.2 Periodic translocation of fluorescently-labeled PH_{Crac} during the early stage of the development taken from Ref. [31]. (A) A image of 4-hr starved *Dictyostelium* cells. The arrows indicate the direction of wave propagation. (B) A image of the cells with translocations of the fluorescent probe. (C) The periodic changes in fluorescence intensity of the cytoplasm. The scale bar represents 30 μ m.

However, the dynamic property of the signaling system has not been fully characterized. Here, to elucidate the molecular origin of the FCD property in cAMP signaling response, we investigate the PIP_3 response and ask how the cells respond to relative change in extracellular cAMP. As was the case in cAMP signaling response, the response property at the PIP_3 level has only been characterized by using step stimuli with 0 M basal level [90, 71]. By clarifying the resetting property of PIP_3 response, we are able to confine possible mechanisms responsible for the response as will be discussed later.

6.2 Results and discussions

6.2.1 PIP_3 response follows fold-change detection.

The cells expressing PH_{Crac}-RFP were well-isolated from other cells in the perfusion chamber and were observed under the microscope. The captured images (such as figure 6.1) were analyzed to obtain time-series data of normalized cytosolic fluorescence of PH_{Crac}-RFP, which reflects inversely the amount of newly-synthesized PIP_3 because elevation of the level of PIP_3 increases the amount of PH_{Crac}-RFP translocating to the membrane [71]. Just like the observation of intracellular cAMP in the perfusion chamber, we exposed to the cells step changes in the concentration of extracellular cAMP by using the same perfusion chamber. During the experiment, cells were treated with a pre-stimulus level and allowed to adapt before elevation of the

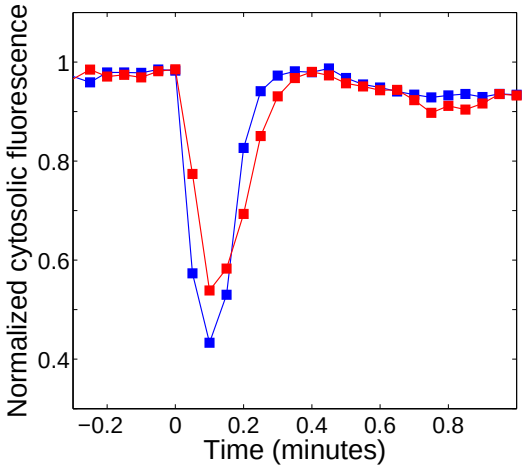

Fig. 6.3 Representative time courses of PIP_3 response. Here the cells were pretreated by 100 pM cAMP before a step change in the concentration of cAMP to 1 μM at $t = 0$. Two different cells are represented by different colors.

stimuli (see chapter 2 for the detailed description of the experimental system and the analysis). Representative time courses of normalized cytosolic fluorescence of PH_{Crac}-RFP are shown in figure 6.3.

We investigated various combinations of pre-stimulus and post-stimulus level of extracellular cAMP. In figure 6.4, the time courses of normalized cytosolic fluorescence are shown, where the pre-stimulus level was initially kept at 100 pM and then elevated at $t = 0$ by 1, 10, 100 and 1000 fold respectively. In the same way as cAMP signaling response, the response intensities of PIP_3 response monotonically increases with increase in the post-stimulus level. In figure 6.5, time courses of normalized cytosolic fluorescence are shown, where the pre-stimulus level was initially kept at 1 nM and then elevated in the same way as the previous one. The monotonic increase is quite similar to those of 100-pM prestimulus level. Importantly, the time scale of the response is also quite similar to each other: the level of cytosolic fluorescence returns to its pre-stimulus level approximately within half a minute.

We then evaluated the response intensity of PIP_3 response as a function of relative increase in the stimulus level. We defined the response intensity as the minimum value of normalized cytosolic fluorescence within 1 minute after the change in the stimulus level. The results are summarized in figure 6.6 (and 6.7 for raw data). Despite 10-fold difference in absolute stimulus level, the two lines overlap significantly. That is to say, the data clearly shows that the response intensity is determined not by absolute level (or absolute change) in input stimulus but relative change. Considering the independence of time scales of the responses to the absolute stimulus level, these data demonstrates that PIP_3 response follows FCD.

To probe the dynamic range over which the FCD property holds, we plotted the response intensity to 10-fold change in input stimuli over various pre-stimulus levels. Figure 6.8 (and figure 6.9 for raw data), summarizes the results. This shows that PIP_3 response shows the FCD property over approximately one-order of magnitude

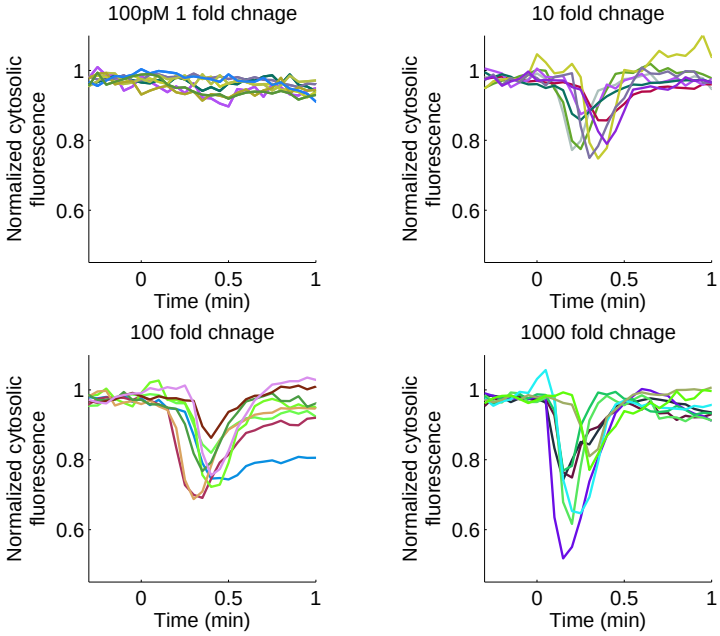

Fig. 6.4 Representative time courses of PIP_3 response with 100 pM pre-stimulus level. The stimulus level is elevated at $t = 0$ by 1, 10, 100 and 1000 fold respectively. Eight different cells are represented by different colors.

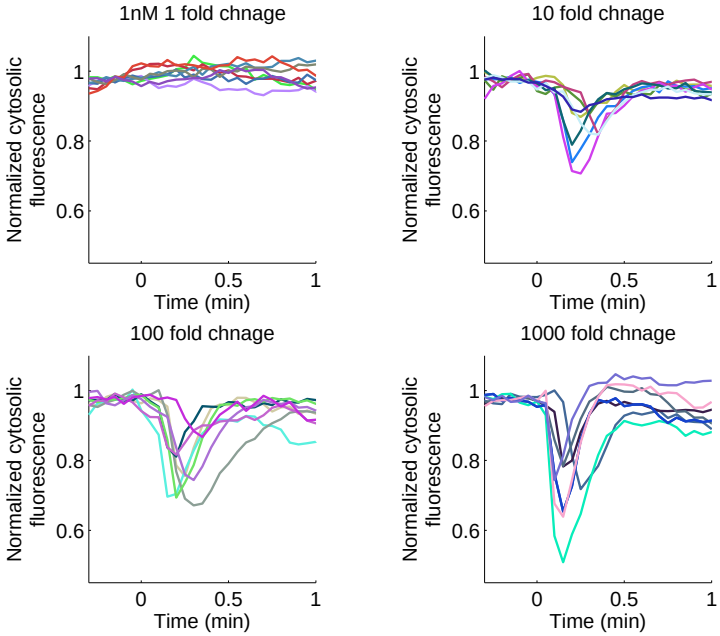

Fig. 6.5 Representative time courses of PIP_3 response with 1n M pre-stimulus level. The stimulus level is elevated at $t = 0$ by 1, 10, 100 and 1000 fold respectively. Eight different cells are represented by different colors.

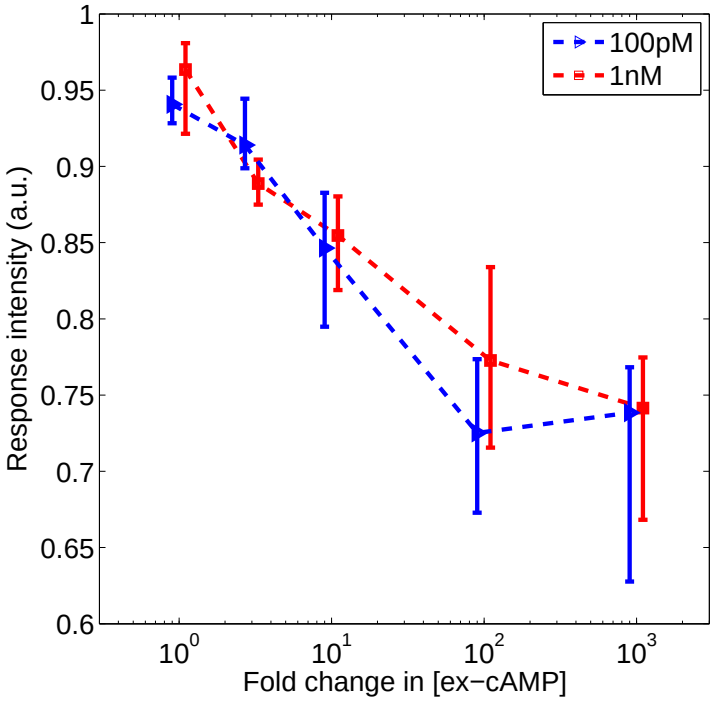

Fig. 6.6 Response intensity of PIP_3 response as a function of fold change in the concentration of extracellular cAMP. The markers and bars represent median value and quartile of the data.

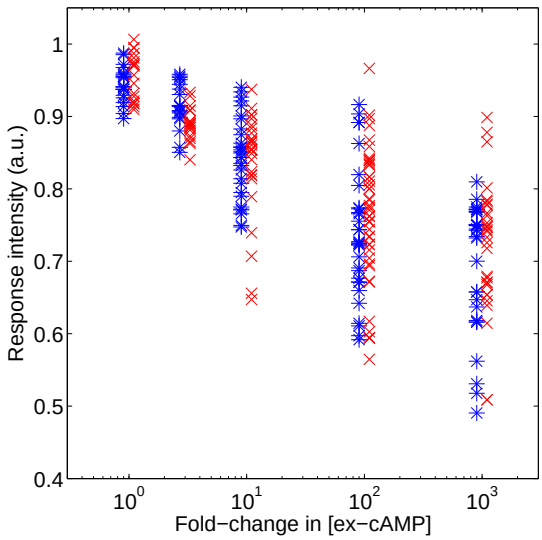

Fig. 6.7 Raw data of figure 6.6.

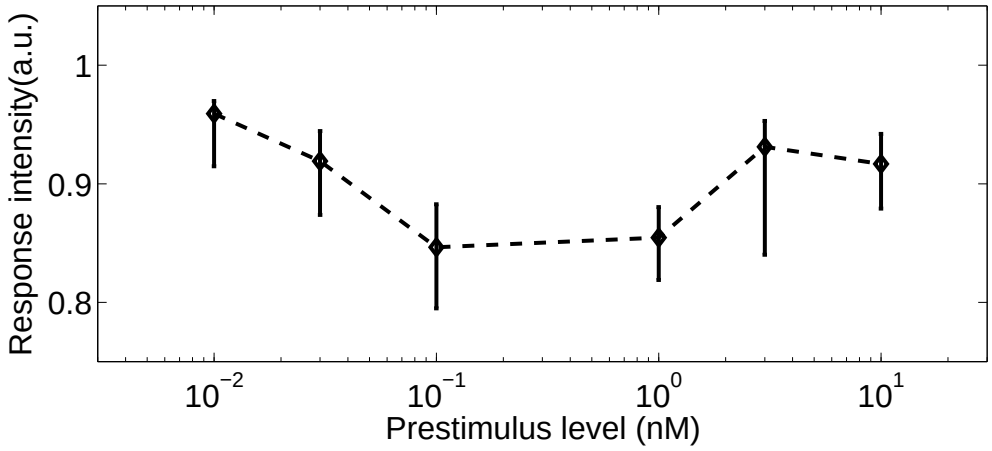

Fig. 6.8 Range over which the FCD property holds. The response intensities to10-fold change in input stimuli are plotted over wide pre-stimulus levels. The markers and bars represent median value and quartile of the data.

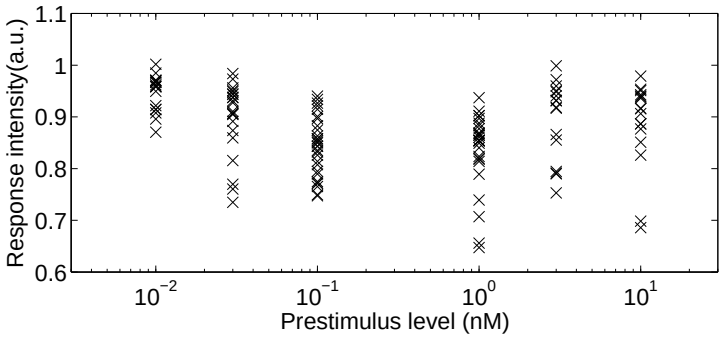

Fig. 6.9 Raw data of figure 6.6.

(∼0.1 nM to ∼1nM).

Discussion1: Relationships to the dose-response curves in cAMP signaling response.
Here we discuss relations between dose-response curves of PIP_3 response and that of cAMP signaling response. First, note that the response amplitude of cAMP signaling response saturates faster that that of PIP_3 response: The amplitude of cAMP signaling response to a few 10-fold change is almost maximum whereas that of PIP_3 response to 10-fold change is only one-half of the maximum amplitude. This is consistent with the assumption that PI3K signaling pathway is upstream of ACA. From the view point of information theory [21], a saturated response amplitude would not be able to 'encode' the difference in stimuli and therefore cannot transmit the difference to a downstream factor.

Second, note that the dynamic range over which PIP_3 response follows FCD (∼0.1 nM to ∼1 nM) is significantly overlaps but a little bit smaller than the dynamic range of FCD for cAMP signaling response (∼0.1 nM to ∼3nM). The overlap in the dynamic ranges itself is consistent with the assumption that PI3K signaling pathway

is upstream of ACA. On the other hand, the fact that the dynamic range of PIP_3 is narrower than that of cAMP suggests that the PI3K pathway in not the only pathway that activates ACA. In fact, some preceding studies suggest that PIP_3-independent signaling molecule PKBR1 is involved in the activation of ACA [17, 15, 104]. The molecule may also be contributing to the wider dynamic range of cAMP signaling response.

To conclude, these data suggest that the FCD property of PIP_3 response is responsible for the FCD property at the level of cytosolic cAMP. Although the exact mechanism for the FCD property remains to be determined, it would be much easier to detail the PI3K pathway than to fully describe cAMP signaling pathway because the number of molecular species involved are much smaller [104]. Therefore, the PI3K pathway can serve as an ideal model system to investigate molecular mechanisms of FCD in eukaryotic signaling system.

Discussion2: The FCD property constrain possible mechanisms in the directional sensing module.

For the purpose of constraining possible mechanisms that govern the dynamics of the PI3K signaling pathway, input/output relations of the system have been characterized from various points of view [88, 60]. Among others, the responses to spatially-uniform elevation in the stimulus level and spatially-graded stimulation (and combinations of those) have been characterized. To spatially-uniform step inputs, the response shows adaptation whereas, to spatially-graded inputs, the localization of the signaling molecule PIP_3 persists. However, it had not been investigated before how the cells respond to relative changes in spatially-uniform step inputs. Here, we discuss how the newly-obtained input/output relation of PIP_3 response can further constrain possible mechanisms of the signaling pathway.

As described in chapter 1, it has been considered that the general idea of local-excitation and global inhibition (LEGI) model explains the spatio-temporal dynamics of PI3K signaling pathway. Note that the idea LEGI just concerns spatial distribution of an excitatory pathway and an inhibitory pathway and therefore it does not constrain specific mechanisms. In fact, LEGI-based models has been implemented by adopting a network topology of incoherent feedforward loop (iFFL) [69] without any experimental evidence for the topology[*1]. However, recent study on the signaling pathway have suggested that the system is composed of an iFFL-based mechanism instead of a feedback-based one by using a quantitative analysis of the dynamic property [105, 55].

A type of LEGI-based phenomenological model called a balanced inactivation model [70] has been thought of as one of the best models that explains the input/output relations of the PI3K pathway [54]. The model has succeeded in reproducing a newly-characterized input-output relation of the pathway: Figure 6.10 demonstrates the response property in graded stimuli, in which the same absolute level in input stimuli can elicit totally different responses depending on whether they occur at the front or rear of the cell (figure 6.10 B). However, input-output relationships, once normalized,

[*1] For example, it is also possible to implement a LEGI model based on a negative feedback loop (NFBL) because iFFL and NFBL are the network topology that can achieve adaptation [72] and both can exhibit persistent output to graded inputs.

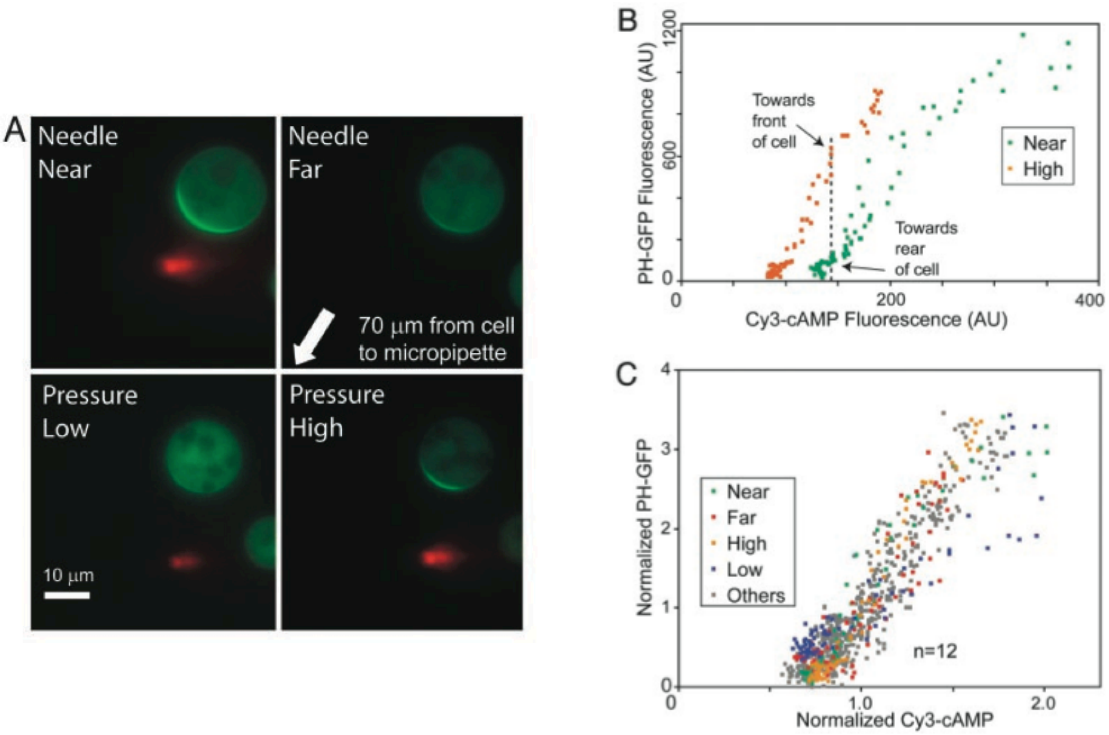

Fig. 6.10 Responses to graded stimuli of varying steepness and absolute level taken from Ref. [60]. (A) The micropipette location and pressure were altered to change the steepness and midpoint of the chemoattractant, Cy3-cAMP, gradient. (B) Input-output relations. x-axis indicates input signal, or Cy3-cAMP fluorescence, at the points just outside the cell perimeter and y-axis indicates output signal, or PH-GFP Fluorescence, at the points just inside the cell perimeter. (C) Normalized input-output relations, where the input signals are normalized by their mean value.

produced curves with nearly identical slopes and thresholds (figure 6.10 C), meaning that the intensity of the response depends on the relative steepness of the gradient rather than the absolute level of the stimulus.

In the model, input stimulus S produces a membrane-bound species A and a cytosolic species B, which diffuses inside the cell and produces another membrane-bound species B_m. A and B_m mutually inactivate each other. In mathematical terms, the model is written as

$$\begin{aligned} \frac{\partial A}{\partial t} &= k_a S - k_{-a} A - k_i A B_m \text{ at the membrane,} \\ \frac{\partial B_m}{\partial t} &= k_b B - k_{-b} B_m - k_i A B_m \text{ at the membrane, and} \\ \frac{\partial B}{\partial t} &= D \nabla^2 B \text{ in the cytosol,} \end{aligned} \tag{6.1}$$

with a boundary condition for the outward pointing normal derivative of the cytosolic component

$$D \frac{\partial B}{\partial n} = k_a S - k_b B.$$

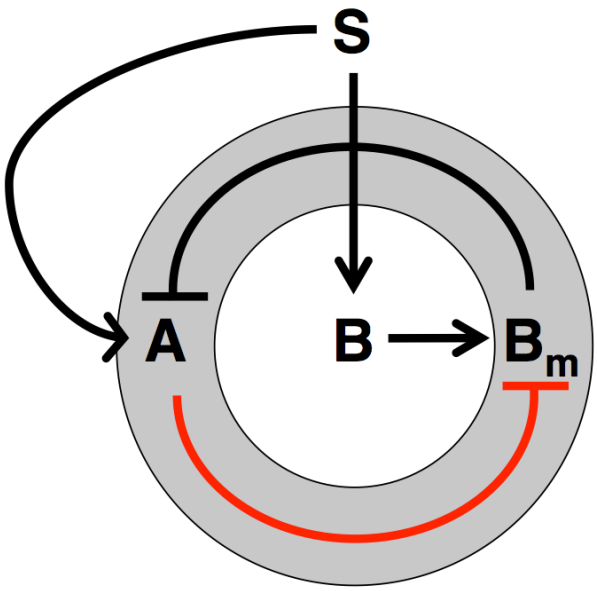

Fig. 6.11 A topological representation of the balanced inactivation model [70].

Figure 6.11 represents a topological representation of the model, where the input variable S control the output variable A through a few internal variables. Note that the model essentially based on an iFFL except that the output variable A negatively regulates an internal variable B_m (red blunt arrow in figure 6.11). However, the negative regulation newly-introduced in the model is not supported by any experimental evidence although the interaction is essential for the model to be able to reproduce the response to graded inputs.

Here we ask whether the model can reproduce the FCD property at the PIP_3 level we have observed in this study. Figure 6.12 is a time course of output variable A obtained by a numerical calculation of the equations 6.12 where successive step-wise changes in the stimulus S were applied to the system (10-fold change at $t = 0$ s and $t = 50$ s). This clearly shows that the FCD property can not be reproduced by the model and therefore the model is not capturing the molecular mechanism of the system.

As a first step towards better understanding of the directional sensing module, here we propose a phenomenological model (a FCD-LEGI model) relying on the framework of LEGI-based model. The model is based on a ODE model that show FCD, which is introduce in chapter 4, to implement the idea of LEGI. The model is written as

$$\begin{aligned}
\frac{\partial A}{\partial t} &= k_a \frac{S^n}{S^n + B_m^n} - k_{-a} A \text{ at the membrane,} \\
\frac{\partial B_m}{\partial t} &= k_b B - k_{-b} B_m \text{ at the membrane, and} \\
\frac{\partial B}{\partial t} &= D \nabla^2 B \text{ in the cytosol,}
\end{aligned} \tag{6.2}$$

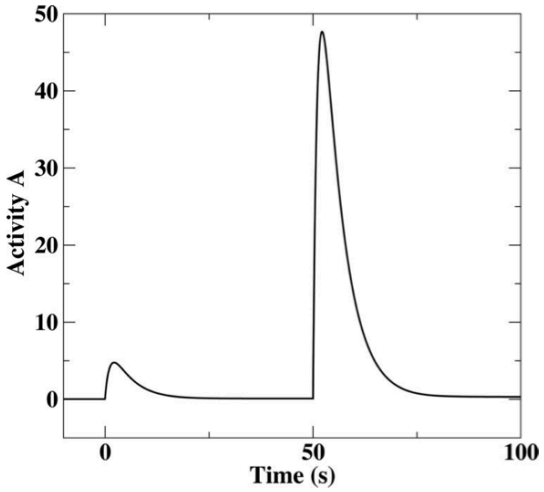

Fig. 6.12 The response of the model (equation) to step-wise changes in uniform stimulus taken from Ref. [70]. The level of the stimulus is changed 10-fold at $t = 0$ s and another 10-fold at $t = 50$ s.

with a boundary condition for the outward pointing normal derivative of the cytosolic component

$$D\frac{\partial B}{\partial n} = k_a S - k_b B.$$

Note that it is obvious that the model is able to show FCD to a spatially-uniform inputs because it is essentially the same as the ODE model that exhibits FCD. To spatially-graded stimuli, it basically follows the LEGI scheme: the output variable A is produced depending on the local level of input stimuli S and the inhibitory variable B is globally distributed by diffusion. Therefore most properties explained by the previously-reported LEGI models, such as amplified responses to shallow graded stimuli, can also be reproduced. Here we consider a simplified one-dimensional geometry, the front and back are single points connected by a finite line segment of length L[*2]. We suppose that S is not uniform but is different at the front, S_f, and at the back, S_b. And we introduce average input level as $\bar{S} = (S_f + S_b)/2$.

The exact solution of the diffusion equation for B is given by a linear profile:

$$B(x) = Gx + H,$$

where $G = (B_f - B_b)/L$ and $H = (B_f + B_b)/2$. The values of B at the front of the cell, B_f, and at the back of the cell, B_b, is obtained by using the boundary condition of the system. It is also easy to obtain the steady-state value of B_m and A both at the front of the cell and at the back of the cell by solving algebraic equations. The

[*2] The same setting has been used to analyze essential features of the models in the previous work [70].

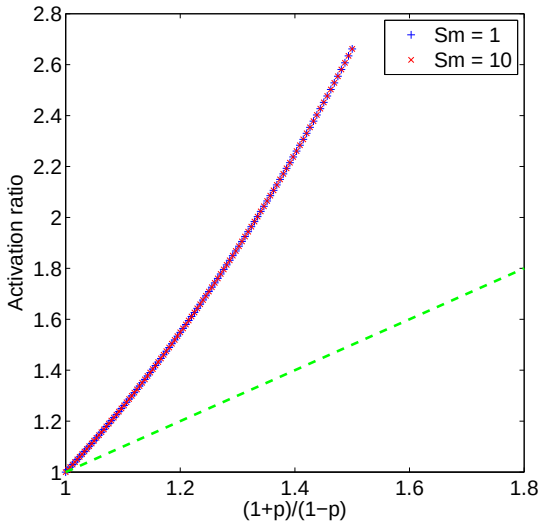

Fig. 6.13 Amplification of graded stimuli in the FCD-LEGI model in a simplified one-dimensional geometry (see the main text). X-axis indicates gradient of the input stimuli (The ratio of the stimulus level at the front of the cell $S_f = Sm(1+p)$ to that at the back of the cell $S_b = Sm(1+p)$). Y-axis indicates the ratio to the output variable A at the front of the cell to that at the back of the cell. The green line represents $y = x$. The parameter values used here are $k_a = 5$, $k_{-a} = 1.5$, $k_b = 4$, $k_{-b} = 1$, $D = 30$, $n = 4$ and $L = 10$.

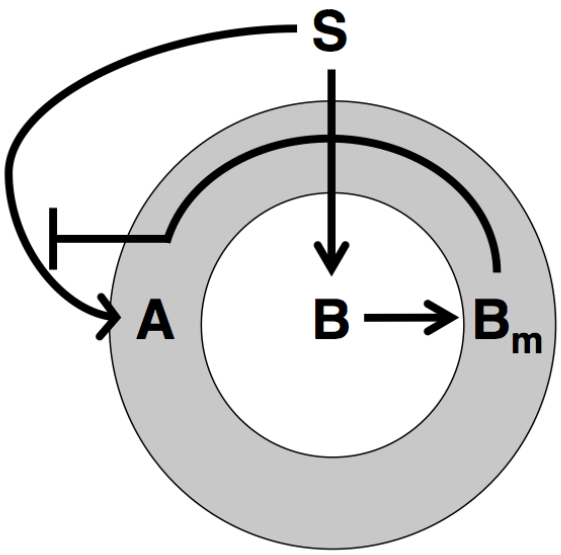

Fig. 6.14 A topological representation of a FCD and LEGI model.

exact solution of the output variable A at the front of the cell is given as

$$A_f = \left(\frac{k_a}{k_{-a}}\right)\frac{S_f^n}{S_f^n + (k_b/k_{-b})^n (B_{m,f})^n}$$
$$= \left(\frac{k_a}{k_{-a}}\right)\frac{(S_f/\bar{S})^n}{(S_f/\bar{S})^n + (k_b/k_{-b})^n (B_{m,f}/\bar{S})^n}.$$

The solution at the back of the cell, A_b, is given by the same expression with S_f and $B_{m,f}$ replaced by S_b and $B_{m,b}$ respectively. The term that appears in the denominator of the solution, $B_{m,f}/\bar{S}$, can be written as

$$\frac{B_{m,f}}{\bar{S}} = \left(\frac{k_b}{k_{-b}}\right)\frac{k_a(S_f/\bar{S}) + (2k_aD/k_bL)}{k_b + 2D/L}. \tag{6.3}$$

From these expressions, it is clear that A_f is dependent only on $S_f/\bar{S}$, the stimulus level at the front of the cell normalized by the average stimulus level. The same holds true for the case of A_b. Note that this is exactly what has been observed in the experiment (figure 6.10 C), i.e., the response depends on the relative steepness of the gradient rather than the absolute level of the stimuli.

Compared to the balanced inactivation model, our model has a few improvement. First of all, our model is capable of FCD, a property which was clearly shown at the PIP_3 level for the first time by our experiments. However, to our knowledge, no previously-reported models for the directional sensing module are able to reproduce the property [61]. Second, the FCD-LEGI model does not assume any new interaction between the molecular species other than iFFL network topology (figure 6.14), although the balanced inactivation model hypothesize new inhibitory interaction.

To conclude, we were able to constrain possible mechanisms of the directional sensing system by the observation of FCD because the FCD property is achieved only by a subset of the models containing iFFL network topology. Also, it has been revealed that the FCD property naturally explains the reason why the responses to graded stimuli are independent of the absolute stimulus level. As a future work, it would be interesting to expand the model to two dimensions and test whether other properties of the signaling system (such as those demonstrated in [60]) is reproduced successfully.

Chapter 7

General relation between fold-change detection and robustness

7.1 Introduction

So far we have discussed the validity of the hypothesis that the FCD property of *Dictyostelium* cells enables cAMP oscillation to be robust to cell density in the perfusion chamber. There, we have assumed that the extracellular environment is described by a kinetic equation ($d[ext - cAMP]/dt = \rho k_t[int - cAMP] - \gamma[ext - cAMP]$). However, the extracellular condition in the perfusion chamber is different from the natural condition of *Dictyostelium* development. In the former case, the extracellular cAMP is constantly diluted by perfusion while, in the latter case, it is degraded by extracellular phosphodiesterase (PDE) secreted by the cells. Therefore it is natural to ask whether the FCD property of the cells make the cell population robust to cell density even in the natural condition.

To investigate the relation between the FCD property and the robustness to cell density in various conditions may help gain insights into cell-cell signaling in general. In the light of the ubiquity of intercellular communication mediated by signaling molecules in single-celled organisms, it is conceivable that the robustness to cell density is a general property of cell-cell signaling; if it were not for such robustness in intercellular communication, collective behavior of cells would rarely be observed in a fluctuating environment. Therefore it would be useful to ask whether FCD can still be a sensible strategy to achieve the robustness even in conditions other than that of *Dictyostelium* cells. To answer these questions, here we explore the possibility that the relation between the FCD property and the robustness to cell density is generalized. Specifically, we ask how the signaling molecule should be secreted and how it should be degraded to achieve the robustness provided that cells are capable of FCD. Based on the mathematical framework we have developed in chapter 4, we show FCD can be an efficient strategy in a broader context.

7.2 Results and discussions

7.2.1 Robustness in an arbitral secretion of signaling molecules

First of all, we note that, when considering general cases, molecular entities of a system's output, y, and secreted molecule, z, can be different from each other, although they are both cAMP in the case of *Dictyostelium*. The molecule y exists in intracellular space while the molecule z is extracellular space. The only assumption here is that the intracellular molecule y somehow determines the rate of secretion of the extracellular signaling molecule z.

Here, we ask what if secretion of signaling molecule z is not proportionate to the output variable y as is the case for *Dictyostelium* cells ($dz/dt = \underline{\rho k_t y} - \gamma z$). In chapter 4, we defined the robustness to variations in cell density as invariance of the equations to a set of transformations. Specifically, the equations we have analyzed so far

$$\begin{aligned}\dot{x} &= f(x, y, z)\\ \dot{y} &= g(x, y, z)\\ \dot{z} &= \rho k_t y - \gamma z,\end{aligned}$$

where f and g satisfies the FCD condition (equation 4.2 and 4.3), shows invariance under the transformation

$$\begin{aligned}x &\to \phi(p, X)\\ z &\to pZ\\ \rho &\to p\rho.\end{aligned} \tag{7.1}$$

The resultant equations are

$$\begin{aligned}\dot{X} &= f(X, y, Z)\\ \dot{y} &= g(X, y, Z)\\ \dot{Z} &= \rho k_t y - \gamma Z.\end{aligned}$$

Observe that, given the FCD property of cells (i.e., subsystem x and y), the invariance holds true if the equation for z is linear in terms of z. It is therefore obvious that the equations

$$\begin{aligned}\dot{x} &= f(x, y, z)\\ \dot{y} &= g(x, y, z)\\ \dot{z} &= \rho h(y) - \gamma z.\end{aligned}$$

is also invariant under the set of transformation. That is, the rate of secretion of the signaling molecule z can be regulated by an arbitrary function of the output variable y as $h(y)$. This means that the system's robustness to variations in cell density is *not* dependent on the way cells regulate the secretion of extracellular signaling molecule z by the output variable y.

7.2.2 Robustness in a cell-density dependent secretion of signaling molecules

Here we consider cases in which cells capable of FCD secrete the signaling molecule z not just depending on the output variable y but also on cell density ρ. In this case, the system would be governed by the equations

$$\begin{aligned} \dot{x} &= f(x, y, z) \\ \dot{y} &= g(x, y, z) \\ \dot{z} &= \xi(\rho)h(y) - \gamma z. \end{aligned} \tag{7.2}$$

Here the cell-density dependence of the equation for z is generalized as $\rho \to \xi(\rho)$. In this case, there exists such q that satisfies the equation

$$\xi(p\rho) = q\xi(\rho).$$

Now we consider the transformations

$$\begin{aligned} x &\to \phi(q, X) \\ z &\to qZ \\ \rho &\to p\rho. \end{aligned} \tag{7.3}$$

This yields that

$$\begin{aligned} \dot{X} &= \frac{1}{\frac{\partial \phi}{\partial X}} f(\phi(q, X), y, qZ) \\ &= f(X, y, Z), \end{aligned}$$

by using one of the condition for FCD (equation 4.2, $f(\phi(p, x), y, pz) = \frac{\partial \phi(p,x)}{\partial x} f(x, y, z)$) and

$$\begin{aligned} \dot{y} &= g(\phi(q, X), y, qZ) \\ &= g(X, y, Z), \end{aligned}$$

by using another condition for FCD (equation 4.3, $g(\phi(p, x), y, pz) = g(x, y, z)$). The equation for z is transformed to

$$\begin{aligned} q\dot{Z} &= \xi(p\rho)h(y) - \gamma qZ \\ \iff \dot{Z} &= \xi(\rho)h(y) - \gamma Z. \end{aligned}$$

Thus the equation 7.2 are transformed to the following form:

$$\begin{aligned} \dot{X} &= f(X, y, Z) \\ \dot{y} &= g(X, y, Z) \\ \dot{Z} &= \xi(\rho)h(y) - \gamma Z. \end{aligned}$$

It was shown that the equations are invariant under the transformation 7.3. That is to say, the system is robust to variations in cell density even when the cells secrete signaling molecule in a cell-density dependent manner.

7.2.3 Robustness in a cell-density dependent degradation of signaling molecules

Here we consider cases where signaling molecule in extracellular space is degraded in cell-density dependent manners. Such assumption may be related to *Dictyostelium* development in a natural condition (e.g., development on an agar substrate). In that case extracellular cAMP would be mainly degraded by secreted PDE [6] and the amount of PDE per unit area can be dependent on cell density. In that case the system is written as

$$\begin{aligned}\dot{x} &= f(x, y, z)\\ \dot{y} &= g(x, y, z)\\ \dot{z} &= \rho k_t y - \gamma(\rho) z,\end{aligned}$$

where γ is a function of cell density ρ.

A case in which the kinetics of extracellular signaling molecule is fast.
First we investigate a situation where the kinetics of the variable z is much faster than that of other variables[*1]. In such a case, it is valid to assume a quasi-steady state for z, whose kinetic equation would then be reduced to the algebraic relation:

$$z = \frac{\rho k_t}{\gamma(\rho)} y \equiv \Theta(\rho) y.$$

In such a condition, the system is governed by the two differential equations:

$$\begin{aligned}\dot{x} &= f(x, y, \Theta(\rho)y)\\ \dot{y} &= g(x, y, \Theta(\rho)y).\end{aligned}$$

Note that there exists such q that satisfies the equation

$$\Theta(p\rho) = q\Theta(\rho).$$

[*1] In the case of the early stage of *Dictyostelium* development, it seems reasonable to assume that the kinetics of extracellular molecule is sufficiently fast. In the perfusion experiment, it was shown that the periodicity of cAMP oscillation is almost constant at 6 minutes even in a sufficiently high dilution rate [47]. This strongly suggests that not the kinetics of *extracellular* space but the kinetics of *intracellular* system is a rate-limiting process and therefore determines the period of the oscillation. On the other hand, the periodicity of the oscillation on an agar substrate is also 6 minutes. These facts suggest that the extracellular kinetics even in the natural condition would not be a rate-limiting process. In other words, the kinetics of the extracellular cAMP is sufficiently fast compared to that of intracellular signaling system. Such a fast kinetics would be achieved if there exist sufficient amount of enzyme that degrade signaling molecules (i.e., PDE) in extracellular space.

We now consider the transformations

$$\begin{aligned} x &\to \phi(q, X) \\ \rho &\to p\rho. \end{aligned} \tag{7.4}$$

This yields that

$$\begin{aligned} \dot{X} &= \frac{1}{\frac{\partial \phi}{\partial X}} f(\phi(q, X), y, \Theta(p\rho)y) \\ &= f(X, y, \Theta(\rho)y), \end{aligned}$$

by using the condition 4.2 and

$$\begin{aligned} \dot{y} &= g(\phi(q, X), y, \Theta(p\rho)y) \\ &= g(X, y, \Theta(\rho)y) \end{aligned}$$

by using the condition 4.3. Therefore we obtain a two-variable system:

$$\begin{aligned} \dot{X} &= f(X, y, \Theta(\rho)y) \\ \dot{y} &= g(X, y, \Theta(\rho)y). \end{aligned}$$

That is, the system is invariant under the transformation 7.4, meaning the system is robust to variations in cell density.

A general case in which the kinetics of extracellular signaling molecule is not so fast.
Then, what if a general case where such a time-scale separation is not validated? The cell-density dependence of the degradation rate of signaling molecule entails that the cell density (ρ) and the degradation rate (γ) are no longer independent of each other like those in the perfusion chamber. The idea is graphically described by introducing a $\gamma - \rho$ plane in figure 7.1. Each point on the plane corresponds to a certain extracellular condition and therefore to a state (e.g., equilibrium or oscillation and so on) of the system.

In the case of the perfusion experiment, an extracellular condition defined by a set of values, (γ, ρ), is arbitrarily selectable. On the other hand, when the degradation rate is dependent on cell density, possible extracellular conditions are restricted on the curve $\gamma = \gamma(\rho)$.

With the FCD property (which refers to the property of the subsystem x and y), the trajectory of the output variable y is independent of ρ as we have discussed so far (figure 7.1 right panel). Without the FCD property, on the other hand, the states are dependent on ρ in general as well as γ (figure 7.1 left panel). Because the FCD property expands the region consists of qualitatively equivalent states towards ρ direction, the curve $\gamma = \gamma(\rho)$ would have larger overlap with the region when the cells are capable of FCD. This means that the range of cell density ($\rho_{min} < \rho < \rho_{max}$) in which the system exhibits a functional state (e.g., oscillatory state) expands by the property of FCD. In other words, the FCD property increases the system's robustness to variations in cell density even when the degradation rate is dependent on cell density. Note that the above discussions hold true even when the term representing secretion of signaling molecule is generalized as $\rho k_t y \to \xi(\rho)h(y)$.

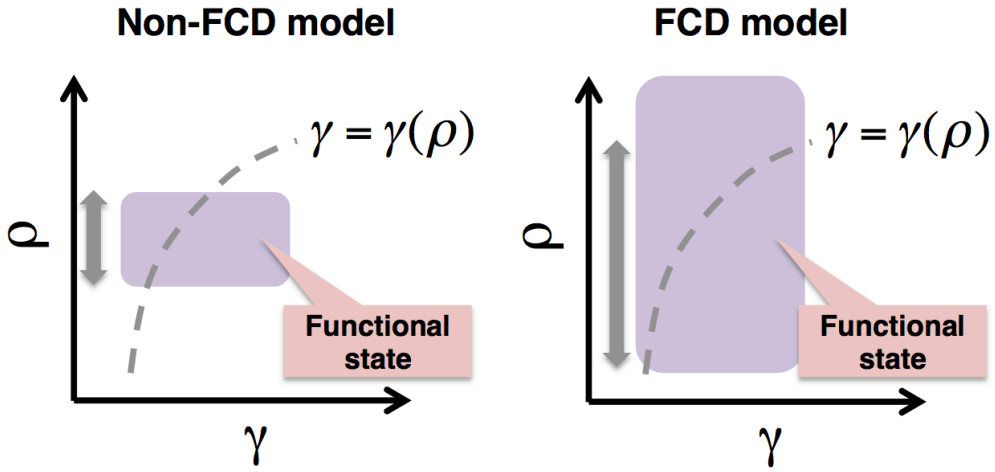

Fig. 7.1 A graphical explanation showing that FCD increases the robustness to cell density even when the rate of degradation of extracellular signaling molecule (z) is degraded in a cell-density dependent manner. In the case of FCD model (right panel) the states of the system (e.g. an oscillatory state or an equilibrium state etc.) are independent of ρ, whereas in the case of non-FCD model (left panel) the states depend both on ρ and γ in general (purple region, where the systems exhibit "functional state"). When the degradation rate of signaling molecule γ depends on cell density ρ, possible conditions of the system are restricted on a curve $\gamma = \gamma(\rho)$ (dotted line) whereas, in the case of perfusion experiment, the both parameters are independent of each other. Because the FCD model expands the "functional state" region towards ρ direction, even if the degradation rate is dependent cell density, the range of ρ that can exhibit "functional state" become larger (double-headed arrows) compared to non-FCD model.

7.2.4 Robustness in a diffusively-coupled system

Lastly, we consider a case where the signaling molecules secreted by the cells diffuse and stimulate the neighboring cells (diffusion coupling) instead of global coupling as we have assumed so far. The assumption of diffusion coupling would be appropriate when, for example, describing cell-cell signaling in the early stage of the *Dictyostelium* development[*2].

In that case, the system is governed by the equations:

$$\begin{aligned} \frac{dx}{dt} &= f(x, y, z) \\ \frac{dy}{dt} &= g(x, y, z) \\ \frac{\partial z}{\partial t} &= \rho k_t y - \gamma z + D\nabla^2 z, \end{aligned} \tag{7.5}$$

[*2] In fact, the kinetic equation for z with a diffusion term in the following equations (equations 7.5) has been used in the models of the early stage of *Dictyostelium* development [44, 67].

where D is a diffusion constant. Observe that the equation for z is linear in terms of the variable z and therefore the equations are invariant under the transformation 7.1. Thus, even in a situation where the extracellular field is inhomogeneous because of diffusion coupling of the cells, FCD enables a system to be robust to cell density.

7.2.5 Cell-cell communications in other microbial systems

In this chapter, we have shown that the robustness to variations in cell density emerges in rather general conditions, given that the constituent cells are capable of FCD. Although it is a prominent feature of *Dictyostelium* cells that cAMP is utilized in both intracellular and extracellular signaling, molecular entities of these don't have to be the same to achieve a FCD-based cell-cell signaling. Moreover, the relation between FCD and the robustness to cell density is independent of the way the cells secrete the signaling molecule. The discussion above suggests that the FCD strategy for the robustness to cell density is a sensible way even in a different conditions from that of *Dictyostelium* cells. It is widely accepted that synchronized activities in single-celled microorganisms on a population-wide scale result from cell-cell communication mediated by extracellular signaling molecule. One of the well-studied examples is cell-cell communication in bacteria called quorum sensing [115, 16, 83]. As in *Dictyostelium* cells, this process also involves detecting, producing, releasing and responding to signaling molecules. For example, in the case of an gram-negative bacteria *Vibro fischeri*, the extracellular signaling molecule acyl-hormoserine lactone (AHL) are synthesized by LuxI, which is synthesized after detection of AHL by the cytoplasmic receptor LuxR (figure 7.2). The concentration of AHL increases as a function of increasing cell density. The bacteria detect the accumulation of the molecule and, at a certain cell density, they alter gene expression in a collective way. To our knowledge, researchers in the field of quorum sensing in bacteria have focused their attention to cell-density *dependent* behavior rather than cell-density *independent* behavior. However, it is conceivable that bacteria also have a mode of cell-cell signaling in which some output variables behave in a cell-density-independent manner to handle with the inevitable fluctuation in cell density. In fact, in our scenario, quorum-sensing ability of the cells and cell-density independence in some output responses are not mutually exclusive; the information of cell density is preserved in the internal variable x, in our notation, while the output variable y is independent of cell density by definition. Therefore, it is possible to make the cells behave in a cell-density dependent manner by making use of the concentration of the internal variable x. There are also several cases in which suspensions of yeast cells [23, 22, 24] or catalytic microparticles in BZ reaction solution [107] communicate with each other through chemical exchange. It would be interesting to test whether the logic we have proposed here can apply to these cases in the future.

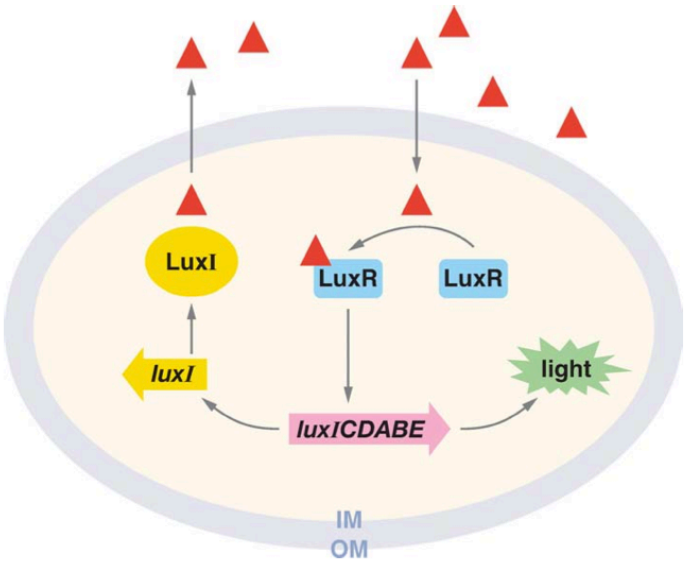

Fig. 7.2 A schematic representation of quorum sensing in *Vibrio fischeri* taken from Ref. [115]. Red triangles represents signaling molecules called AHL, which freely diffuses in and out of the cells. The signaling molecule is synthesized by LuxI and detected by the receptor molecule LuxR.

Chapter 8

Summary and outlook

8.1 Summary of the results

In this study, we investigated adaptation in cAMP signaling response in the social amoeba *Dictyostelium discoideum* at the single-cell level. Binding of extracellular cAMP (input signal) to the membrane-bound receptors elicit transient synthesis and secretion of intracellular cAMP (output signal) through a series of complex signaling cascade [104]. As explained in chapter 2, to monitor the real-time change in cytosolic cAMP, we carried out time-lapse live-cell imaging of the cells expressing Förster Resonance Energy Transfer (FRET)-based cAMP sensor [84, 47]. The FRET signal was fully corrected to obtain an index that is independent of expression level of the sensor. This enabled us to compare amplitudes of cAMP signaling response between cells [14]. Moreover, cells were isolated in a small perfusion chamber to prevent cell-cell interaction and well-defined time-varying input signal was delivered by employing syringe pumps.

Using these experimental setups, in chapter 3, we characterized adaptation in cAMP signaling response. Specifically, we exposed the cells to step increase in extracellular cAMP from nonzero basal level to evaluate response intensity to relative change in the input stimulus. We found that the main initial peaks observed immediately after the step increase follows fold-change detection (FCD). Moreover, despite its marked cell-cell variability, the peak amplitude of the initial peak was found to be reproducible in each individual cells when they are exposed to successive step inputs with identical fold-change but different absolute level. These results suggest that FCD is a robust property to cell-cell variation.

In *Dictyostelium* development, cell-cell signaling mediated by cAMP signaling response results in a collective oscillation in the concentration of cAMP. In chapter 4, we therefore asked whether there are any advantages of FCD in cell-cell signaling. One of the characteristics of the collective oscillation in cAMP is its robustness to variations in cell density. An analysis of a mathematical model describing communicating cells capable of FCD revealed that FCD renders the output of the system, which corresponds to intracellular cAMP, independent of the parameter of cell density. To corroborate the predictions of the model, in chapter 5, we studied populations of cells interacting with each other in the perfusion chamber. It was shown that the dynamic properties of both intracellular and extracellular cAMP are consistent with

those of the models. Thus, we conclude that cell-cell signaling in *Dictyostelium* development achieves robustness to variations in cell density by the FCD property of the constituent cells.

In chapter 6, we asked how the FCD property in cAMP signaling response is implemented in the signal transduction system in the cells. To address this question, we observed the activity of the PI3K signaling pathway responding to relative changes in the input by measuring spatio-temporal dynamics of phosphotidylinositol-(3,4,5)-triphosphate (PIP_3). The PI3K signaling pathway is known to exist upstream of adenylyl cyclase ACA that synthesizes intracellular cAMP [74] and its dynamics has been explained by a network model consisting of a incoherent feedforward loop [69, 114, 55]. By using the perfusion system, we showed that PIP_3 response also follows FCD at the single-cell level. The result suggests that the PI3K signaling pathway is responsible for the FCD property in cAMP signaling response. Moreover, the result enabled us to choose a special type of incoherent feedforward loop as a model of the pathway.

Although we have discussed cell-cell signaling by focusing *Dictyostelium* cells in the perfusion chamber, we asked, in chapter 7, whether the relation between FCD and the robustness to cell density can be generalized to other situations. By examining equations that describes communicating cells capable of FCD, we found that the relation is not specific to *Dictyostelium* cells. Rather, the robustness to cell density can be observed in a wide range of conditions as far as the constituent cells have the FCD property. Considering the generality of cell-cell signaling in single-celled microorganism, the result suggests that other organisms may also use the FCD strategy to alleviate cell-density dependence in their communication with each other.

8.2 cAMP signaling response in *Dictyostelium* cells as an ideal model system for further studies of FCD

In chapter 3, we have shown that the initial peak in cAMP signaling response follows FCD. The result provides a unique experimental demonstration of FCD in eukaryotic cells. Furthermore, our results are the first direct observation of FCD at the single-cell level. This enables us to analyze deeper aspect of FCD than other systems. For example, we have demonstrated the robustness of the FCD property to cell-cell variation. Such an experiment would not be possible in a population-level measurement.

Because there are a lot of experimental and theoretical tools available for analyzing the system, cAMP signaling response can serve as an ideal model system for further studies of FCD, from the level of molecular mechanism to its physiological implications. Regarding its molecular mechanism, we have suggested in chapter 6 that the FCD property in the PI3K pathway may be implemented by a type of incoherent feedforward loop. It is interesting to ask which, if any, molecular species compose such network topology in the signal transduction system.

In addition to that, several preceding works have mentioned possible advantages of the fold-change detection (FCD) property in signal processing of the cells. Goentoro and co-workers have suggested that FCD may provide advantages in coping with cell-cell variations in the concentrations of regulatory proteins and in maintaining

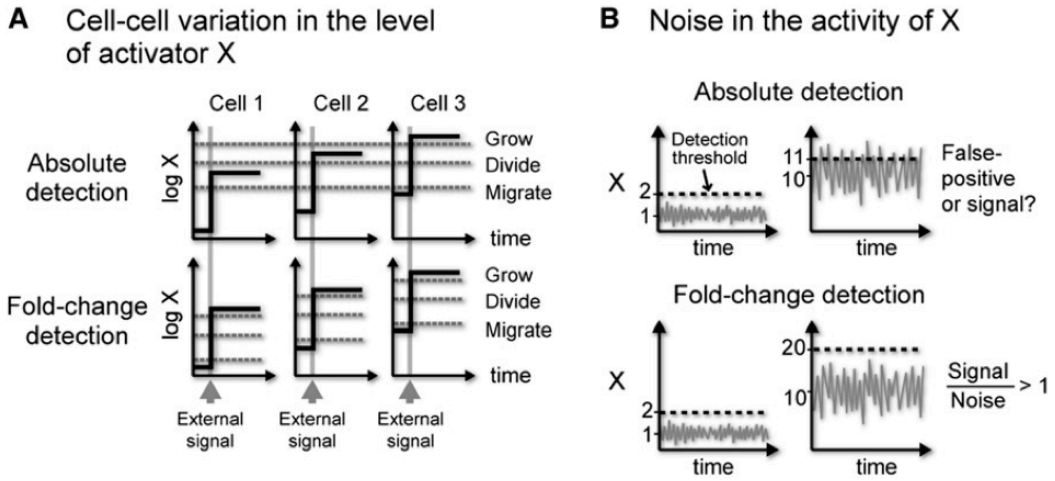

Fig. 8.1 Schematics representing possible advantages of FCD in cellular information processing taken from Ref. [43]. (A) An increase in activator X is detected by the cells. Consider a situation where basal concentrations of X are variable between cells but its fold-change is equal among the cells. In that case a system capable of fold-change detection ensures that each cell responds reliably to an external signal despite the variation in the basal level of the signal X (lower part). A system which detect absolute-level (or absolute-change) of the signal would fail to cope with the variation in the basal level of X (upper part). (B) Then what if a system where the level of an external signal X is increased by a constant level (absolute-change generation) and the change in the signal is detected by an absolute-change detector? Is it work as well as a system where the signal X is increased by a constant *ratio* (fold-change generation) and the change in the signal is detected by an fold-change detector? Again the system composed of absolutes-change detector would fail to overcome the basal-level variation in cellular environment because the amplitude of fluctuations of the signal also increases with the absolute level of basal activity of X. As a result, such systems would result in reacting to false positives (upper part) more often than the system composed of fold-change detector (lower part).

sensitivity to noisy environment [43] (figure 8.1). However, whether the strategy is the one really utilized by cells remain to be examined. Further investigation of cAMP signaling system in *Dictyostelium* cells can provide useful information on this problem.

8.3 Robustness as a scale invariance in developmental biology

In this study, we have shown that the robustness of cAMP oscillation to variations in cell density can be understood as a consequence of the FCD property in cAMP signaling response in *Dictyostelium cells*. As described in chapter 4, the relation between the robustness and FCD can be summarized succinctly by using a set of

equations; The cells in the perfusion chamber are described as

$$\begin{aligned}\dot{x} &= f(x, y, z)\\ \dot{y} &= g(x, y, z)\\ \dot{z} &= \rho k_t y - \gamma z.\end{aligned}$$

If the cells exhibit FCD, i.e., if f and g satisfy the FCD condition (equation 4.2 and 4.3), then the system is invariant under the transformation

$$\begin{aligned}x &\to \phi(p, x)\\ z &\to pz\\ \rho &\to p\rho.\end{aligned}$$

In other words, the oscillation is robust to variations in cell density because the system has a scale-invariant property.

A mathematically similar mechanism for robustness can be found in the study of developing animals. As described in section 1.4, developing embryo often utilizes morphogen gradient that scales with the size of the embryo to keep accurate proportions within and between tissues [9]. This means that the system can be invariant under the transformation in the size of the field L (figure 8.2):

$$L \to pL.$$

This suggests that robustness as a scale-invariant property can be found in biological parameters other than cell density. To our knowledge, our results provide a unique demonstration of the robustness to cell density as a scale-invariant property. It would be interesting to test whether such robustness to other biological parameters can be observed in other biological systems.

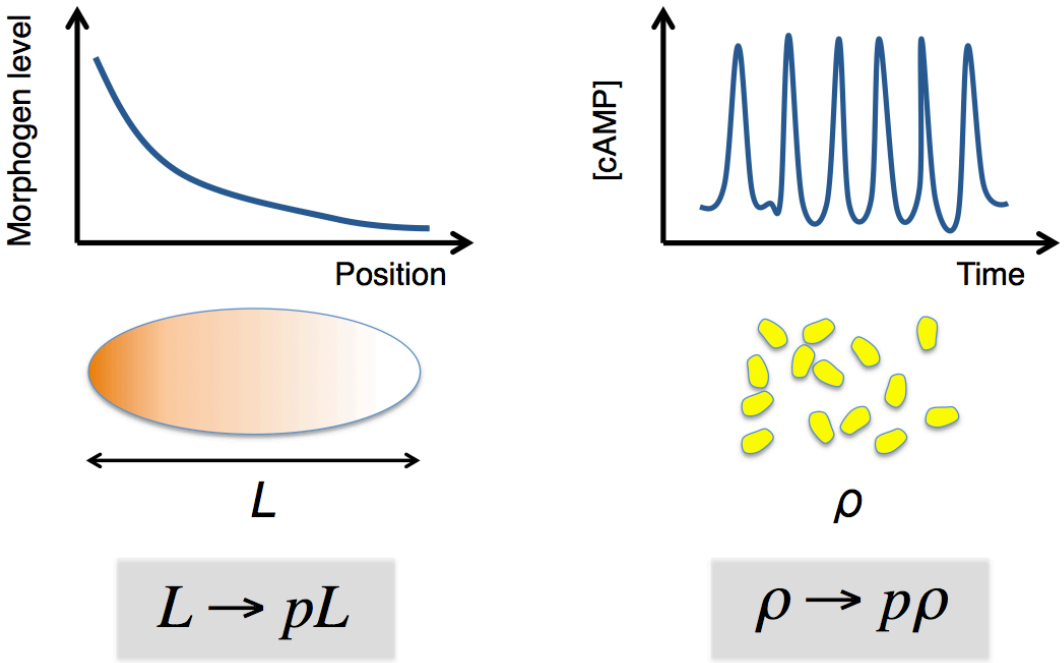

Fig. 8.2 Robustness as a scale invariance in developmental biology. (Left) Morphogen gradient often scales with the size of the embryo. (Right) cAMP oscillation scales with cell density.

Appendix A

Appendix

A.1 Source codes for data analysis

In this work, processing and analysis of data were performed by using MATLAB (MahtWorks). Here we provide some of the central source codes used in the analyses.

A.1.1 FRET analysis

The raw images for FRET measurement were processed and analyzed as shown in the following code;

```
clear all;
%
Input = [18];
Pos = 5;
%
Start=1;
Finish=200;
n=Finish-Start+1;
Interval=10; %the interval(sec) of images
NameofCFP='130131_1_Epac1AX4__w1FRET-CFP_s';
NameofYFP='130131_1_Epac1AX4__w2FRET-YFP_s';
NameofYFPDIR='130131_1_Epac1AX4_pre_w4YFP_s';
%
EndTime=(n-1).*Interval;
Time=linspace(0,EndTime,n);
InputTime = (Input-1).*Interval./60;
Time = Time./60;
%
mkdir(DIR);
%
%Parameters for correction
alpha=0.50312;
beta=3.1085;
%
```

```
for l=1:Pos;
    %
    v=genvarname(['Color' int2str(l)]);
    eval([v '=rand(1,3);']);
    %
    v=genvarname(['CFPMed' int2str(l)]);
    eval([v '=zeros(1,n);']);
    v=genvarname(['YFPMed' int2str(l)]);
    eval([v '=zeros(1,n);']);
    v=genvarname(['YFPcorr' int2str(l)]);
    eval([v '=zeros(1,n);']);
    v=genvarname(['YFPDirMed' int2str(l)]);
    eval([v '=zeros(1,1);']);
    v=genvarname(['FRETratio' int2str(l)]);
    eval([v '=zeros(1,n);']);
    v=genvarname(['BGCFPMed' int2str(l)]);
    eval([v '=zeros(1,n);']);
    v=genvarname(['BGYFPMed' int2str(l)]);
    eval([v '=zeros(1,n);']);
    %
    YFPDIR=imread([NameofYFPDIR,num2str(l),'_t1.TIF' ]);
    if max(YFPDIR(:)) > 1.9661e+04
        disp('YFPDIR is adjusted incorrectly');
        break
    end
    YFPDIR2=imadjust(YFPDIR,[0 0.3],[0 1]);
    %Making a mask
    ImB = PreprocessForCYFP(YFPDIR2);
    [MaskYFPDIR L] = SingleMask(ImB);
    [YFPDirMed BGYFPDirMed] = CFRETIntensityCell(YFPDIR,MaskYFPDIR);
    srNew=['YFPDirMed' int2str(l) '=YFPDirMed;'];
    eval(srNew)
    %
    for k=Start:Finish
        CFP=imread([NameofCFP,num2str(l),'_t',num2str(k),'.TIF' ]);
        YFP=imread([NameofYFP,num2str(l),'_t',num2str(k),'.TIF' ]);
        %
        %Making a mask
        ImB= PreprocessForCYFP(CFP);
        [MaskCFP L] = SingleMask(ImB);
        ImB= PreprocessForCYFP(YFP);
        [MaskYFP L] = SingleMask(ImB);
        Mask = MaskCFP & MaskYFP;
        %
        [YFPMed BGYFPMed] = CFRETIntensityCell(YFP,Mask);
        [CFPMed BGCFPMed] = CFRETIntensityCell(CFP,Mask);
```

```
        %
        YFPcorr=double(YFPMed)-alpha*double(CFPMed)-beta*double(YFPDirMed);
        FRETratio=double(CFPMed)/double(YFPcorr);
        %
        sr1=['CFPMed' int2str(l) '(k)=CFPMed;'];
        eval(sr1)
        sr2=['YFPMed' int2str(l) '(k)=YFPMed;'];
        eval(sr2)
        sr3=['YFPcorr' int2str(l) '(k)=YFPcorr;'];
        eval(sr3)
        sr4=['FRETratio' int2str(l) '(k)=FRETratio;'];
        eval(sr4)
        sr5=['BGCFPMed' int2str(l) '(k)= BGCFPMed;'];
        eval(sr5);
        sr6=['BGYFPMed' int2str(l) '(k)= BGYFPMed;'];
        eval(sr6);
    end
end
%
FH=figure;AH=axes;
for FRETi=1:Pos
    plot(Time,eval(['FRETratio',num2str(FRETi)]),'Color',eval(['Color' ...
        int2str(FRETi)]),'LineWidth',2);hold on
end
Bar = linspace(1, 4);%linspace(min of YLim, max of YLim, 10)
[X, Y]=meshgrid(InputTime,Bar);
plot(X,Y,'--k','LineWidth',1);
xlabel('Time (min.)','FontSize',20);ylabel('FRET index (a.u.)','FontSize',20);
set(AH,'FontSize',20);
axis([Time(1) Time(n) 1.45 2.45]);

function ImC = PreprocessForCYFP(Im)
%
SEA=strel('disk',30);
ImA=imtophat(Im,SEA);
SEB=strel('disk',10);
ImB=imclose(ImA,SEB);
SEC=strel('disk',10);
ImC=imopen(ImB,SEC);
end

function [Mask L]  = SingleMask(ImB)
%
Mask = im2bw(ImB,graythresh(ImB));
[L,num]=bwlabel(Mask,4);
while num>1
    STATS=regionprops(L,'Area');
```

```
    [M idx]=max([STATS.Area]);
    Mask=ismember(L,idx);
    [L,num]=bwlabel(Mask,4);
end
Mask=imfill(Mask,'holes');
end

function [CellMedian BGMedian] = CFRETIntensityCell(Image,Mask)
%
BGMask=~Mask;
SE=strel('disk',30);
BGMask=imerode(BGMask,SE);
BGMaskedImage=im2uint16(im2double(Image).*BGMask);
[r_finalBG,c_finalBG,v_finalBG]=find(BGMaskedImage);
BGMedian=median(v_finalBG);
%
Image=Image-BGMedian;
MaskedImage=im2uint16(im2double(Image).*Mask);
[r_finalCell,c_finalCell,v_finalCell]=find(MaskedImage);
CellMedian=median(v_finalCell);
end
```

A.1.2 Quantifying the responses of PH_{Crac}-RFP/AX4

The raw images of PH_{Crac}-RFP/AX4 were processed and analyzed as shown in the following code;

```
clear all
%
Input =[10];
Pos = 2;
Start=1;
Finish=30;
n=Finish-Start+1;
Interval=3; %the interval(sec) of images
NameofRFP='121102_2_DagAAX4_4__w1CSU-HcRed_s';
%
EndTime=(n-1).*Interval;%The time of last Image
Time=linspace(0,EndTime,n);
InputTime = (Input-1).*Interval./60;
Time = Time./60;
MinInt=2000;
MaxInt=20000;
%
se = strel('square',8);
%
```

```
for l=1:Pos;
    v=genvarname(['Color' int2str(l)]);
    eval([v '=rand(1,3);']);
    v=genvarname(['Cyt_med' int2str(l)]);
    eval([v '=zeros(1,n);']);
    v=genvarname(['Cyt_std' int2str(l)]);
    eval([v '=zeros(1,n);']);
    v=genvarname(['BackGro_med' int2str(l)]);
    eval([v '=zeros(1,n);']);
    v=genvarname(['BackGro_std' int2str(l)]);
    eval([v '=zeros(1,n);']);
    v=genvarname(['Ic_med' int2str(l)]);
    eval([v '=zeros(1,n);']);
    v=genvarname(['Ic_std' int2str(l)]);
    eval([v '=zeros(1,n);']);
    %
    for k=Start:Finish;
        Im=imread([NameofRFP,num2str(l),'_t',num2str(k),'.TIF' ]);
        %
        %Making a Mask
        Mask = MakeMask2(Im);
        DilatedMask=imdilate(Mask,se);
        [r_O c_O v_O]=find(DilatedMask==0);
        BackGro=zeros(1,length(r_O));
        for a=1:length(r_O);
            BackGro(a)=Im(r_O(a),c_O(a));
        end
        sr1=['BackGro_med' int2str(l) '(k)=median(BackGro);'];
        eval(sr1)
        sr2=['BackGro_std' int2str(l) '(k)=std(BackGro);'];
        eval(sr2)
        [L,num]=bwlabel(Mask,4);
        while num>1
            STATS=regionprops(L,'Area');
            [M idx]=max([STATS.Area]);
            Mask=ismember(L,idx);
            [L,num]=bwlabel(Mask,4);
        end
        Mask=imfill(Mask,'holes');
        %
        STATS=regionprops(L,'Centroid');
        G=round([STATS.Centroid]);
        G2=[G(2);G(1)];
        %
        Im=Im(max(1,G2(1)-50):max(1,G2(1)+50),max(1,G2(2)-50):max(1,G2(2)+50));
        MedfiltIm=medfilt2(Im,[5 5],'symmetric');
```

```
            Mask=Mask(max(1,G2(1)-50):max(1,G2(1)+50),max(1,G2(2)-50):max(1,G2(2)+50)
            Mask2=imerode(Mask,se);
            ErodedRegion=Mask-Mask2;
            MaskedIm=im2uint16(im2double(Im).*Mask);
            MaskedIm2=im2uint16(im2double(Im).*Mask2);
            MaskedMedfiltIm=im2uint16(im2double(MedfiltIm).*Mask2);
            %
            [r,c,v]=find(MaskedIm2);
            %
            [r_high,c_high]=find(MaskedMedfiltIm>prctile(v,85));
            [r_low,c_low]=find(Mask2&(MaskedMedfiltIm<prctile(v,10)));
            %
            FinalIm=MaskedIm2;
            for i=1:length(r_high)
                FinalIm(r_high(i),c_high(i))=0;
            end
            for i=1:length(r_low)
                FinalIm(r_low(i),c_low(i))=0;
            end
            [r_final,c_final,v_final]=find(FinalIm);
            %
            sr3=['Cyt_med' int2str(l) '(k)=median(v_final);'];
            eval(sr3)
            sr4=['Cyt_std' int2str(l) '(k)=std(double(v_final));'];
            eval(sr4)
        end
        %
        if Input~=0
            Ic0=eval(['mean(Cyt_med' int2str(l) '(Input(1)-5:Input(1)-1))']);
        elseif Input == 0
            Ic0=eval(['Cyt_med' int2str(l) '(1)']);
        end
        sr5=['Ic_med' int2str(l) '=(Cyt_med' int2str(l) '-BackGro_med' int2str(l) ...
            ')./(Ic0-BackGro_med' int2str(l) ');'];
        eval(sr5)
        sr6=['Ic_std' int2str(l) '=(Cyt_std' int2str(l) ').//(Ic0-BackGro_med'...
            int2str(l) ');'];
        eval(sr6)
    end
    %
    figure;AHCyt=axes;hold on
    for l=1:Pos
        plot(Time,eval(['Ic_med' int2str(l)]),'Color',...
            eval(['Color' int2str(l)]),'LineWidth',1,'Marker','s','MarkerSize'...
            ,10,'MarkerFaceColor',eval(['Color' int2str(l)]));
    end
```

```
set(AHCyt,'YLim',[0.4 1.3],'XLim',[0 max(Time)],'FontSize',15);
Bar = linspace(0.4,1.3);%linspace(min of YLim, max of YLim, 10)
[X, Y]=meshgrid(InputTime,Bar);
plot(X,Y,'--k','LineWidth',1);
ylabel('Normalized cytosolic fluorescence (a.u.)');
xlabel('Time (minutes)');
```

Acknowledgements

First of all, I would like to thank my Ph.D. adviser, Dr. Satoshi Sawai, for giving me a chance to carry out this project. I am very fortunate to be able to start my career as an experimental biologist by using a well-designed experimental system, which has stimulated my interest in dynamic aspects of biological systems. I am also grateful to Dr. Yohei Kondo for his cooperation, stimulating discussions and his friendship. I have genuinely enjoyed exchanges of constructive ideas with him on a daily basis. I have also learned enormous amounts of mathematical ideas in biology, through conversations with him. The results of this study, especially in its theoretical parts, owe much to his collaborations.

Many thanks to the following people for generously sharing their physical and biological knowledge with me and helping me think more clearly throughout the course of my study: Dr. Kunihiko Kaneko, Dr. Koichi Fujimoto, Dr. Thomas Gregor, Dr. Yuichi Wakamoto, Dr. Noritaka Masaki, Dr. Daisuke Taniguchi Dr. Akihiko Nakajima, Dr. Shuji Ishihara, Dr. Soo Hyeon Kim, Dr. Tom Shimizu, Mr. Mani Hamidi, Dr. David Colliaux, and others.

Thanks are also due to my lab mates for their advice on carrying out experiments and constant encouragement: Ms. Mai Honda-Kitahara, Ms. Emi Hada, Dr. Nao Shimada, Mr. Norio Tanaka, Mr. Takehiko Onuki, Dr. Yuka Shirokawa, Mr. Kei Takahashi, Mr. Ryosuke Iri, Mr. Fumihito Fukujin, Mr. Daisuke Imoto, Ms. Yuko Chida, Ms. Kie Hayashi and Mr. Taihei Fujimori.

This project was supported by Grant-in-Aid for Research Fellow of the Japan Society for the Promotion of Science.

Bibliography

[1] Afonso, P. V. and Parent, C. A. PI3K and chemotaxis: a priming issue?, *Science signaling*, **4**, 170 (2011), pe22.

[2] Alcantara, F. and Monk, M. Signal propagation during aggregation in the slime mould Dictyostelium discoideum., *Journal of general microbiology*, **85**, 2 (Dec. 1974), 321–334.

[3] Alon, U. *An Introduction to Systems Biology*, Design Principles of Biological Circuits, Chapman & Hall/CRC (2007).

[4] Alon, U. Network motifs: theory and experimental approaches., *Nature reviews. Genetics*, **8**, 6 (June 2007), 450–461.

[5] Alon, U., Surette, M. G., Barkai, N. and Leibler, S. Robustness in bacterial chemotaxis., *Nature*, **397**, 6715 (Jan. 1999), 168–171.

[6] Bader, S., Kortholt, A. and Van Haastert, P. J. M. Seven Dictyostelium discoideum phosphodiesterases degrade three pools of cAMP and cGMP, *Biochemical Journal*, **402**, 1 (Feb. 2007), 153.

[7] Barad, O., Hornstein, E. and Barkai, N. Robust selection of sensory organ precursors by the Notch-Delta pathway., *Current opinion in cell biology*, **23**, 6 (Dec. 2011), 663–667.

[8] Barkai, N. and Leibler, S. Robustness in simple biochemical networks., *Nature*, **387**, 6636 (June 1997), 913–917.

[9] Ben-Zvi, D., Shilo, B.-Z. and Barkai, N. Scaling of morphogen gradients., *Current opinion in genetics & development*, **21**, 6 (Dec. 2011), 704–710.

[10] Berg, H. C. *E. Coli in Motion*, Springer Verlag (2004).

[11] Berg, H. C. and Brown, D. A. Chemotaxis in Escherichia coli analysed by three-dimensional tracking, *Nature*, **239**, 5374 (1972), 500–504.

[12] Block, S. M., Segall, J. E. and Berg, H. C. Adaptation kinetics in bacterial chemotaxis., *Journal of bacteriology*, **154**, 1 (Apr. 1983), 312–323.

[13] Bonner, J. T., Barkley, D. S., Hall, E. M., Konijn, T. M., Mason, J. W., O'Keefe, G., III and Wolfe, P. B. Acrasin, acrasinase, and the sensitivity to acrasin in Dictyostelium discoideum, *Developmental Biology*, **20**, 1 (July 1969), 72–87.

[14] Börner, S., Schwede, F., Schlipp, A., Berisha, F., Calebiro, D., Lohse, M. J. and Nikolaev, V. O. FRET measurements of intracellular cAMP concentrations and cAMP analog permeability in intact cells, *Nature Protocols*, **6**, 4 (Mar. 2011), 427–438.

[15] Cai, H., Das, S., Kamimura, Y., Long, Y., Parent, C. A. and Devreotes, P. N. Ras-mediated activation of the TORC2-PKB pathway is critical for chemotaxis., *The Journal of cell biology*, **190**, 2 (July 2010), 233–245.

[16] Camilli, A. and Bassler, B. L. Bacterial small-molecule signaling pathways., *Science (New York, N.Y.)*, **311**, 5764 (Feb. 2006), 1113–1116.

[17] Charest, P. G., Shen, Z., Lakoduk, A., Sasaki, A. T., Briggs, S. P. and Firtel, R. A. A Ras signaling complex controls the RasC-TORC2 pathway and directed cell migration., *Developmental cell*, **18**, 5 (May 2010), 737–749.

[18] Cohen, M. H. and Robertson, A. ScienceDirect.com - Journal of Theoretical Biology - Wave propagation in the early stages of aggregation of cellular slime molds, *Journal of theoretical biology* (1971).

[19] Cohen-Saidon, C., Cohen, A. A., Sigal, A., Liron, Y. and Alon, U. Dynamics and variability of ERK2 response to EGF in individual living cells., *Molecular cell*, **36**, 5 (Dec. 2009), 885–893.

[20] Comer, F. I. and Parent, C. A. Phosphoinositide 3-kinase activity controls the chemoattractant-mediated activation and adaptation of adenylyl cyclase., *Molecular biology of the cell*, **17**, 1 (Jan. 2006), 357–366.

[21] Cover, T. M. and Thomas, J. A. *Elements of Information Theory*, Wiley-Interscience (Nov. 2012).

[22] Danø, S., Madsen, M. F. and Sørensen, P. G. Quantitative characterization of cell synchronization in yeast., *Proceedings of the National Academy of Sciences of the United States of America*, **104**, 31 (July 2007), 12732–12736.

[23] Danø, S., Sørensen, P. G. and Hynne, F. Sustained oscillations in living cells : Abstract : Nature, *Nature*, **402**, 6759 (Nov. 1999), 320–322.

[24] De Monte, S., d'Ovidio, F., Danø, S. and Sørensen, P. G. Dynamical quorum sensing: Population density encoded in cellular dynamics., *Proceedings of the National Academy of Sciences of the United States of America*, **104**, 47 (Nov. 2007), 18377–18381.

[25] Devreotes, P. N. Cyclic 3',5' AMP relay in Dictyostelium discoideum. II. Requirements for the initiation and termination of the response, *The Journal of cell biology*, **80**, 2 (Feb. 1979), 300–309.

[26] Devreotes, P. N., Derstine, P. L. and Steck, T. L. Cyclic 3',5' AMP relay in Dictyostelium discoideum. I. A technique to monitor responses to controlled stimuli., *The Journal of cell biology*, **80**, 2 (Feb. 1979), 291–299.

[27] Dinauer, M. C., MacKay, S. A. and Devreotes, P. N. Cyclic 3',5'-AMP relay in Dictyostelium discoideum III. The relationship of cAMP synthesis and secretion during the cAMP signaling response., *The Journal of cell biology*, **86**, 2 (Aug. 1980), 537–544.

[28] Dinauer, M. C., Steck, T. L. and Devreotes, P. N. Cyclic 3',5'-AMP relay in Dictyostelium discoideum IV. Recovery of the cAMP signaling response after adaptation to cAMP., *The Journal of cell biology*, **86**, 2 (Aug. 1980), 545–553.

[29] Dinauer, M. C., Steck, T. L. and Devreotes, P. N. Cyclic 3',5'-AMP relay in Dictyostelium discoideum V. Adaptation of the cAMP signaling response during cAMP stimulation., *The Journal of cell biology*, **86**, 2 (Aug. 1980), 554–561.

[30] Dormann, D., Kim, J. Y., Devreotes, P. N. and Weijer, C. J. cAMP receptor affinity controls wave dynamics, geometry and morphogenesis in Dictyostelium., *Journal of cell science*, **114**, Pt 13 (July 2001), 2513–2523.

[31] Dormann, D., Weijer, G., Parent, C. A., Devreotes, P. N. and

Weijer, C. J. Visualizing PI3 kinase-mediated cell-cell signaling during Dictyostelium development., *Current biology : CB*, **12**, 14 (July 2002), 1178–1188.

[32] Driever, W. and Nüsslein-Volhard, C. A gradient of bicoid protein in Drosophila embryos., *Cell*, **54**, 1 (July 1988), 83–93.

[33] Driever, W. and Nüsslein-Volhard, C. The bicoid protein determines position in the Drosophila embryo in a concentration-dependent manner., *Cell*, **54**, 1 (July 1988), 95–104.

[34] Durston, A. J. Dictyostelium discoideum aggregation fields as excitable media., *Journal of theoretical biology*, **42**, 3 (Dec. 1973), 483–504.

[35] Durston, A. J. ScienceDirect.com - Developmental Biology - Pacemaker activity during aggregation in Dictyostelium discoideum, *Developmental Biology* (1974).

[36] Elowitz, M. B., Levine, A. J., Siggia, E. D. and Swain, P. S. Stochastic gene expression in a single cell., *Science (New York, N.Y.)*, **297**, 5584 (Aug. 2002), 1183–1186.

[37] Forgacs, G. and Newman, S. A. Biological Physics of the Developing Embryo (Nov. 2005).

[38] Geberth, D. and Hütt, M.-T. Predicting the distribution of spiral waves from cell properties in a developmental-path model of Dictyostelium pattern formation., *PLoS computational biology*, **5**, 7 (July 2009), e1000422.

[39] Gerisch, G. and Hess, B. Cyclic-AMP-controlled oscillations in suspended Dictyostelium cells: their relation to morphogenetic cell interactions., *Proceedings of the National Academy of Sciences of the United States of America*, **71**, 5 (May 1974), 2118–2122.

[40] Gerisch, G. and Wick, U. Intracellular oscillations and release of cyclic AMP from Dictyostelium cells., *Biochemical and biophysical research communications*, **65**, 1 (July 1975), 364–370.

[41] Gingle, A. R. Critical density for relaying in Dictyostelium discoideum and its relation to phosphodiesterase secretion into the extracellular medium., *Journal of cell science*, **20**, 1 (Jan. 1976), 1–20.

[42] Goentoro, L. and Kirschner, M. W. ScienceDirect.com - Molecular Cell - Evidence that Fold-Change, and Not Absolute Level, of β-Catenin Dictates Wnt Signaling, *Molecular cell* (2009).

[43] Goentoro, L., Shoval, O., Kirschner, M. W. and Alon, U. The incoherent feedforward loop can provide fold-change detection in gene regulation., *Molecular cell*, **36**, 5 (Dec. 2009), 894–899.

[44] Goldbeter, A. *Biochemical Oscillations and Cellular Rhythms*, The Molecular Bases of Periodic and Chaotic Behaviour, Cambridge University Press (Apr. 1997).

[45] Gordon, G. W., Berry, G., Liang, X. H., Levine, B. and Herman, B. Quantitative fluorescence resonance energy transfer measurements using fluorescence microscopy., *Biophysical journal*, **74**, 5 (May 1998), 2702–2713.

[46] Gregor, T., Bialek, W., Steveninck, de Ruyter van R. R., Tank, D. W. and Wieschaus, E. F. Diffusion and scaling during early embryonic pattern formation., *Proceedings of the National Academy of Sciences of the United States of America*, **102**, 51 (Dec. 2005), 18403–18407.

[47] Gregor, T., Fujimoto, K., Masaki, N. and Sawai, S. The onset of collective behavior in social amoebae., *Science (New York, N.Y.)*, **328**, 5981 (May 2010), 1021–1025.

[48] Gregor, T., Tank, D. W., Wieschaus, E. F. and Bialek, W. Probing the Limits to Positional Information, *Cell*, **130**, 1 (July 2007), 153–164.

[49] Gregor, T., Wieschaus, E. F., McGregor, A. P. and Bialek, W. ScienceDirect.com - Cell - Stability and Nuclear Dynamics of the Bicoid Morphogen Gradient, *Cell* (2007).

[50] Hashimoto, Y., Cohen, M. H. and Robertson, A. Cell density dependence of the aggregation characteristics of the cellular slime mould Dictyostelium discoideum., *Journal of cell science*, **19**, 1 (Oct. 1975), 215–229.

[51] Hosoya, K.-I., Amagai, A., Chida, J. and Maeda, Y. Unique behavior and function of the mitochondrial ribosomal protein S4 (RPS4) in early Dictyostelium development., *Zoological science*, **20**, 12 (Dec. 2003), 1455–1465.

[52] Howard, P. K., Ahern, K. G. and Firtel, R. A. Establishment of a transient expression system for Dictyostelium discoideum., *Nucleic acids research*, **16**, 6 (Mar. 1988), 2613–2623.

[53] Huang, Y. E., Iijima, M., Parent, C. A., Funamoto, S., Firtel, R. A. and Devreotes, P. Receptor-mediated regulation of PI3Ks confines PI(3,4,5)P3 to the leading edge of chemotaxing cells., *Molecular biology of the cell*, **14**, 5 (May 2003), 1913–1922.

[54] Iglesias, P. A. Spatial regulation of PI3K signaling during chemotaxis., *Wiley interdisciplinary reviews. Systems biology and medicine*, **1**, 2 (Sept. 2009), 247–253.

[55] Iglesias, P. A. Chemoattractant Signaling in Dictyostelium: Adaptation and Amplification, *Science signaling*, **5**, 213 (Feb. 2012), pe8.

[56] Iijima, M., Huang, Y. E., Luo, H. R., Vazquez, F. and Devreotes, P. N. Novel mechanism of PTEN regulation by its phosphatidylinositol 4,5-bisphosphate binding motif is critical for chemotaxis., *The Journal of biological chemistry*, **279**, 16 (Apr. 2004), 16606–16613.

[57] Insall, R., Kuspa, A., Lilly, P. J., Shaulsky, G., Levin, L. R., Loomis, W. F. and Devreotes, P. CRAC, a cytosolic protein containing a pleckstrin homology domain, is required for receptor and G protein-mediated activation of adenylyl cyclase in Dictyostelium., *The Journal of cell biology*, **126**, 6 (Sept. 1994), 1537–1545.

[58] Izhikevich, E. M. *Dynamical Systems in Neuroscience*, The Geometry of Excitability And Bursting, The MIT Press (2007).

[59] Janetopoulos, C., Jin, T. and Devreotes, P. Receptor-mediated activation of heterotrimeric G-proteins in living cells., *Science (New York, N.Y.)*, **291**, 5512 (Mar. 2001), 2408–2411.

[60] Janetopoulos, C., Ma, L., Devreotes, P. N. and Iglesias, P. A. Chemoattractant-induced phosphatidylinositol 3,4,5-trisphosphate accumulation is spatially amplified and adapts, independent of the actin cytoskeleton, *Proceedings of the ...* (2004).

[61] Jilkine, A. and Edelstein-Keshet, L. A comparison of mathematical models for polarization of single eukaryotic cells in response to guided cues., *PLoS*

computational biology, **7**, 4 (Apr. 2011), e1001121.

[62] Johnson, R. L., Van Haastert, P. J., Kimmel, A. R., Saxe, C. L., Jastorff, B. and Devreotes, P. N. The cyclic nucleotide specificity of three cAMP receptors in Dictyostelium., *The Journal of biological chemistry*, **267**, 7 (Mar. 1992), 4600–4607.

[63] Kamino, K., Fujimoto, K. and Sawai, S. Collective oscillations in developing cells: insights from simple systems., *Development, growth & differentiation*, **53**, 4 (May 2011), 503–517.

[64] Kaneko, K. and Furusawa, C. Consistency principle in biological dynamical systems., *Theory in biosciences = Theorie in den Biowissenschaften*, **127**, 2 (June 2008), 195–204.

[65] Kessin, R. H. Dictyostelium (2001).

[66] Konijn, T. M., Van De Meene, J. G., Bonner, J. T. and Barkley, D. S. The acrasin activity of adenosine-3',5'-cyclic phosphate., *Proceedings of the National Academy of Sciences of the United States of America*, **58**, 3 (Sept. 1967), 1152–1154.

[67] Lauzeral, J., Halloy, J. and Goldbeter, A. Desynchronization of cells on the developmental path triggers the formation of spiral waves of cAMP during Dictyostelium aggregation., *Proceedings of the National Academy of Sciences of the United States of America*, **94**, 17 (Aug. 1997), 9153–9158.

[68] Lazova, M. D., Ahmed, T., Bellomo, D., Stocker, R. and Shimizu, T. S. Response rescaling in bacterial chemotaxis., *Proceedings of the National Academy of Sciences of the United States of America*, **108**, 33 (Aug. 2011), 13870–13875.

[69] Levchenko, A. and Iglesias, P. A. Models of eukaryotic gradient sensing: application to chemotaxis of amoebae and neutrophils., *Biophysical journal*, **82**, 1 Pt 1 (Jan. 2002), 50–63.

[70] Levine, H., Kessler, D. A. and Rappel, W.-J. Directional sensing in eukaryotic chemotaxis: a balanced inactivation model., *Proceedings of the National Academy of Sciences of the United States of America*, **103**, 26 (June 2006), 9761–9766.

[71] Loovers, H. M., Postma, M., Keizer-Gunnink, I., Huang, Y. E., Devreotes, P. N. and Van Haastert, P. J. M. Distinct roles of PI(3,4,5)P3 during chemoattractant signaling in Dictyostelium: a quantitative in vivo analysis by inhibition of PI3-kinase., *Molecular biology of the cell*, **17**, 4 (Apr. 2006), 1503–1513.

[72] Ma, W., Trusina, A., El-Samad, H., Lim, W. A. and Tang, C. Defining network topologies that can achieve biochemical adaptation., *Cell*, **138**, 4 (Aug. 2009), 760–773.

[73] Martiel, J. L. and Goldbeter, A. A Model Based on Receptor Desensitization for Cyclic AMP Signaling in Dictyostelium Cells., *Biophysical journal*, **52**, 5 (Nov. 1987), 807–828.

[74] McMains, V. C., Liao, X.-H. and Kimmel, A. R. Oscillatory signaling and network responses during the development of Dictyostelium discoideum., *Ageing research reviews*, **7**, 3 (July 2008), 234–248.

[75] Mesibov, R., Ordal, G. W. and Adler, J. The range of attractant concen-

trations for bacterial chemotaxis and the threshold and size of response over this range. Weber law and related phenomena., *The Journal of general physiology*, **62**, 2 (Aug. 1973), 203–223.

[76] Mettetal, J. T., Muzzey, D., Gómez-Uribe, C. and Oudenaarden, van A. The frequency dependence of osmo-adaptation in Saccharomyces cerevisiae., *Science (New York, N.Y.)*, **319**, 5862 (Jan. 2008), 482–484.

[77] Milo, R., Shen-Orr, S., Itzkovitz, S., Kashtan, N., Chklovskii, D. and Alon, U. Network Motifs: Simple Building Blocks of Complex Networks, *Science signaling*, **298**, 5594 (Oct. 2002), 824.

[78] Munsky, B., Neuert, G. and Oudenaarden, van A. Using gene expression noise to understand gene regulation., *Science (New York, N.Y.)*, **336**, 6078 (Apr. 2012), 183–187.

[79] Muratov, C. B., Vanden-Eijnden, E. and E, W. Noise can play an organizing role for the recurrent dynamics in excitable media, *Proceedings of the National Academy of Sciences of the United States of America*, **104**, 3 (Jan. 2007), 702–707.

[80] Muzzey, D., Gómez-Uribe, C. A., Mettetal, J. T. and Oudenaarden, van A. A systems-level analysis of perfect adaptation in yeast osmoregulation., *Cell*, **138**, 1 (July 2009), 160–171.

[81] Muzzey, D. and Oudenaarden, van A. Quantitative time-lapse fluorescence microscopy in single cells., *Annual review of cell and developmental biology*, **25** (2009), 301–327.

[82] Nanjundiah, V. Periodic stimuli are more successful than randomly spaced ones for inducing development in Dictyostelium discoideum., *Bioscience reports*, **8**, 6 (Dec. 1988), 571–577.

[83] Ng, W.-L. and Bassler, B. L. Bacterial quorum-sensing network architectures., *Annual review of genetics*, **43** (2009), 197–222.

[84] Nikolaev, V. O., Bünemann, M., Hein, L., Hannawacker, A. and Lohse, M. J. Novel Single Chain cAMP Sensors for Receptor-induced Signal Propagation, *Journal of Biological ...* (2004).

[85] Novák, B. and Tyson, J. J. Design principles of biochemical oscillators., *Nature reviews. Molecular cell biology*, **9**, 12 (Dec. 2008), 981–991.

[86] Pálsson, E. A cAMP signaling model explains the benefit of maintaining two forms of phosphodiesterase in Dictyostelium., *Biophysical journal*, **97**, 9 (Nov. 2009), 2388–2398.

[87] Parent, C. A., Blacklock, B. J., Froehlich, W. M., Murphy, D. B. and Devreotes, P. N. G protein signaling events are activated at the leading edge of chemotactic cells., *Cell*, **95**, 1 (Oct. 1998), 81–91.

[88] Parent, C. A. and Devreotes, P. N. A cell's sense of direction., *Science (New York, N.Y.)*, **284**, 5415 (Apr. 1999), 765–770.

[89] Postma, M., Bosgraaf, L., Loovers, H. M. and Van Haastert, P. J. M. Chemotaxis: signalling modules join hands at front and tail., *EMBO reports*, **5**, 1 (Jan. 2004), 35–40.

[90] Postma, M., Roelofs, J., Goedhart, J., Gadella, T. W. J., Visser, A. J. W. G. and Van Haastert, P. J. M. Uniform cAMP stimulation of Dictyostelium cells induces localized patches of signal transduction

and pseudopodia., *Molecular biology of the cell*, **14**, 12 (Dec. 2003), 5019–5027.

[91] Purvis, J. E. and Lahav, G. Encoding and Decoding Cellular Information through Signaling Dynamics., *Cell*, **152**, 5 (Feb. 2013), 945–956.

[92] Rappel, W.-J., Nicol, A., Sarkissian, A., Levine, H. and Loomis, W. Self-organized Vortex State in Two-Dimensional Dictyostelium Dynamics, *Phys Rev Lett*, **83**, 6 (Aug. 1999), 1247–1250.

[93] Robertson, A., Drage, D. J. and Cohen, M. H. Control of Aggregation in Dictyostelium discoideum by an External Periodic Pulse of Cyclic Adenosine Monophosphate., *Science (New York, N.Y.)*, **175**, 4019 (Jan. 1972), 333–335.

[94] Saran, S., Meima, M. E., Alvarez-Curto, E., Weening, K. E., Rozen, D. E. and Schaap, P. cAMP signaling in Dictyostelium, *Journal of Muscle Research & Cell Motility*, **23**, 7-8 (2002), 793–802.

[95] Shimizu, T. S., Tu, Y. and Berg, H. C. A modular gradient-sensing network for chemotaxis in Escherichia coli revealed by responses to time-varying stimuli., *Molecular systems biology*, **6** (June 2010), 382.

[96] Shoval, O., Alon, U. and Sontag, E. Symmetry invariance for adapting biological systems, *SIAM Journal on Applied Dynamical Systems*, **10**, 3 (2011), 857–886.

[97] Shoval, O., Goentoro, L., Hart, Y., Mayo, A., Sontag, E. and Alon, U. Fold-change detection and scalar symmetry of sensory input fields., *Proceedings of the National Academy of Sciences of the United States of America*, **107**, 36 (Sept. 2010), 15995–16000.

[98] Sigal, A., Danon, T., Cohen, A., Milo, R., Geva-Zatorsky, N., Lustig, G., Liron, Y., Alon, U. and Perzov, N. Generation of a fluorescently labeled endogenous protein library in living human cells., *Nature Protocols*, **2**, 6 (2007), 1515–1527.

[99] Sourjik, V. and Berg, H. C. Binding of the Escherichia coli response regulator CheY to its target measured in vivo by fluorescence resonance energy transfer., *Proceedings of the National Academy of Sciences of the United States of America*, **99**, 20 (Oct. 2002), 12669–12674.

[100] Sourjik, V. and Berg, H. C. Receptor sensitivity in bacterial chemotaxis., *Proceedings of the National Academy of Sciences of the United States of America*, **99**, 1 (Jan. 2002), 123–127.

[101] Sourjik, V. and Berg, H. C. Receptor sensitivity in bacterial chemotaxis, ... *of the National Academy of Sciences* (2002).

[102] Sourjik, V. and Berg, H. C. Functional interactions between receptors in bacterial chemotaxis., *Nature*, **428**, 6981 (Mar. 2004), 437–441.

[103] Strogatz, S. H. *Nonlinear dynamics and chaos*, with applications to physics, biology, chemistry, and engineering, Sarat Book Distributors (1994).

[104] Swaney, K. F., Huang, C.-H. and Devreotes, P. N. Eukaryotic chemotaxis: a network of signaling pathways controls motility, directional sensing, and polarity., *Annual review of biophysics*, **39** (2010), 265–289.

[105] Takeda, K., Shao, D., Adler, M., Charest, P. G., Loomis, W. F., Levine, H., Groisman, A., Rappel, W.-J. and Firtel, R. A. Incoherent feedforward control governs adaptation of activated ras in a eukaryotic chemotaxis pathway., *Science signaling*, **5**, 205 (Jan. 2012), ra2.

[106] Taniguchi, D., Ishihara, S., Oonuki, T., Honda-Kitahara, M., Kaneko, K. and Sawai, S. Phase geometries of two-dimensional excitable waves govern self-organized morphodynamics of amoeboid cells., *Proceedings of the National Academy of Sciences of the United States of America* (Mar. 2013).

[107] Taylor, A. F., Tinsley, M. R., Wang, F., Huang, Z. and Showalter, K. Dynamical quorum sensing and synchronization in large populations of chemical oscillators., *Science (New York, N.Y.)*, **323**, 5914 (Jan. 2009), 614–617.

[108] Theibert, A. and Devreotes, P. N. Cyclic 3', 5'-AMP relay in Dictyostelium discoideum: adaptation is independent of activation of adenylate cyclase., *The Journal of cell biology*, **97**, 1 (July 1983), 173–177.

[109] Tomchik, K. J. and Devreotes, P. N. Adenosine 3',5'-monophosphate waves in Dictyostelium discoideum: a demonstration by isotope dilution–fluorography., *Science (New York, N.Y.)*, **212**, 4493 (Apr. 1981), 443–446.

[110] Tyson, J. J., Alexander, K. A. and Manoranjan, V. S. ScienceDirect.com - Physica D: Nonlinear Phenomena - Spiral waves of cyclic amp in a model of slime mold aggregation, *Physica D: Nonlinear ...* (1989).

[111] Tyson, J. J. and Murray, J. D. Cyclic AMP waves during aggregation of Dictyostelium amoebae., *Development*, **106**, 3 (July 1989), 421–426.

[112] Ueda, M. and Shibata, T. Stochastic signal processing and transduction in chemotactic response of eukaryotic cells., *Biophysical journal*, **93**, 1 (July 2007), 11–20.

[113] Wang, B. and Kuspa, A. Dictyostelium development in the absence of cAMP., *Science (New York, N.Y.)*, **277**, 5323 (July 1997), 251–254.

[114] Wang, C. J., Bergmann, A., Lin, B., Kim, K. and Levchenko, A. Diverse sensitivity thresholds in dynamic signaling responses by social amoebae., *Science signaling*, **5**, 213 (Feb. 2012), ra17.

[115] Waters, C. M. and Bassler, B. L. Quorum sensing: cell-to-cell communication in bacteria., *Annual review of cell and developmental biology*, **21** (2005), 319–346.

[116] Wolpert, L. Positional information and patterning revisited., *Journal of theoretical biology*, **269**, 1 (Jan. 2011), 359–365.

[117] Xia, Z. and Liu, Y. Reliable and global measurement of fluorescence resonance energy transfer using fluorescence microscopes., *Biophysical journal*, **81**, 4 (Oct. 2001), 2395–2402.

[118] Yi, T. M., Huang, Y., Simon, M. I. and Doyle, J. Robust perfect adaptation in bacterial chemotaxis through integral feedback control., *Proceedings of the National Academy of Sciences of the United States of America*, **97**, 9 (Apr. 2000), 4649–4653.